UNITED STATES DEPARTMENT OF THE INTERIOR
GEOLOGICAL SURVEY

Numerical Study of Attenuation of High Frequency Lg-Waves in the New Madrid Seismic Region

by

John J. Dwyer, Robert B. Herrmann, and Otto W. Nuttli

Open-File Report 81-112
1981

CONTENTS

PREFACE

This report was prepared by John J. Dwyer, Robert B. Herrmann and Otto W. Nuttli, Department of Earth and Atmospheric Sciences, Saint Louis University, Saint Louis, Missouri, under a grant contract No. 52480 U.S. Geological Survey. This effort is part of a continuing program at the U.S. Geological Survey in the study of short-period seismic wave attenuation in the United States, sponsored by the project of "Seismic Wave Attenuation in Conterminous United States" of the Office of Earthquake Studies in Denver, Colorado.

INTRODUCTION

Any study of seismic risk in regions of seismic activity must take into account, along with other important factors, the rate of attenuation of seismic energy with distance in the region. It is known that the coefficient of anelastic attenuation for 1 Hz and 10 Hz Lg waves is lower in the central United States than in the western United States (Nuttli, 1973; Street, 1976; Nuttli, 1978; Bollinger, 1979). Since the frequencies of damaging ground motion usually lie between 1 and 10 Hz, a study of the attenuation of waves in this frequency range is important. Some work has already been done in this area, using narrow-bandpass filtered time-domain data (Nuttli and Dwyer, 1978; Dwyer and Nuttli, 1978).

This study presents an attempt to use a numerical least-squares method to determine a value for the coefficient of anelastic attenuation at various frequencies, using both broadband and narrow-bandpass filtered time-domain data. The filtered data were obtained from events occurring in the New Madrid seismic zone. A network of microearthquake seismographs located in the active seismic region, funded by the U.S. Geological Survey, and operated by Saint Louis University, was used to provide a data base.

DATA

The data base for this study consists of 35 events occurring in the New Madrid seismic zone. The events were recorded by the Southeast Missouri Regional Seismic Network, operated by Saint Louis University. The network consists presently of twenty-four stations. Figure 1 shows the network, as well as the seismicity of the area, as recorded since the installation of the network. Figure 2 shows the events used in this study. Each station consists of one vertical short-period seismometer, preamplifier/VCO, and a telemetry package. Signals are transmitted from the station to a collection point, and then transmitted via phone line to the Seismic Data Center in the Department of Earth and Atmospheric Sciences of Saint Louis University. Here they are recorded on 16 mm film using develocorders, on paper using pen and ink drum monitors, and on magnetic tape using two slow-speed sixteen-channel magnetic FM tape recorders. The data for this study were obtained from the analog tape records.

The calibration of the magnetic-tape playback system was made using a shake table calibration of one of the seismometers. The output of the tape playback goes to the galvanometers of a Brush oscillograph, which puts the record on dry photographic paper, from which amplitudes are read. The seismometer-tape playback-Brush oscillograph system response curve is shown in Figure 3. We can see that the system peaks at about 8 hz, and provides a good window for looking at the frequency range of interest.

In order to study Lg phase amplitudes at a variety of frequencies, the analog tape data are passed to the Brush oscillograph through

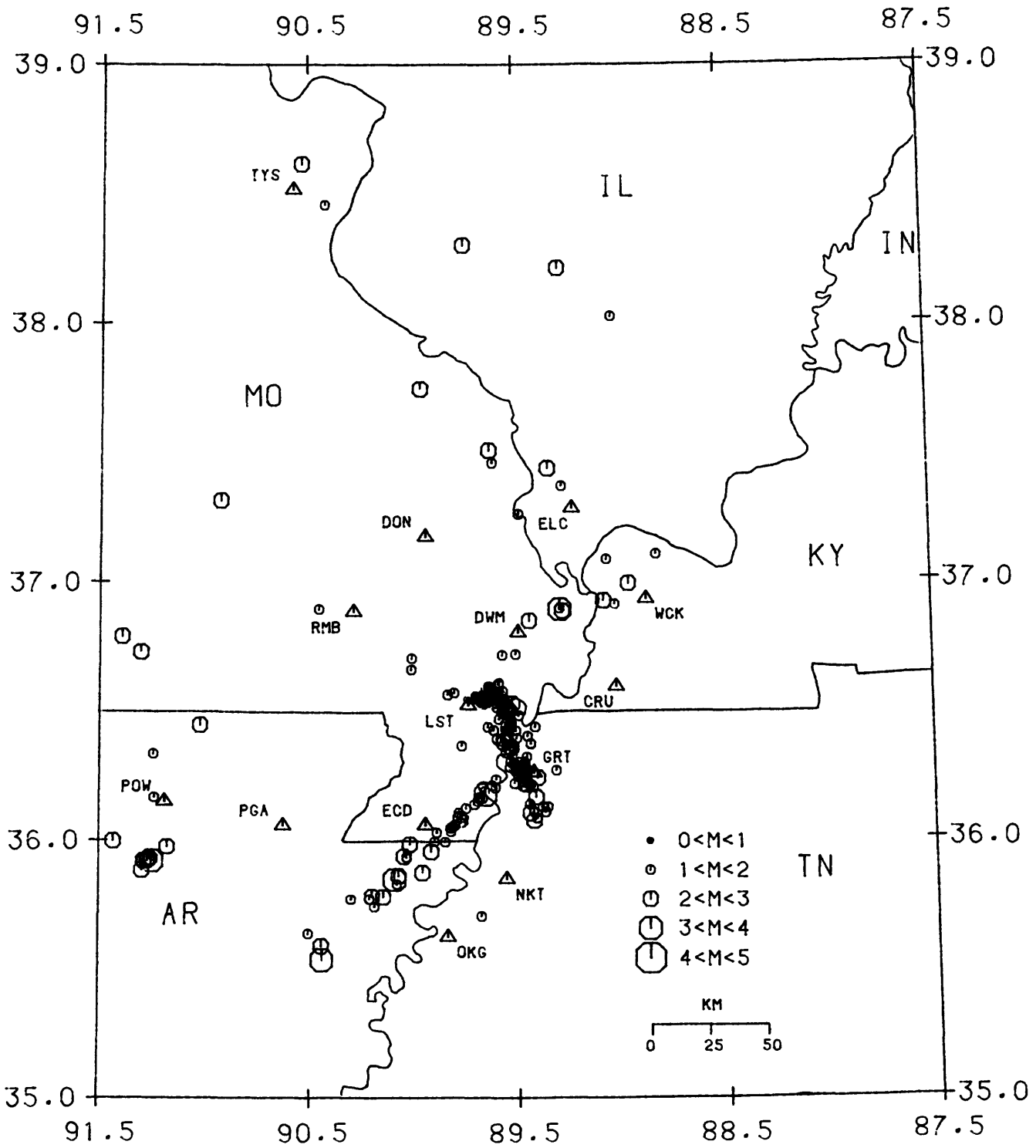

FIGURE 1

CUMULATIVE PERIOD 01 JAN 1979 TO 31 DEC 1979

LEGEND . ▲ STATION ⊙ EPICENTER

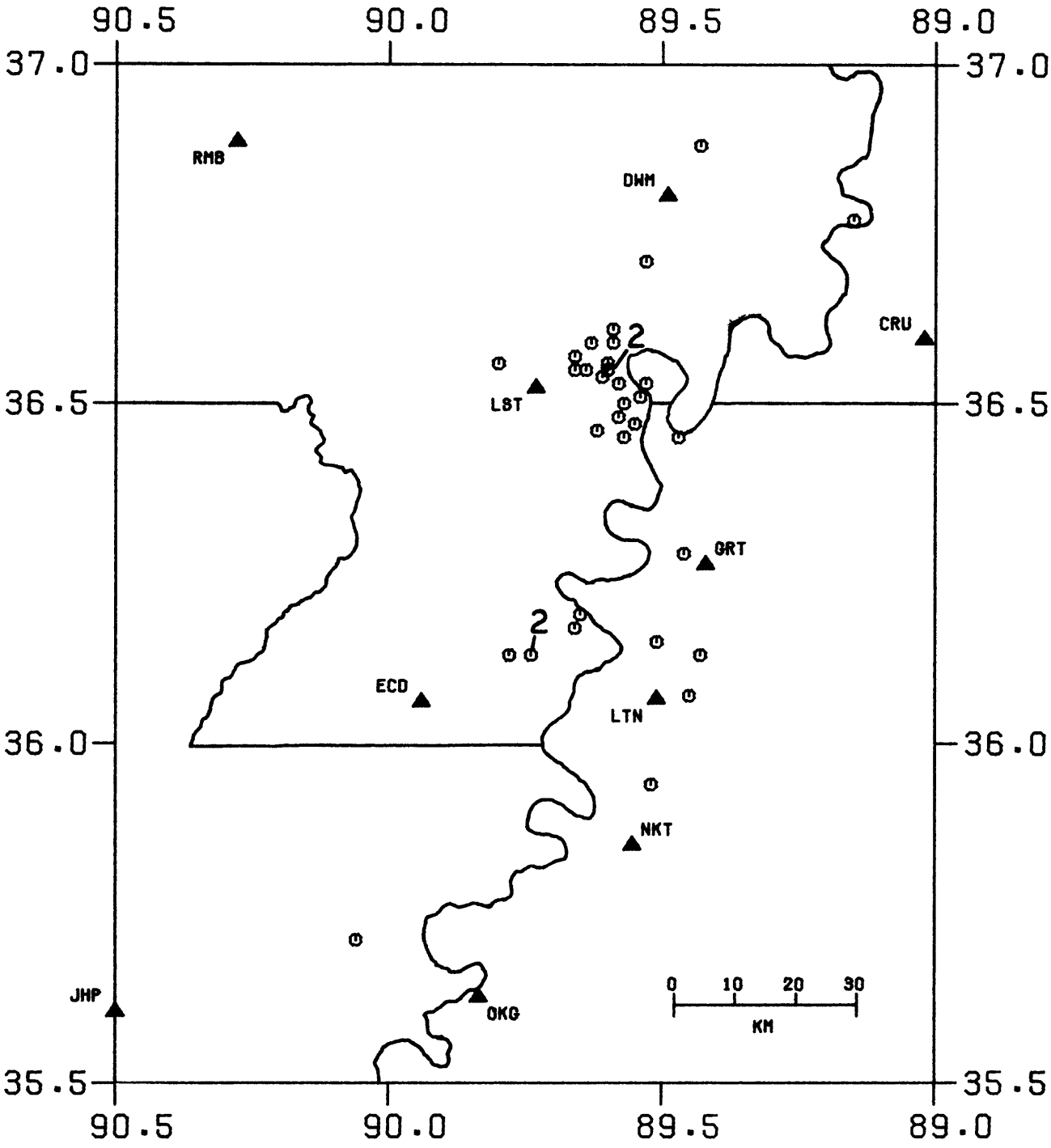

Fig. 2 Location of Epicenters of Earthquakes Used in this Study

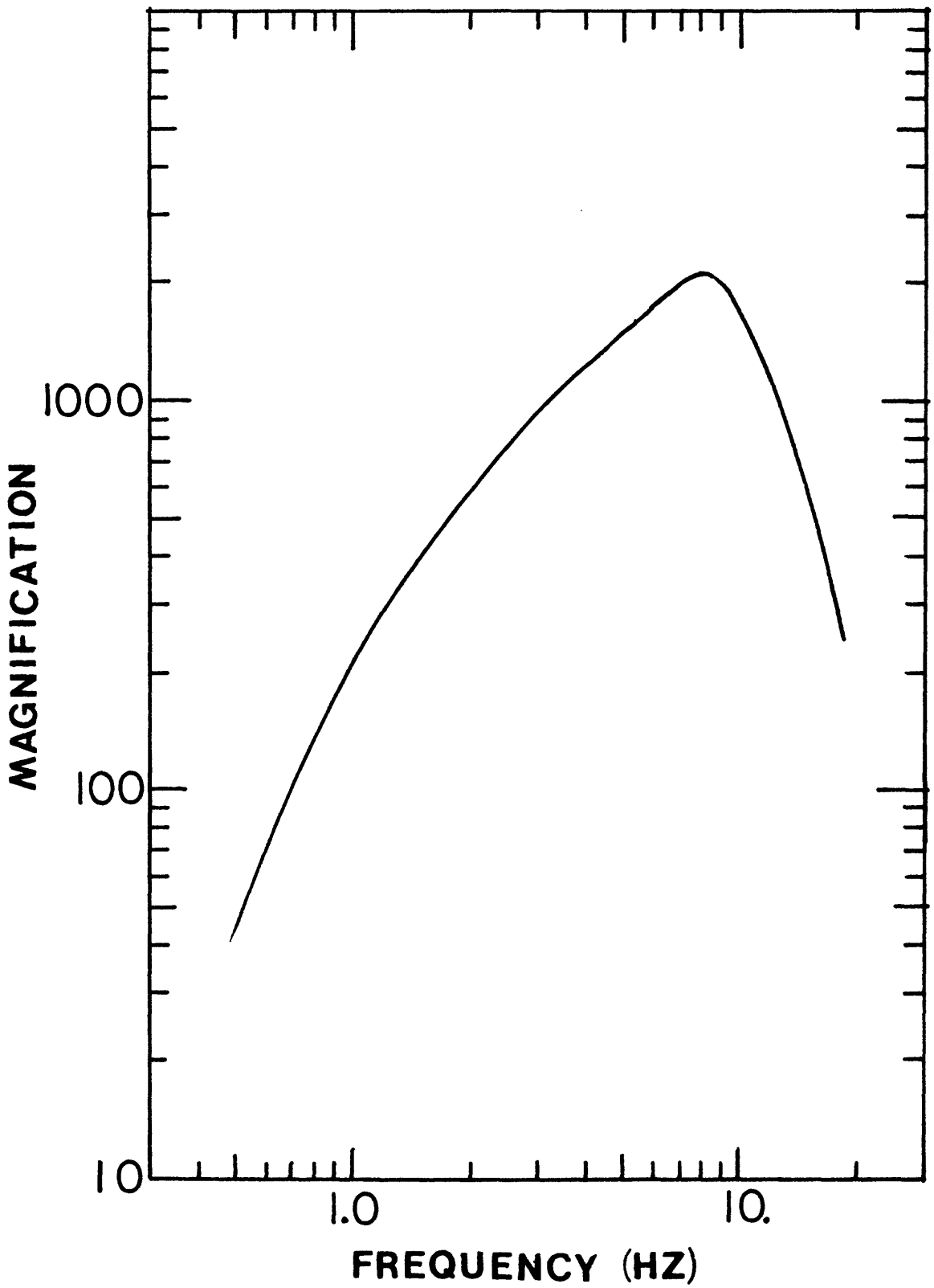

Fig. 3 Tape Playback Response Curve

several Kronhite filters. The magnification curve of the filtered system is found by passing the calibrated seismograph data on analog tape through the Kronhites. Seven filter settings on the Kronhite filters have been used in the present study, with peak frequencies of 1, 1.5, 2, 3, 5, 8, and 10.5 hz. (The 12.5 hz filter setting peaked at 10.5 hz.) The magnification curves for these narrow-bandpass filter settings are seen in Figure 4. With these curves, all one needs to know to determine the actual ground amplitude at a given frequency are the gain of the field station with respect to the calibrated seismometer, and the gain setting on the Brush oscillograph.

The stations available for use as analog tape data are listed in Table 1. Also listed are the station gains relative to the calibrated seismometer, and the date on which the station data first were recorded on analog tape.

The epicenters used in this study are listed in Table 2. The magnitudes have been calculated using the recently revised magnitude scale for the central U.S. (Stauder et al., 1979). An attempt was made to examine data from larger magnitude events at larger epicentral distances in order to improve the range of epicentral distances involved. This meant, however, that for a given event, the spread of distances was no longer large enough to show any significant data trend. As with the other earthquakes examined, if a general decrease in Lg amplitude with increase in epicentral distance was not evident, the data were rejected. The term Lg amplitude refers to the sustained maximum amplitude, defined as that equalled or excelled by the three largest cycles of motion (Nuttli, 1973).

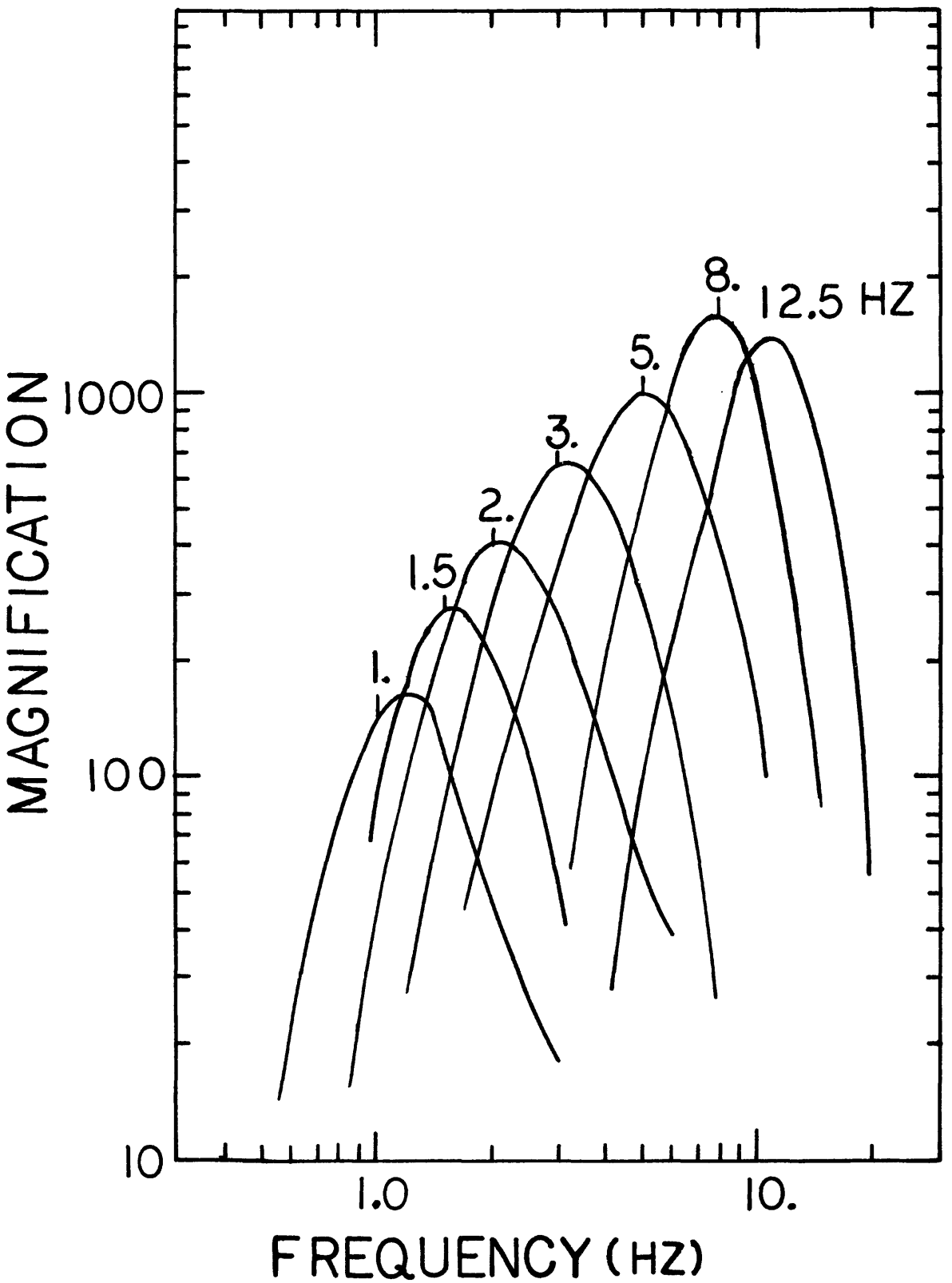

Fig. 4 Filtered Playback Response Curves

TABLE 1

LIST OF SEISMOGRAPH STATIONS

CODE	LOCATION	LATITUDE °N	LATITUDE °W	STATION GAIN*	START OF ANALOG TAPE RECORDING
TYS	Tyson Valley, MO	38.515	90.568	32	2-19-74
DWM	Dogwood, MO	36.805	89.490	8	9-06-74
ELC	Elco, IL	37.285	89.227	128	9-06-74
WCK	Wilson Creek, KY	36.934	88.874	32	9-06-74
CRU	Crutchfield, KY	36.595	89.020	32	9-06-74
GRT	Gratio, TN	36.264	89.425	32	9-06-74
LST	Lone Star, MO	36.523	89.731	16	9-06-74
RMB	Rombauer, MO	36.886	90.278	64	9-06-74
DON	Dongola, MO	37.176	89.933	128	9-06-74
OKG	Oak Grove, TN	35.626	89.835	32	6-09-75
PGA	Paragould, AR	36.060	90.620	16	4-15-77
ECD	Elk Chute Ditch, MO	36.060	89.940	16	4-15-77
NKT	Nankipoo, TN	35.850	89.544	16	4-15-77

* relative to calibrated seismometers

TABLE 2

EVENTS ANALYSED

NO.	DATE	ORIGIN TIME U.T.	LATITUDE ^{o}N	LONGITUDE ^{o}W	m_b
1	01 JUN 75	03:40:11.9	36.28	89.60	2.0
2	28 JUN 75	13:11:01.3	36.57	89.66	1.8
3	05 JUL 75	18:38:16.7	36.13	89.78	1.7
4	09 AUG 75	06:40:24.9	36.59	89.59	2.0
5	09 AUG 75	19:08:39.4	36.88	89.43	2.2
6	05 SEP 75	21:46:14.5	36.13	89.43	2.0
7	17 SEP 75	00:00:34.2	36.59	89.63	2.1
8	03 DEC 75	10:54:42.2	36.56	89.80	1.7
9	07 DEC 75	12:18:28.7	35.71	90.06	2.0
10	05 JAN 76	03:46:30.0	35.94	89.52	2.0
11	10 JAN 76	10:28:35.9	36.13	89.72	1.5
12	23 JAN 76	00:56:39.6	36.55	89.60	2.1
13	28 FEB 76	00:14:35.2	36.51	89.54	2.1
14	26 MAR 76	08:50:37.4	36.61	89.59	1.9
15	10 APR 76	02:47:55.9	36.55	89.66	1.7
16	23 MAY 76	08:37:09.5	36.13	89.74	1.9
17	24 MAY 76	07:30:17.5	36.07	89.45	1.8
18	04 JUL 76	03:02:50.5	36.77	89.15	2.0
19	15 DEC 76	11:57:07.1	36.07	89.80	2.0
20	02 JAN 77	20:29:36.2	36.45	89.57	1.7
21	02 JAN 77	20:33:23.2	36.47	89.55	1.7
22	29 JAN 77	22:08:37.8	36.53	89.58	2.2
23	08 FEB 77	10:20:42.5	36.50	89.57	1.8
24	17 FEB 77	08:34:00.8	36.15	89.51	2.0
25	04 AUG 77	01:05:19.3	36.55	89.60	2.0
26	10 SEP 77	21:36:04.5	36.55	89.64	1.7
27	12 SEP 77	23:48:38.9	36.53	89.53	1.7
28	26 SEP 77	17:19:17.4	36.46	89.62	2.1
29	28 SEP 77	21:45:20.1	36.71	89.53	2.0
30	25 OCT 77	19:22:29.7	36.45	89.47	2.2
31	04 NOV 77	11:21:06.8	34.01	89.22	3.5
32	22 NOV 77	06:42:50.9	36.48	89.58	2.0
33	24 DEC 77	00:00:28.8	36.17	89.66	2.2
34	14 Jan 78	12:46:50.0	36.19	89.65	1.9
35	20 JAN 78	10:25:44.3	36.54	89.61	1.9

The Lg ground displacement amplitude data for four of the events are listed in Tables 3-6, and plotted versus epicentral distance in Figures 5-32. The error bars shown represent the level of background noise. The procedure of data analysis was as follows: the analog tape record of an event recorded at a particular station was passed through the filter at a given filter setting, yielding a filtered trace on the Brush oscillograph. The largest sustained maximum amplitude was read off (as was the background noise level), then corrected for galvanometer gain, station gain, and filtered playback response to yield a ground displacement amplitude. In this study, these ground displacement amplitude and corresponding epicentral distance data were used to numerically determine a value for the coefficient of anelastic attenuation at the peak frequency of each filter setting.

TABLE 3

AMPLITUDE AND DISTANCE DATA FOR EVENT 1

3a) 1-Hz Narrow Bandpass Data

Peak Magnification: 190

STA	DIST. (km)	RECORD AMPLITUDE (mm)	RECORD NOISE (mm)	GALVANOMETER GAIN	STATION GAIN	GROUND DISPLACEMENT (μ)	NOISE (μ)	AZIMUTH
ELC	98.3	5.1	1.8	8.9	128	.0118	.0042	35
WCK	97.7	5.9	2.2	8.9	32	.0545	.0203	65
GRT	51.5	8.8	1.8	8.9	32	.0813	.0166	130
LST	12.7	8.4	1.4	8.9	16	.1552	.0259	110
RMB	51.5	17.0	1.6	8.9	128	.0393	.0037	314
DON	68.4	13.7	1.0	8.9	128	.0316	.0023	355

TABLE 3

(continued)

3b) 1.5-Hz Narrow Bandpass Data

Peak Magnification: 250

STA	DIST. (km)	RECORD AMPLITUDE (mm)	RECORD NOISE (mm)	GALVANOMETER GAIN	STATION GAIN	GROUND DISPLACEMENT (μ)	NOISE (μ)	AZIMUTH
ELC	98.3	15.9	2.7	13.7	128	.0181	.0031	35
WCK	97.7	9.2	2.9	13.7	32	.0420	.0132	65
GRT	51.5	12.4	1.8	13.7	32	.0566	.0082	130
LST	12.7	24.0	4.9	13.7	16	.2190	.0429	110
RMB	51.5	19.1	1.4	8.9	128	.0335	.0025	314
DON	68.5	19.3	1.5	8.9	128	.0339	.0026	355

TABLE 3

(continued)

3c) 2.0-Hz Narrow Bandpass Data

Peak Magnification: 250

STA	DIST. (km)	RECORD AMPLITUDE (mm)	RECORD NOISE (mm)	GALVANOMETER GAIN	STATION GAIN	GROUND DISPLACEMENT (μ)	NOISE (μ)	AZIMUTH
ELC	98.3	7.8	1.5	8.9	128	.0070	.0013	35
WCK	97.7	11.1	2.3	8.9	32	.0398	.0078	65
GRT	51.5	15.0	1.1	8.9	32	.0537	.0039	130
LST	12.7	31.6	4.3	8.9	16	.2264	.0308	110
RMB	51.5	38.4	2.3	8.9	128	.0344	.0021	314
DON	68.4	25.2	2.2	8.9	128	.0226	.0020	355

TABLE 3

(continued)

3d) 3-Hz Narrow Bandpass Data

Peak Magnification: 850

STA	DIST. (km)	RECORD AMPLITUDE (mm)	RECORD NOISE (mm)	GALVANOMETER GAIN	STATION GAIN	GROUND DISPLACEMENT (μ)	NOISE (μ)	AZIMUTH
ELC	98.3	17.8	2.0	8.9	128	.0092	.0010	35
WCK	97.7	18.2	3.8	8.9	32	.0376	.0066	65
GRT	51.5	12.2	1.3	3.8	32	.0590	.0063	130
LST	12.7	20.6	2.9	3.8	16	.1993	.0526	110
RMB	51.5	31.7	2.9	3.8	128	.0383	.0035	314
DON	68.5	13.7	1.2	3.8	128	.0166	.0015	355

TABLE 3

(continued)

3e) 5-Hz Narrow Bandpass Data

Peak Magnification: 1240

STA	DIST. (km)	RECORD AMPLITUDE (mm)	RECORD NOISE (mm)	GALVANOMETER GAIN	STATION GAIN	GROUND DISPLACEMENT (μ)	NOISE (μ)	AZIMUTH
ELC	98.5	27.0	3.6	8.9	128	.0096	.0013	35
WCK	97.7	25.8	5.7	8.9	32	.0365	.0081	65
GRT	51.5	18.0	1.6	3.8	32	.0597	.0053	130
LST	12.7	21.6	3.0	3.8	16	.1433	.0199	110
RMB	51.5	21.4	2.7	2	128	.0337	.0043	314
DON	68.4	19.0	1.2	2	128	.0299	.0019	355

TABLE 3

(continued)

3f) 8-Hz Narrow Bandpass Data

Peak Magnification: 2050

STA	DIST. (km)	RECORD AMPLITUDE (mm)	RECORD NOISE (mm)	GALVANOMETER GAIN	STATION GAIN	GROUND DISPLACEMENT (μ)	NOISE (μ)	AZIMUTH
ELC	98.3	19.8	3.4	3.8	128	.0099	.0017	35
WCK	97.7	16.1	4.5	3.8	32	.0323	.0090	65
GRT	51.5	19.6	1.3	2	32	.0747	.0013	130
LST	12.7	18.3	2.4	2	16	.1395	.0183	110
RMB	51.5	24.2	4.2	2	128	.0231	.0040	314
DON	68.5	26.8	1.0	1	128	.0511	.0019	355

Table 3

(continued)

3g) 12.5-Hz Narrow Bandpass Data

Peak Magnification: 1300

STA	DIST. (km)	RECORD AMPLITUDE (mm)	RECORD NOISE (mm)	GALVANOMETER GAIN	STATION GAIN	GROUND DISPLACEMENT (μ)	NOISE (μ)	AZIMUTH
ELC	98.3	16.7	3.9	8.9	128	.0056	.0013	35
WCK	97.7	11.3	5.8	3.8	32	.0357	.0183	65
GRT	51.5	31.9	2.8	3.8	32	.1009	.0089	130
LST	12.7	24.8	3.3	3.8	16	.1569	.0209	110
RMB	51.5	16.8	3.7	2	128	.0252	.0056	314
DON	68.5	32.0	1.8	2	128	.0481	.0027	355

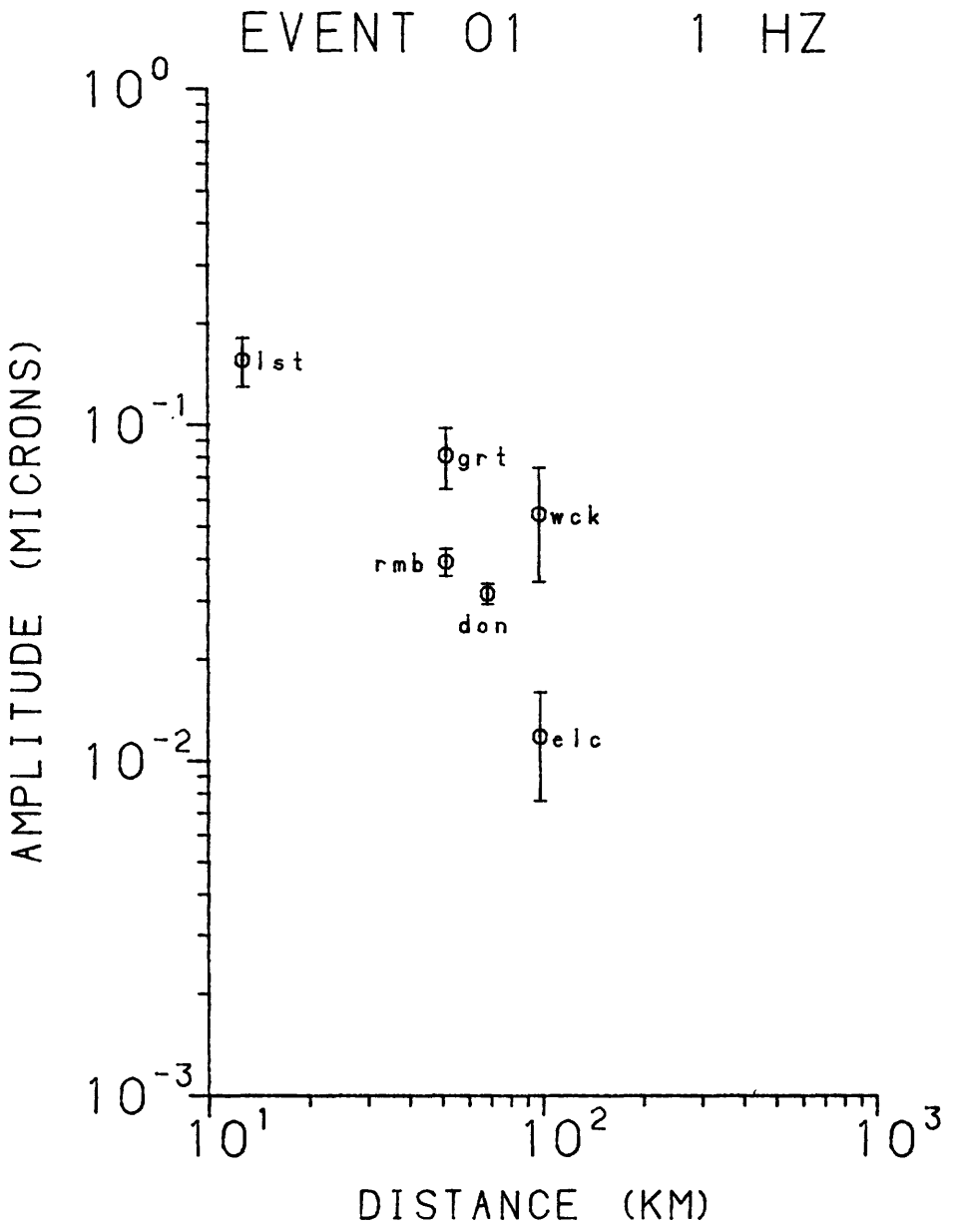

Figure 5. 1-Hz amplitudes of Lg-Z waves for Event No. 1.

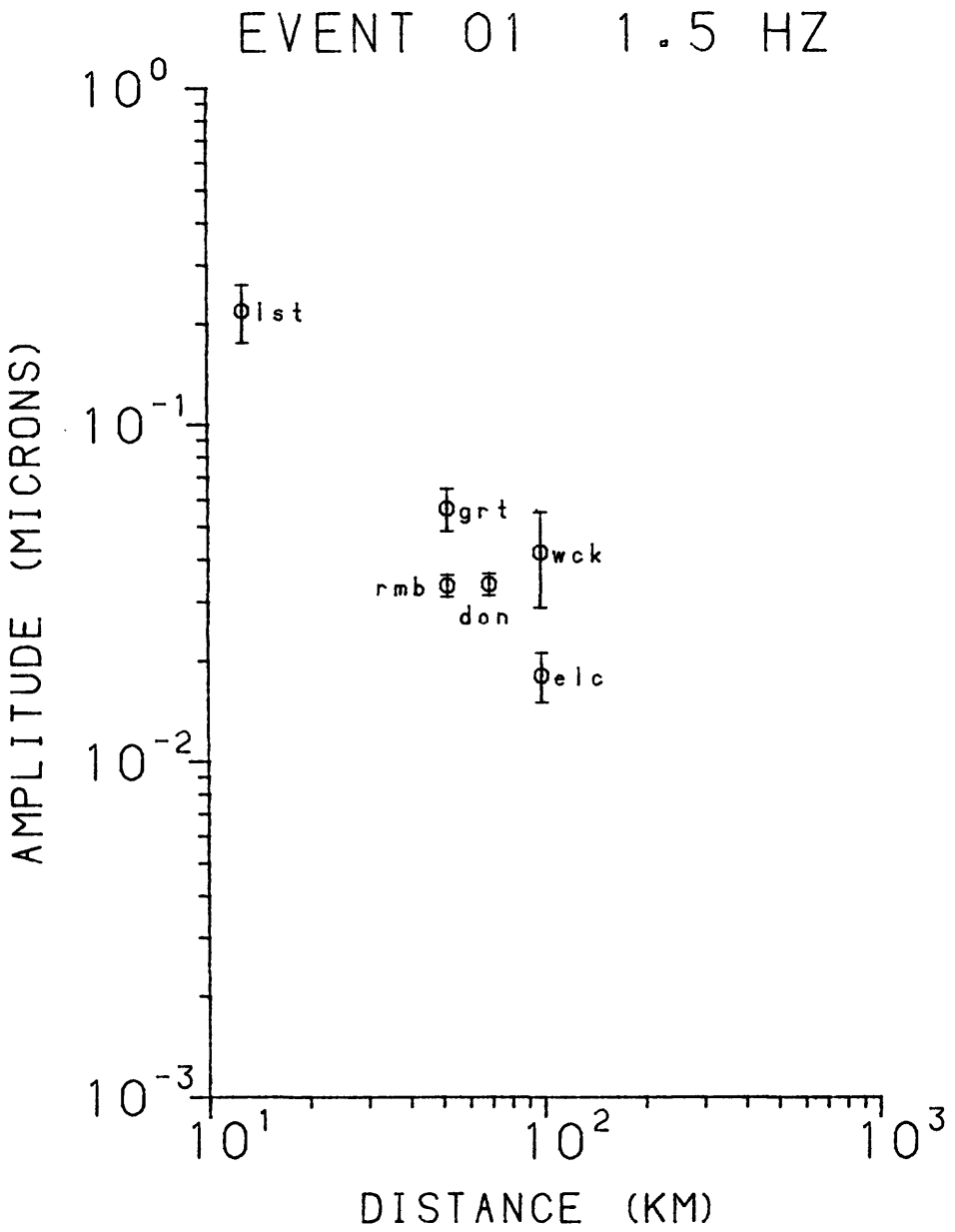

Figure 6. 1.5-Hz amplitudes of Lg-Z for Event No. 1.

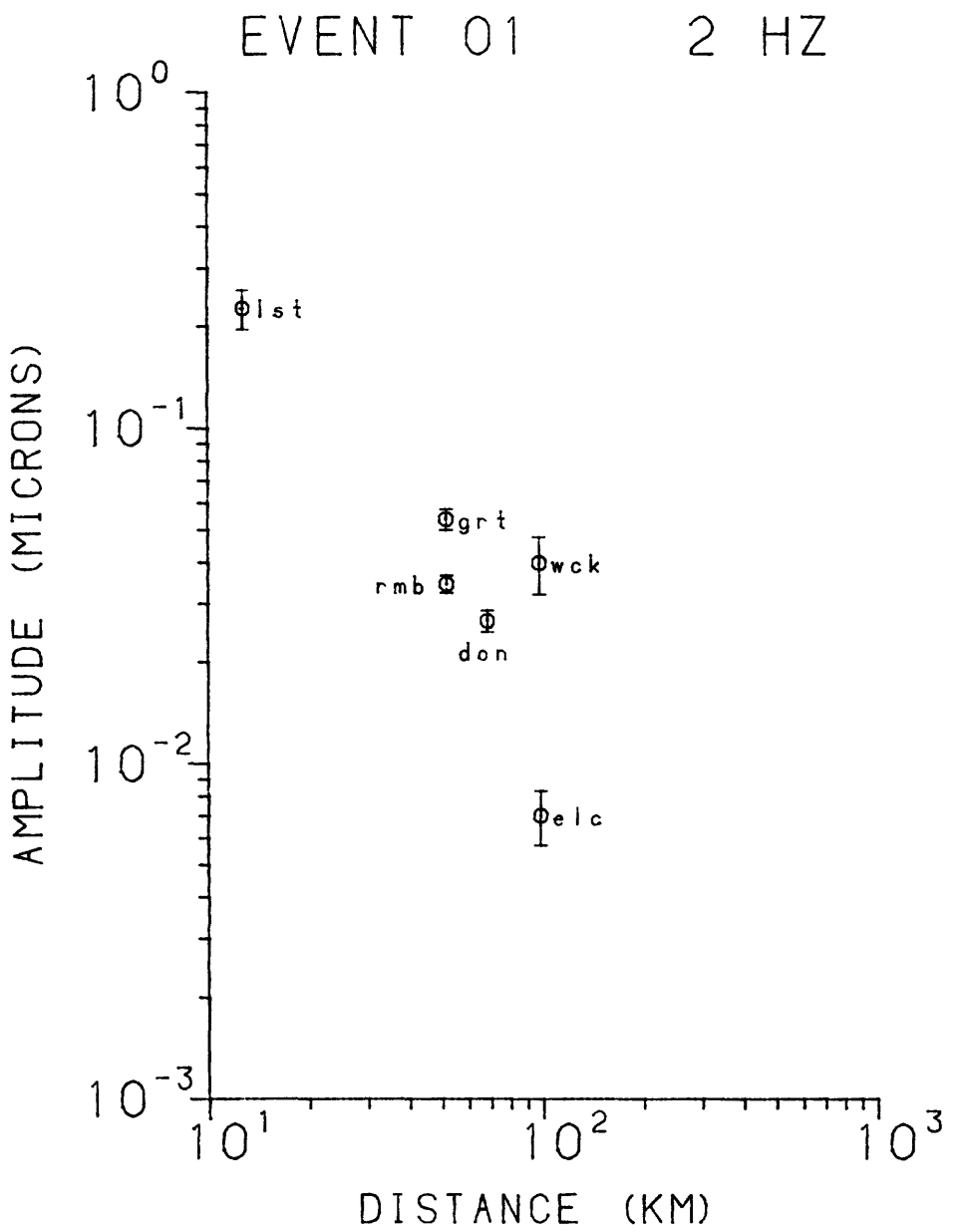

Figure 7. 2-Hz amplitudes of Lg-Z waves for Event No. 1.

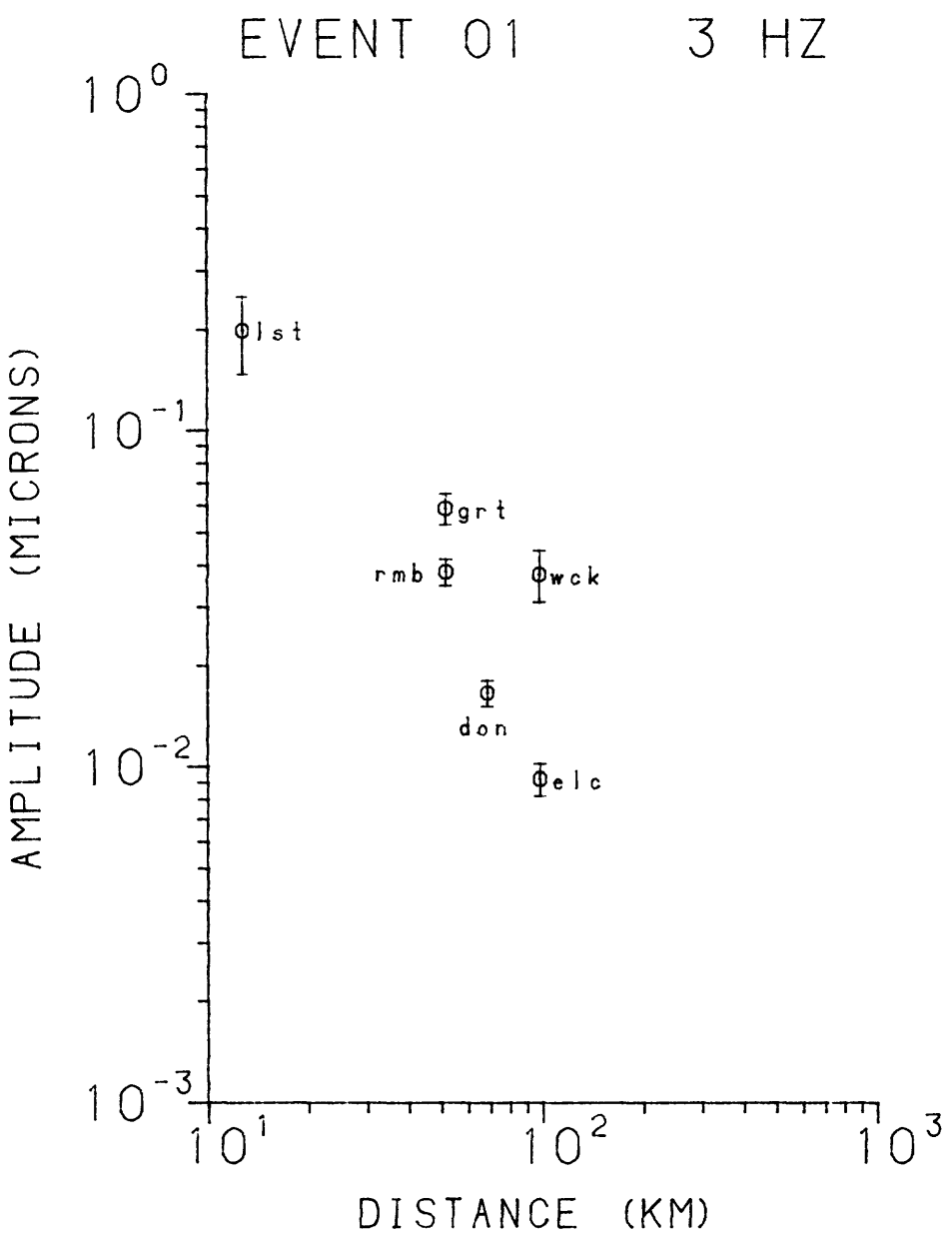

Figure 8. 3-Hz amplitudes of Lg-Z waves for Event No. 1.

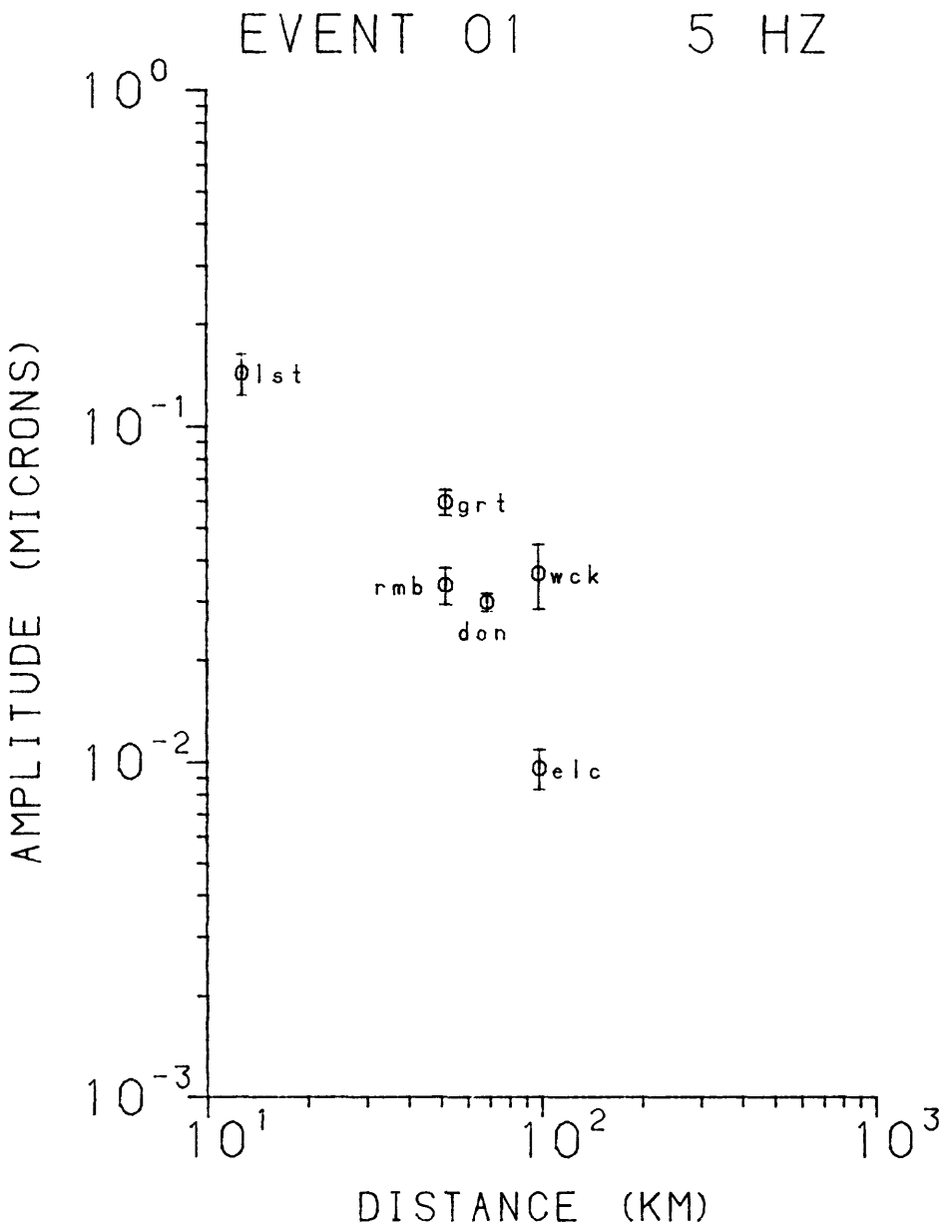

Figure 9. 5-Hz amplitudes of Lg-Z waves for Event No. 1.

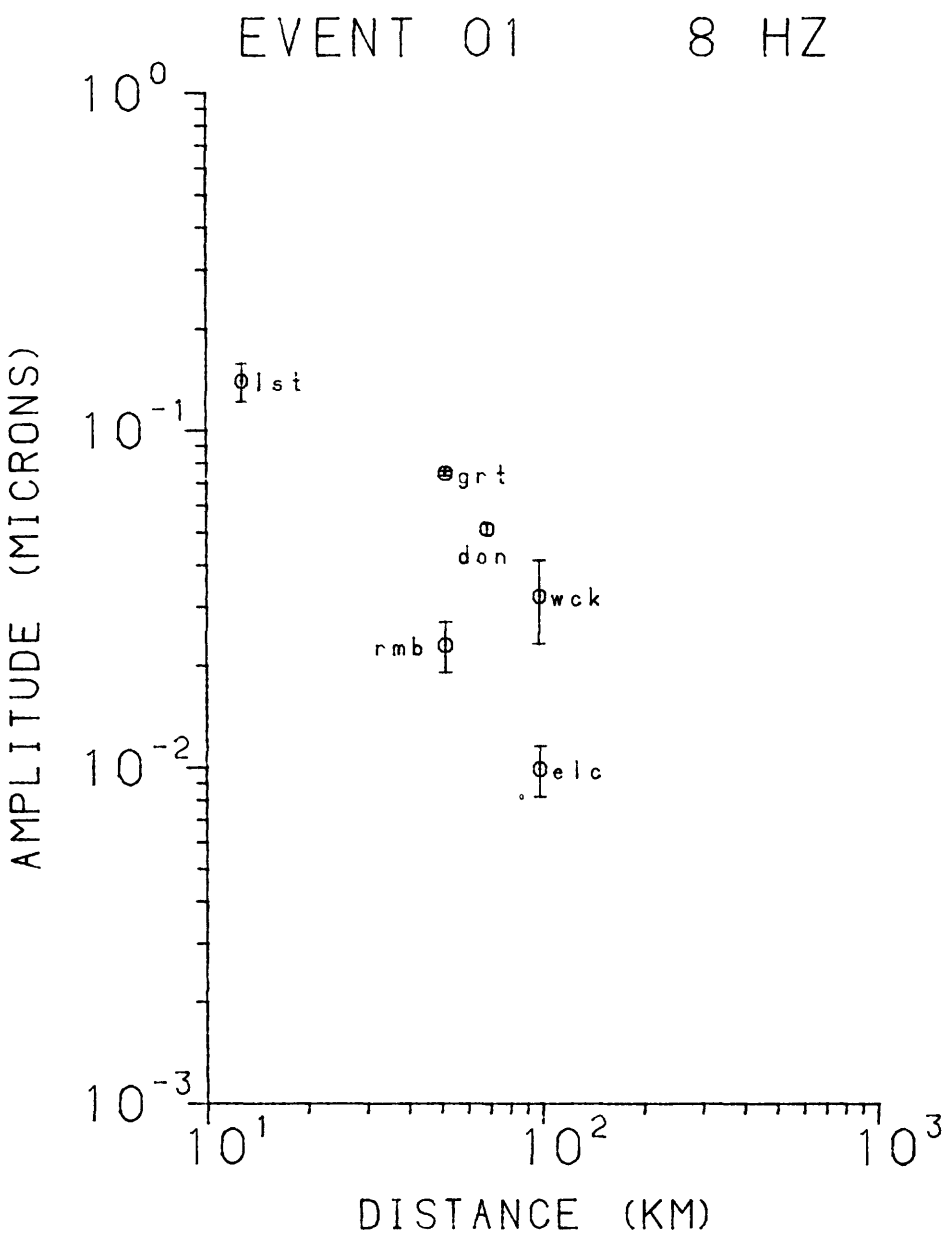

Figure 10. 8-Hz amplitudes of Lg-Z waves for Event No. 1.

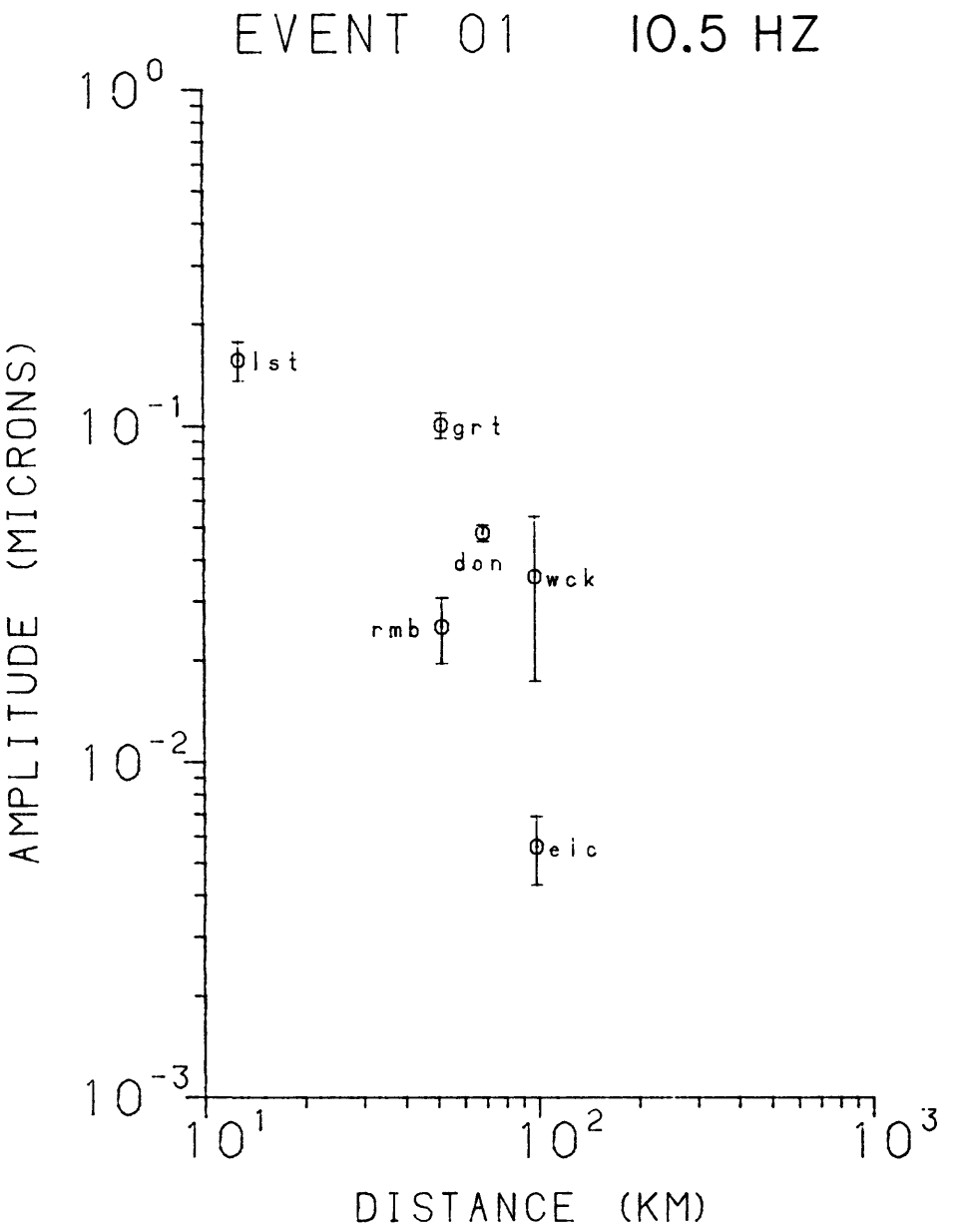

Figure 11. 10.5-Hz amplitudes of Lg-Z waves for Event No. 1.

Table 4

AMPLITUDE AND DISTANCE DATA FOR EVENT 18

4a) 1 -Hz Narrow Bandpass Data

Peak Magnification: 190

STA	DIST. (km)	RECORD AMPLITUDE (mm)	RECORD NOISE (mm)	GALVANOMETER GAIN	STATION GAIN	GROUND DISPLACEMENT (μ)	NOISE (μ)	AZIMUTH
TYS	230.3	4.3	1.0	8.9	32	.0040	.0009	327
DWM	30.5	6.0	1.1	8.9	8	.0222	.0041	277
ELC	57.2	23.3	1.0	8.9	128	.0054	.0002	353
WCK	30.4	31.9	2.2	8.9	32	.0295	.0020	54
CRU	22.9	21.2	1.3	3.8	32	.0459	.0028	149
LST	58.9	12.9	3.1	8.9	16	.0238	.0057	242
RMB	101.4	22.1	1.1	8.9	64	.0102	.0005	277
DON	82.8	19.1	1.2	8.9	128	.0044	.0003	303
PGA	153.8	10.2	1.7	8.9	16	.0188	.0031	239
POW	194.9	13.2	1.4	8.9	128	.0030	.0003	249

TABLE 4

(continued)

4b) 1.5-Hz Narrow Bandpass Data

Peak Magnification: 250

STA	DIST. (km)	RECORD AMPLITUDE (mm)	RECORD NOISE (mm)	GALVANOMETER GAIN	STATION GAIN	GROUND DISPLACEMENT (μ)	NOISE (μ)	AZIMUTH
TYS	230.3	7.8	1.3	13.7	32	.0356	.0059	327
DWM	30.5	10.8	1.9	13.7	8	.1971	.0347	277
ELC	57.2	19.2	1.1	8.9	128	.0337	.0019	353
WCK	30.4	40.8	1.8	8.9	32	.2865	.0126	54
CRU	22.9	17.9	2.1	3.8	32	.2944	.0345	149
LST	58.9	10.1	2.2	8.9	16	.1418	.0309	242
RMB	101.4	15.8	1.0	8.9	64	.0555	.0035	277
DON	21.6	17.2	1.0	8.9	128	.0302	.0018	303
POW	194.9	40.1	2.7	13.7	128	.0457	.0031	249

TABLE 4

(continued)

4c) 2-Hz Narrow Bandpass Data

Peak Magnification: 490

STA	DIST. (km)	RECORD AMPLITUDE (mm)	RECORD NOISE (mm)	GALVANOMETER GAIN	STATION GAIN	GROUND DISPLACEMENT (μ)	NOISE (μ)	AZIMUTH
TYS	230.3	9.0	1.3	8.9	32	.0032	.0004	327
DWM	30.5	11.8	2.1	8.9	8	.0169	.0030	277
ELC	57.2	29.5	1.0	8.9	128	.0026	.0001	353
WCK	30.4	39.4	1.3	8.9	32	.0141	.0009	54
CRU	22.9	26.8	2.7	3.8	32	.0225	.0023	149
LST	58.9	14.3	1.9	8.9	16	.0102	.0013	242
RMB	101.4	10.9	.8	3.8	64	.0046	.0003	277
DON	82.8	11.2	.9	8.9	128	.0010	.0001	303
PGA	153.8	22.2	2.9	8.9	16	.0159	.0021	239
POW	194.9	29.2	2.5	8.9	128	.0026	.0002	249

TABLE 4

(continued)

4d) 3 -Hz Narrow Bandpass Data

Peak Magnification: 850

STA	DIST. (km)	RECORD AMPLITUDE (mm)	RECORD NOISE (mm)	GALVANOMETER GAIN	STATION GAIN	GROUND DISPLACEMENT (μ)	NOISE (μ)	AZIMUTH
TYS	230.3	26.7	2.3	8.9	32	.0055	.0005	327
DWM	30.5	21.1	4.7	8.9	8	.0174	.0039	277
ELC	57.2	14.1	.9	2	128	.0032	.0002	353
WCK	30.4	11.1	.7	1	32	.0204	.0013	54
CRU	22.9	12.8	1.4	1	32	.0235	.0026	149
LST	58.9	13.3	1.2	3.8	16	.0129	.0012	242
RMB	101.4	25.1	1.3	3.8	64	.0061	.0003	277
DON	82.8	14.9	.8	2	128	.0034	.0002	303
PGA	153.8	11.2	1.2	2	16	.0206	.0022	239
POW	194.9	21.4	2.0	3.8	128	.0026	.0002	249

TABLE 4

(continued)

4e) 5-Hz Narrow Bandpass Data

Peak Magnification: 1240

STA	DIST. (km)	RECORD AMPLITUDE (mm)	RECORD NOISE (mm)	GALVANOMETER GAIN	STATION GAIN	GROUND DISPLACEMENT (μ)	NOISE (μ)	AZIMUTH
TYS	230.3	24.1	2.3	8.9	32	.0034	.0003	327
DWM	30.5	23.2	2.9	8.9	8	.0131	.0006	277
ELC	57.2	20.2	1.1	2	128	.0032	.0002	353
WCK	30.4	11.6	1.0	1	32	.0146	.0013	54
CRU	22.9	15.8	1.0	1	32	.0199	.0013	149
LST	58.9	15.3	1.6	3.8	16	.0102	.0011	242
RMB	101.4	35.2	1.5	3.8	64	.0058	.0002	277
DON	82.8	20.8	.8	1	128	.0066	.0002	303
PGA	153.8	13.9	2.7	2	16	.0175	.0034	239
POW	194.9	23.8	2.4	2	128	.0037	.0004	249

TABLE 4

(continued)

4f) 8-Hz Narrow Bandpass Data

Peak Magnification: 2050

STA	DIST. (km)	RECORD AMPLITUDE (mm)	RECORD NOISE (mm)	GALVANOMETER GAIN	STATION GAIN	GROUND DISPLACEMENT (μ)	NOISE (μ)	AZIMUTH
TYS	230.3	13.5	1.8	8.9	32	.0012	.0002	327
DWM	30.5	22.3	1.3	8.9	8	.0076	.0004	277
ELC	57.2	21.6	.8	2	128	.0020	.0001	353
WCK	30.4	12.0	.6	1	32	.0091	.0004	54
CRU	22.9	27.7	.8	1	32	.0211	.0006	149
LST	58.9	13.8	1.3	3.8	16	.0055	.0005	242
RMB	101.4	33.3	1.1	3.8	64	.0033	.0001	277
DON	82.8	35.0	.9	1	128	.0067	.0002	303
PGA	153.8	12.3	3.2	2	16	.0094	.0024	239
POW	194.9	30.2	3.7	2	128	.0029	.0004	249

TABLE 4

(continued)

4g) 12.5-Hz Narrow Bandpass Data

Peak Magnification: 1300

STA	DIST. (km)	RECORD AMPLITUDE (mm)	RECORD NOISE (mm)	GALVANOMETER GAIN	STATION GAIN	GROUND DISPLACEMENT (μ)	NOISE (μ)	AZIMUTH
TYS	230.3	10.8	2.7	8.9	32	.0146	.0036	327
DWM	30.5	23.3	3.7	8.9	8	.1259	.0200	277
ELC	57.2	18.2	1.1	2	128	.0273	.0016	353
WCK	30.4	14.8	1.2	2	32	.0889	.0072	54
CRU	22.9	43.3	1.5	2	32	.2602	.0090	149
LST	58.9	31.1	2.4	8.9	16	.0840	.0065	242
RMB	101.4	26.1	1.5	3.8	64	.0413	.0024	277
DON	82.8	21.6	1.1	1	128	.0649	.0033	303
POW	194.9	19.8	4.4	2	128	.0297	.0066	249

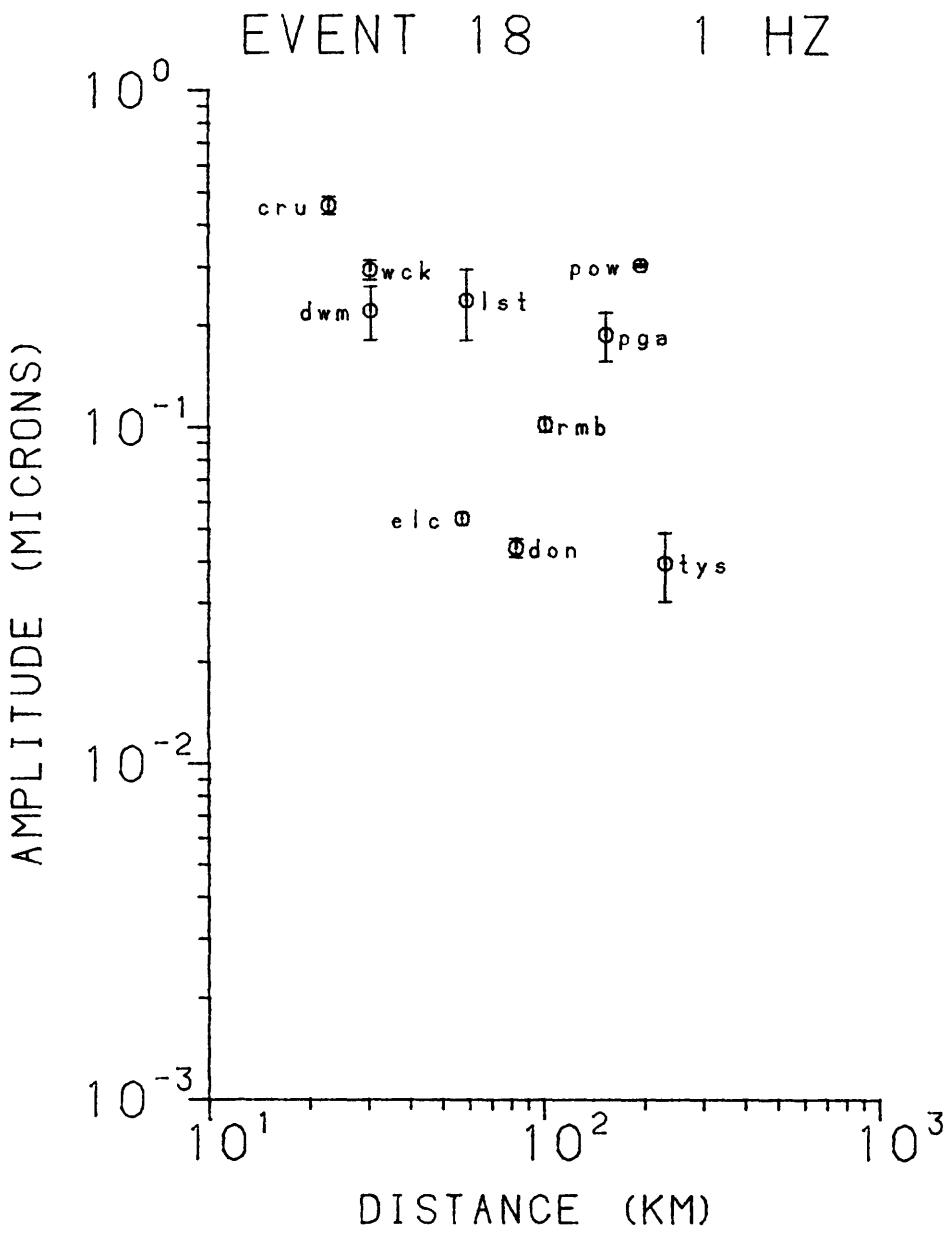

Figure 12. 1-Hz amplitudes of Lg-Z waves for Event No. 18.

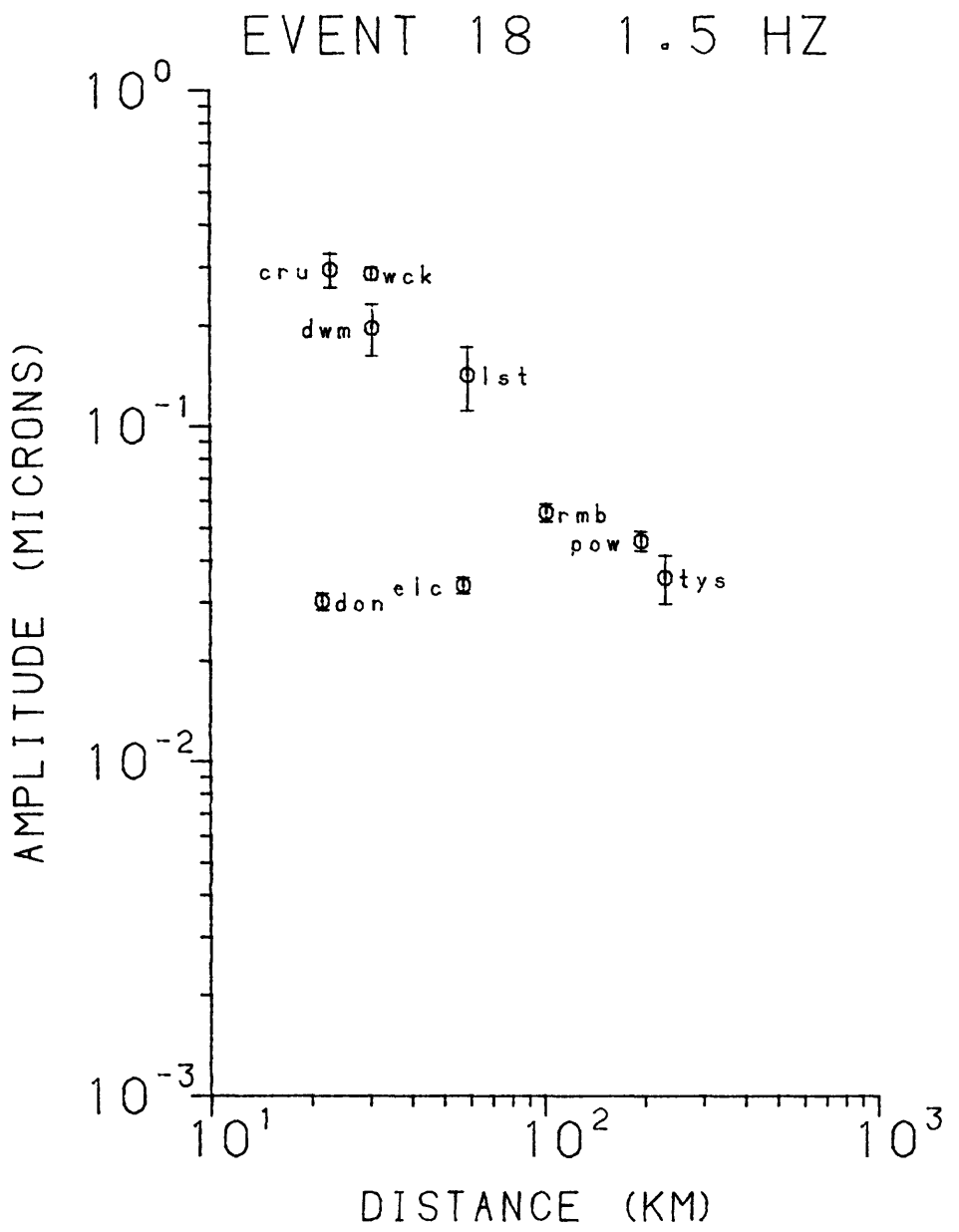

Figure 13. 1.5-Hz amplitudes of Lg-Z waves for Event No. 18.

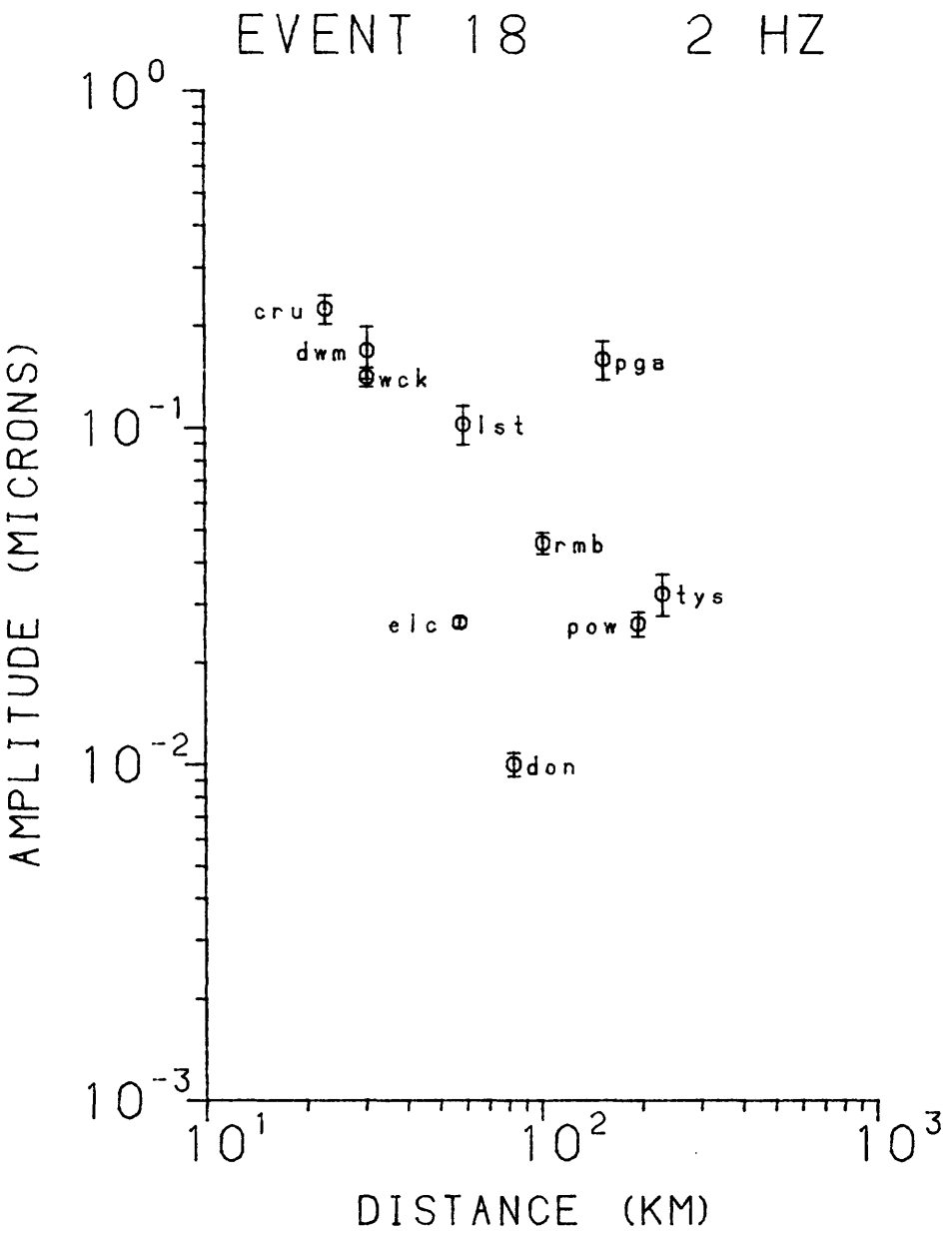

Figure 14. 2-Hz amplitudes of Lg-Z waves for Event No. 18.

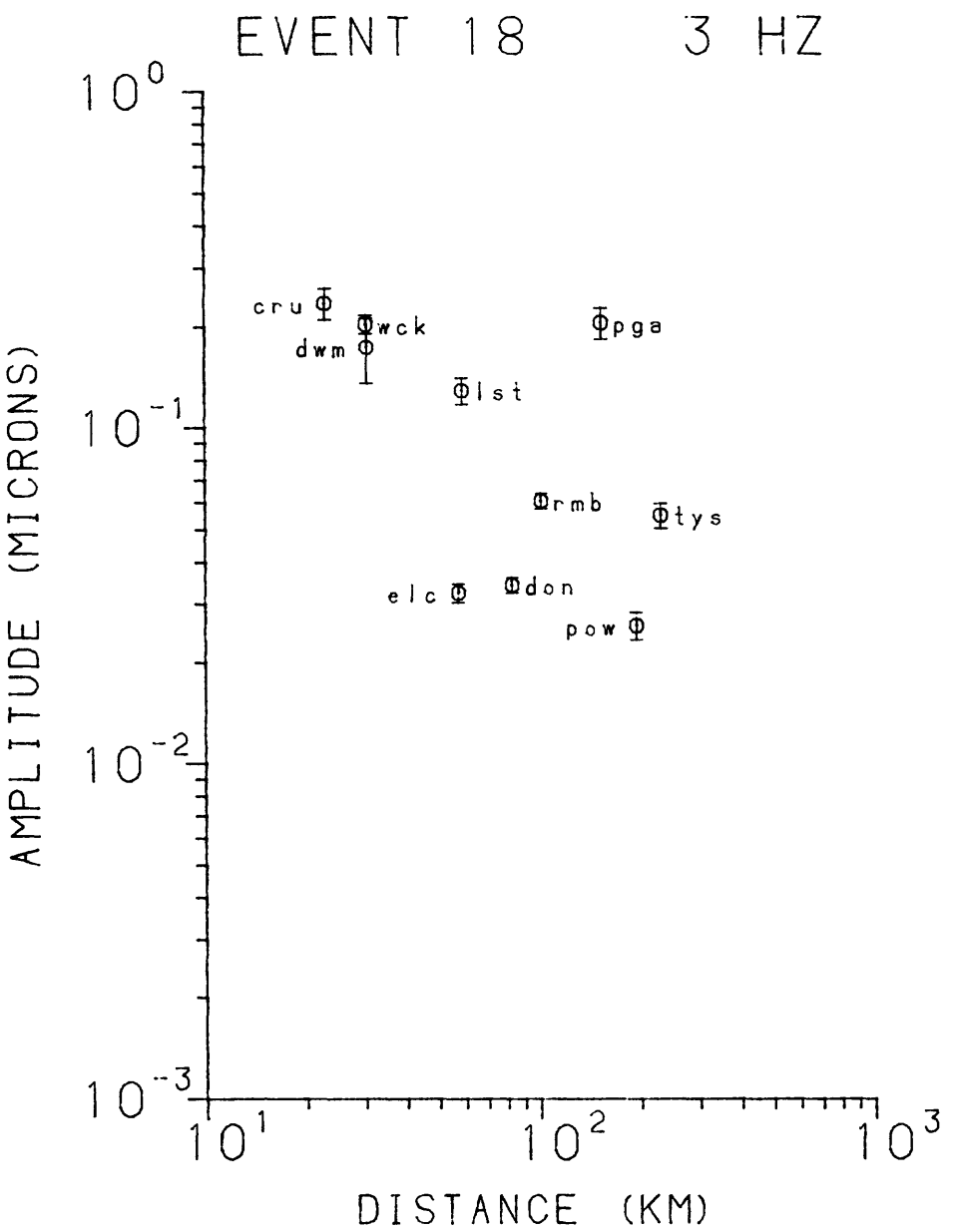

Figure 15. 3-Hz amplitudes of Lg-Z waves for Event No. 18.

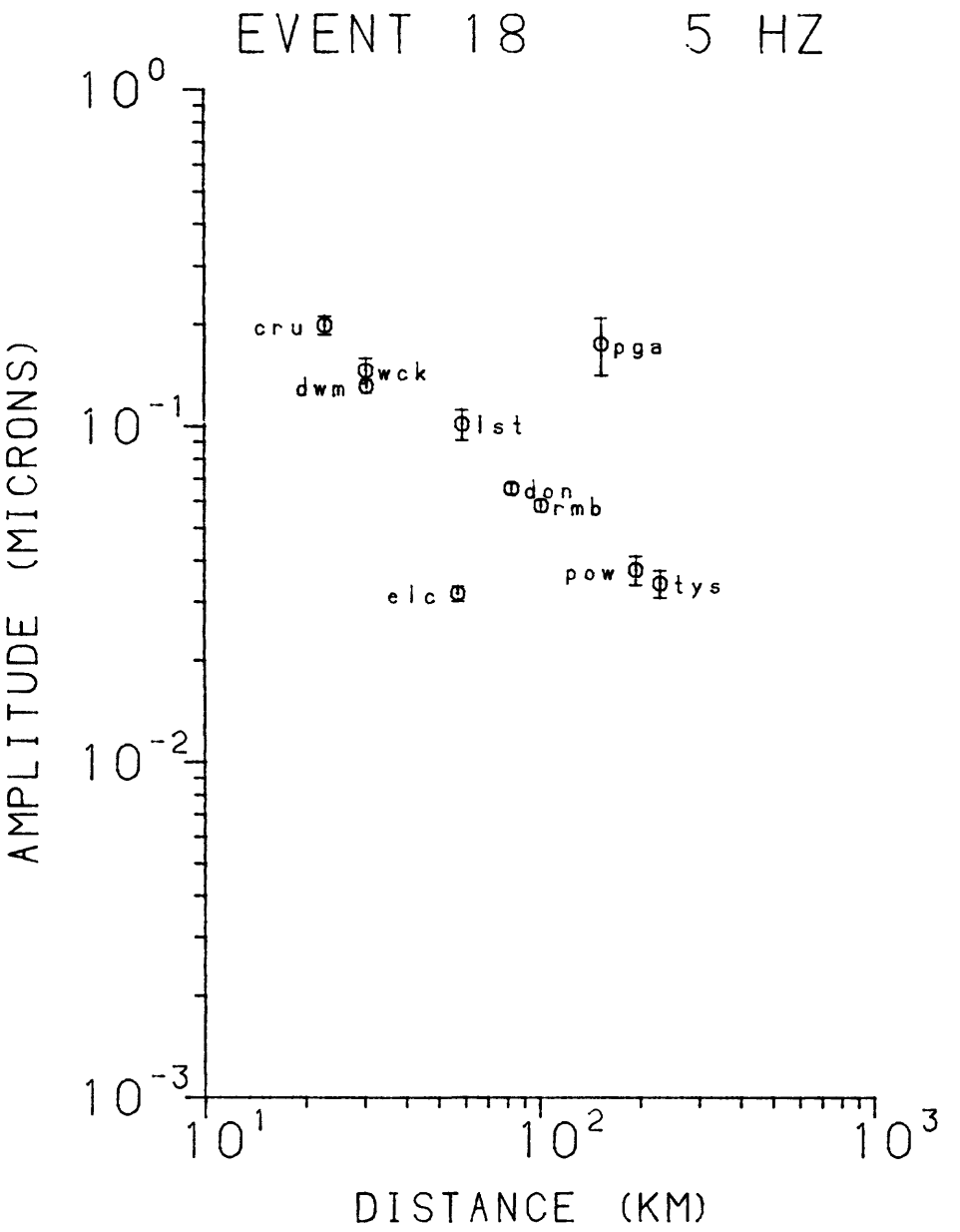

Figure 16. 5-Hz amplitudes of Lg-Z waves for Event No. 18.

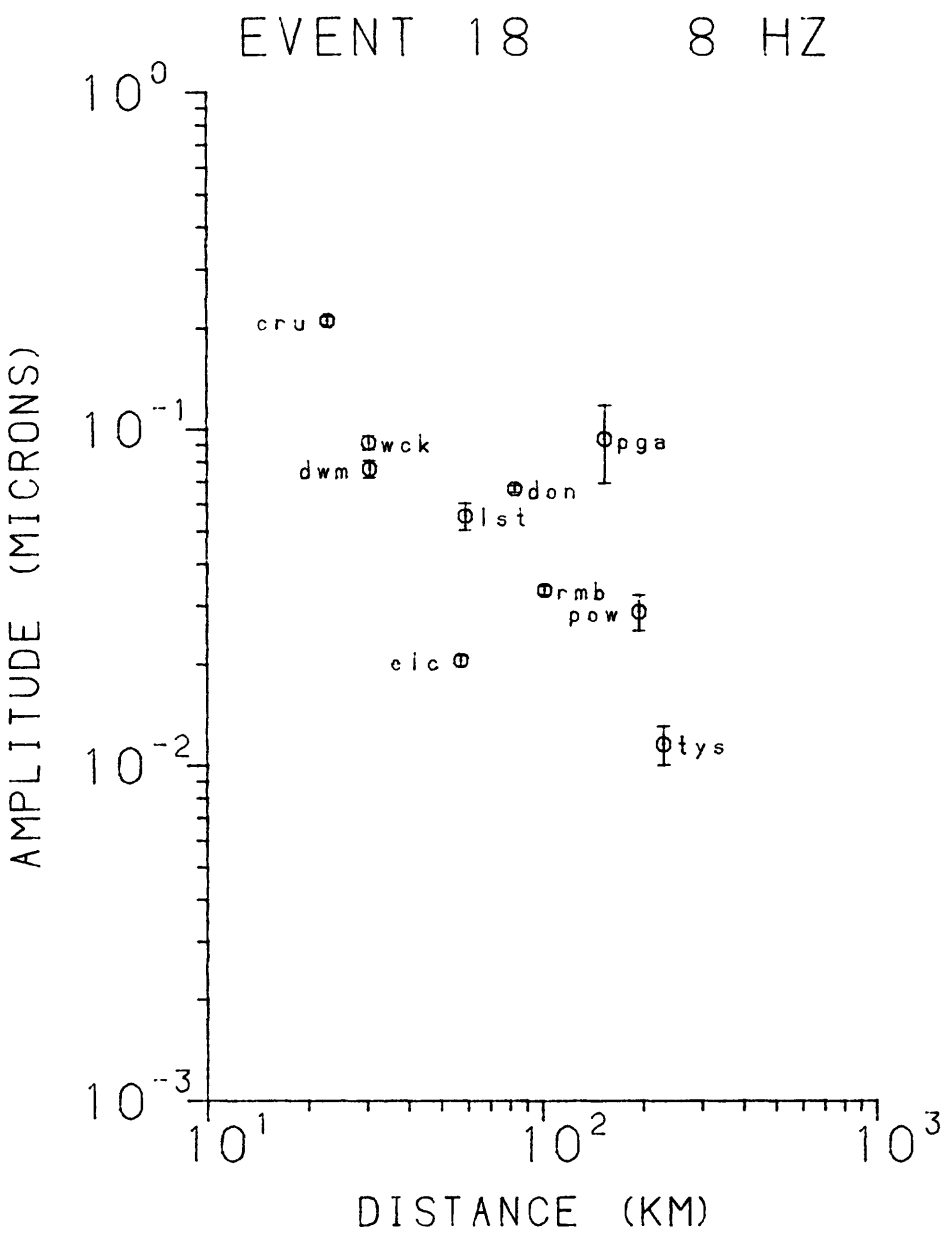

Figure 17. 8-Hz amplitudes of Lg-Z waves for Event No. 18.

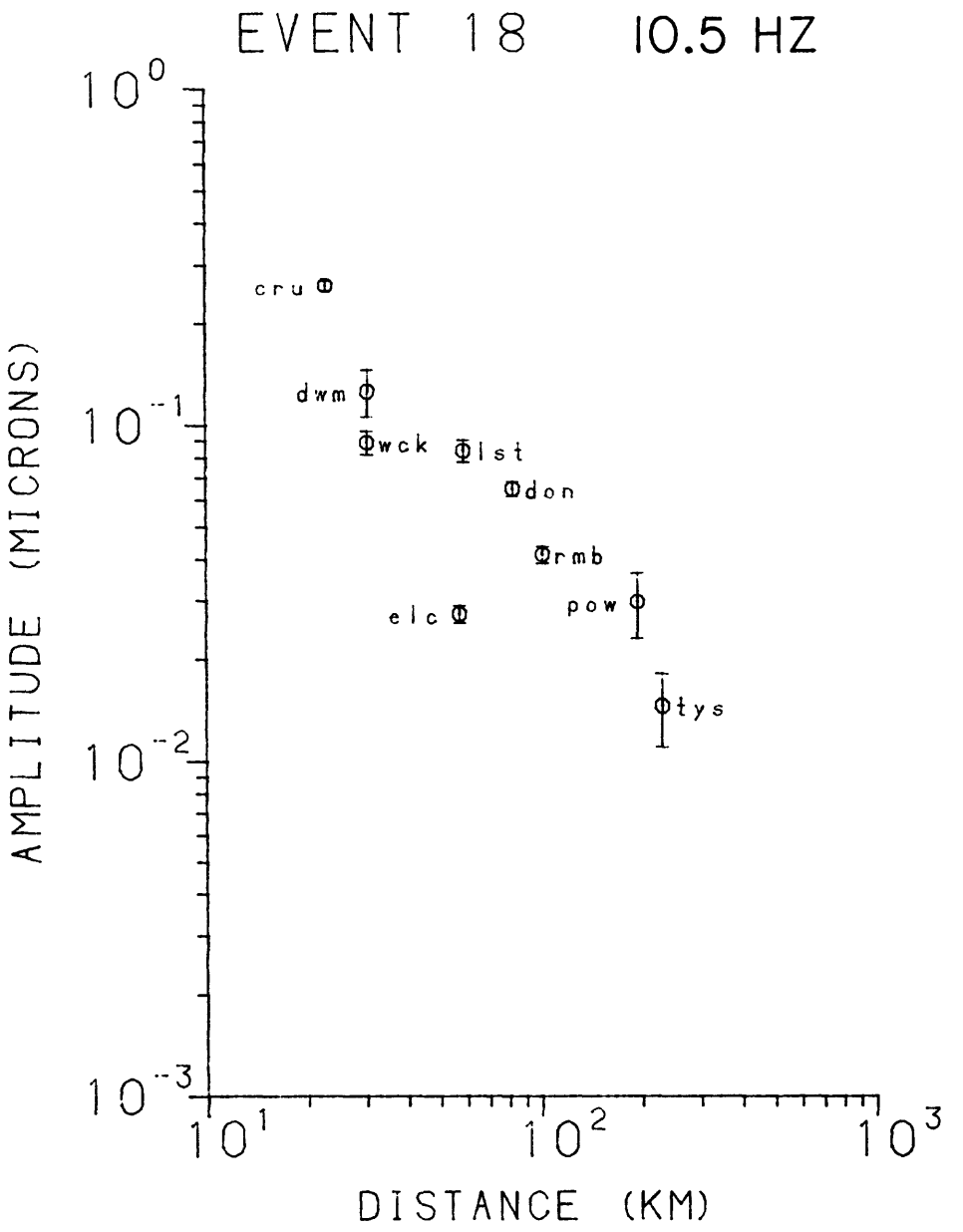

Figure 18. 10.5-Hz amplitudes of Lg-Z waves for Event No. 18.

TABLE 5

AMPLITUDE AND DISTANCE DATA FOR EVENT 25

5a) 1-Hz Narrow Bandpass Data

Peak Magnification: 166

STA	DIST. (km)	RECORD AMPLITUDE (mm)	RECORD NOISE (mm)	GALVANOMETER GAIN	STATION GAIN	GROUND DISPLACEMENT (μ)	NOISE (μ)	AZIMUTH
ELC	87.9	4.1	1.2	8.9	128	**.0108**	**.0032**	22
WCK	77.5	6.9	2.2	8.9	64	**.0365**	**.0116**	57
GRT	35.5	5.4	1.8	8.9	32	**.0571**	**.0190**	154
LST	12.3	6.5	1.2	8.9	16	**.1370**	**.0254**	255
RMB	71.2	8.8	1.0	8.9	64	**.0465**	**.0053**	301
DON	75.5	2.5	.9	8.9	64	**.0132**	**.0048**	337

TABLE 5

(continued)

5b) 1.5-Hz Narrow Bandpass Data

Peak Magnification: 250

STA	DIST. (km)	RECORD AMPLITUDE (mm)	RECORD NOISE (mm)	GALVANOMETER GAIN	STATION GAIN	GROUND DISPLACEMENT (μ)	NOISE (μ)	AZIMUTH
ELC	87.9	9.4	1.9	13.7	128	.0107	.0022	22
GRT	34.9	13.8	3.3	13.7	32	.0630	.0150	154
LST	12.3	14.7	3.2	13.7	16	.1341	.0292	255
RMB	71.2	15.3	1.3	8.9	64	.0537	.0046	301
DON	75.5	8.2	1.5	13.7	64	.0187	.0034	337
NKT	77.9	6.0	1.9	13.7	16	.0547	.0173	177

TABLE 5

(continued)

5c) 2.0 -Hz Narrow Bandpass Data

Peak Magnification: 410

STA	DIST. (km)	RECORD AMPLITUDE (mm)	RECORD NOISE (mm)	GALVANOMETER GAIN	STATION GAIN	GROUND DISPLACEMENT (μ)	NOISE (μ)	AZIMUTH
ELC	87.9	11.0	1.5	8.9	128	.0118	.0016	22
GRT	35.5	11.3	2.2	8.9	32	.0484	.0094	154
LST	12.3	17.5	2.3	8.9	16	.1500	.0197	255
RMB	71.2	23.2	1.3	8.9	64	.0497	.0028	301
DON	75.5	5.9	1.1	8.9	64	.0126	.0024	337
NKT	77.9	17.8	2.8	8.9	16	.1520	.0240	177
POW	149.0	7.4	1.7	8.9	64	.0158	.0036	253

TABLE 5

(continued)

5d) 3.12-Hz Narrow Bandpass Data

Peak Magnification: 675

STA	DIST. (km)	RECORD AMPLITUDE (mm)	RECORD NOISE (mm)	GALVANOMETER GAIN	STATION GAIN	GROUND DISPLACEMENT (μ)	NOISE (μ)	AZIMUTH
ELC	87.9	27.0	2.1	8.9	128	.0176	.0014	22
GRT	35.5	12.1	.9	3.8	32	.0737	.0055	154
LST	12.3	16.0	1.5	3.8	16	.1950	.0183	255
RMB	71.2	14.9	1.0	3.8	64	.0454	.0030	301
DON	75.5	11.6	1.0	8.9	64	.0151	.0013	337
OKG	104.	9.8	2.2	3.8	32	.0597	.0134	168
NKT	77.9	15.7	4.0	8.9	16	.0817	.0208	177

TABLE 5

(continued)

5e) 5.0 -Hz Narrow Bandpass Data

Peak Magnification: 1010

STA	DIST. (km)	RECORD AMPLITUDE (mm)	RECORD NOISE (mm)	GALVANOMETER GAIN	STATION GAIN	GROUND DISPLACEMENT (μ)	NOISE (μ)	AZIMUTH
ELC	87.9	16.1	1.2	3.8	128	.0164	.0012	22
WCK	77.5	12.1	2.7	3.8	64	.0246	.0055	57
CRU	52.0	27.8	4.2	8.9	32	.0483	.0073	85
GRT	35.5	16.5	1.3	3.8	32	.0672	.0053	154
LST	12.3	25.2	1.0	3.8	16	.2050	.0081	255
RMB	71.2	24.2	1.1	3.8	64	.0493	.0022	301
DON	75.5	19.4	1.1	3.8	64	.0394	.0022	337
OKG	104	18.6	1.7	3.8	32	.0757	.0069	168
NKT	77.9	31.8	5.5	8.9	16	.1100	.0191	177
POW	149.0	19.7	3.8	8.9	64	.0171	.0033	253

TABLE 5

(continued)

5f) 8.0-Hz Narrow Bandpass Data

Peak Magnification: 1625

STA	DIST. (km)	RECORD AMPLITUDE (mm)	RECORD NOISE (mm)	GALVANOMETER GAIN	STATION GAIN	GROUND DISPLACEMENT (μ)	NOISE (μ)	AZIMUTH
ELC	87.9	26.1	1.1	3.8	128	.0165	.0007	22
WCK	77.5	24.9	1.8	3.8	64	.0315	.0023	57
CRU	52.0	24.5	1.3	3.8	32	.0620	.0033	85
GRT	35.5	16.8	.9	2	32	.0808	.0043	154
LST	12.3	19.2	1.0	2	16	.1850	.0096	255
RMB	71.2	14.8	.8	2	64	.0356	.0019	301
DON	75.5	27.0	.7	2	64	.0649	.0017	337
OKG	104.	14.7	.9	2	32	.0707	.0043	168
NKT	77.9	44.9	10.0	8.9	16	.0974	.0216	177
POW	149.0	17.4	3.6	3.8	64	.0220	.0046	253

TABLE 5

(continued)

5g) 12.5-Hz Narrow Bandpass Data

Peak Magnification: 1300

STA	DIST. (km)	RECORD AMPLITUDE (mm)	RECORD NOISE (mm)	GALVANOMETER GAIN	STATION GAIN	GROUND DISPLACEMENT (μ)	NOISE (μ)	AZIMUTH
ELC	87.9	30.8	1.7	3.8	128	.0244	.0013	22
WCK	77.5	21.1	2.2	3.8	64	.0334	.0035	57
CRU	52.0	29.8	1.7	3.8	32	.0943	.0054	85
GRT	35.5	34.9	1.8	3.8	32	.1104	.0057	154
LST	12.3	33.4	1.7	3.8	16	.2113	.0108	255
RMB	71.2	24.8	1.8	3.8	64	.0392	.0028	301
DON	75.5	35.9	1.8	3.8	64	.0568	.0028	337
OKG	104.	30.4	1.6	3.8	32	.0962	.0051	192
NKT	77.9	16.1	5.8	3.8	16	.1018	.0367	177
POW	149.0	16.9	5.1	3.8	64	.0267	.0081	253

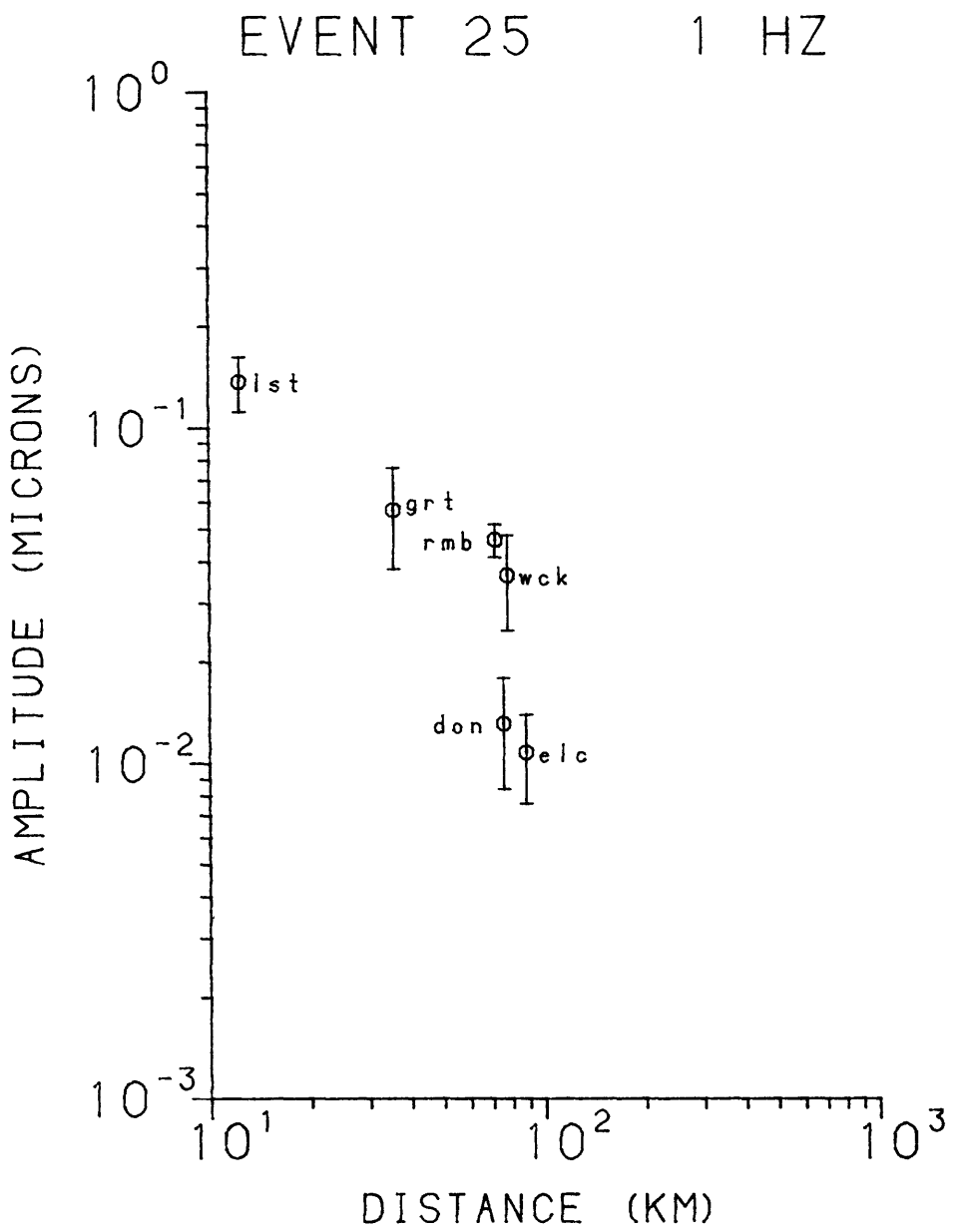

Figure 19. 1-Hz amplitudes of Lg-Z waves for Event No. 25.

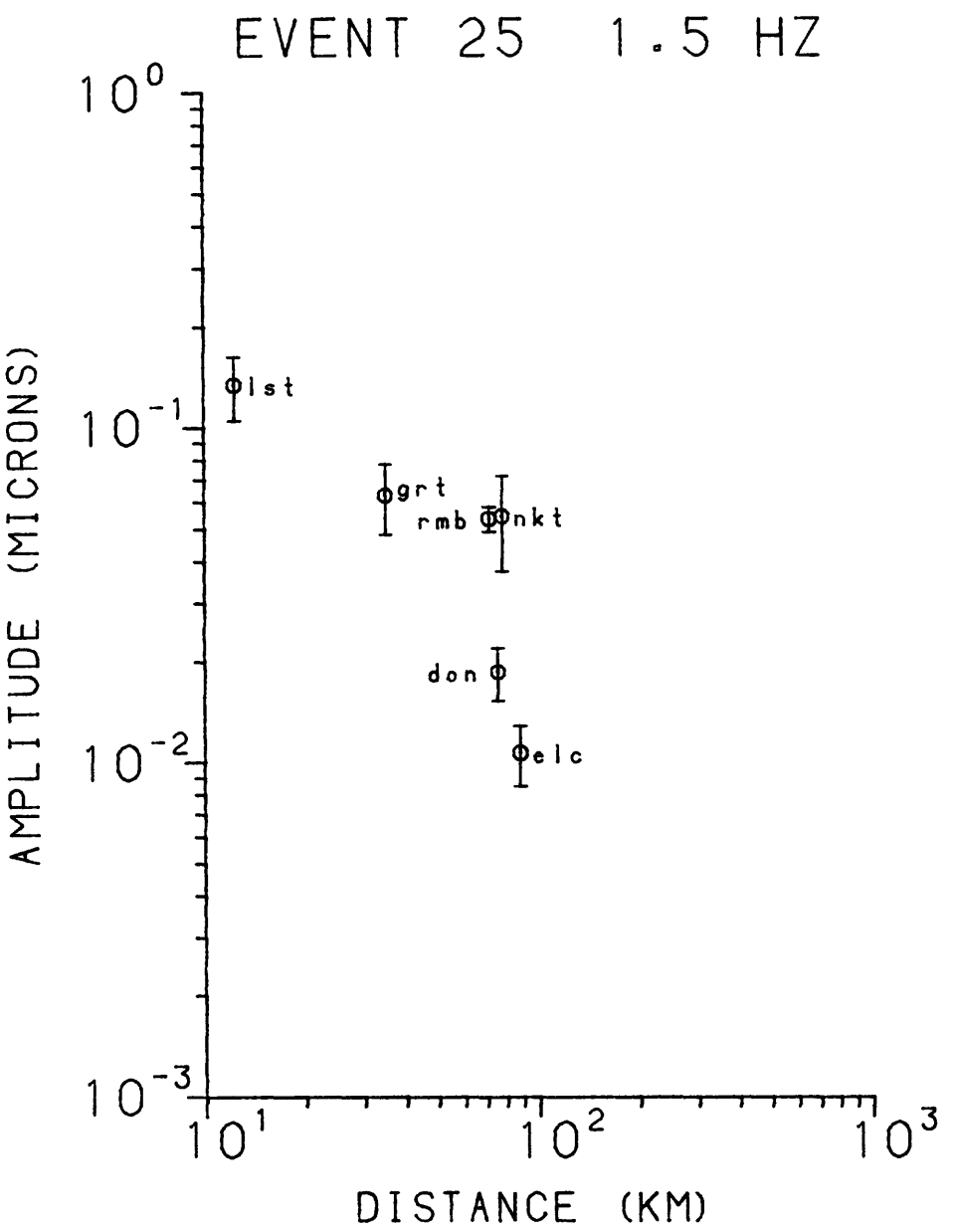

Figure 20. 1.5-Hz amplitudes of Lg-Z waves for Event No. 25.

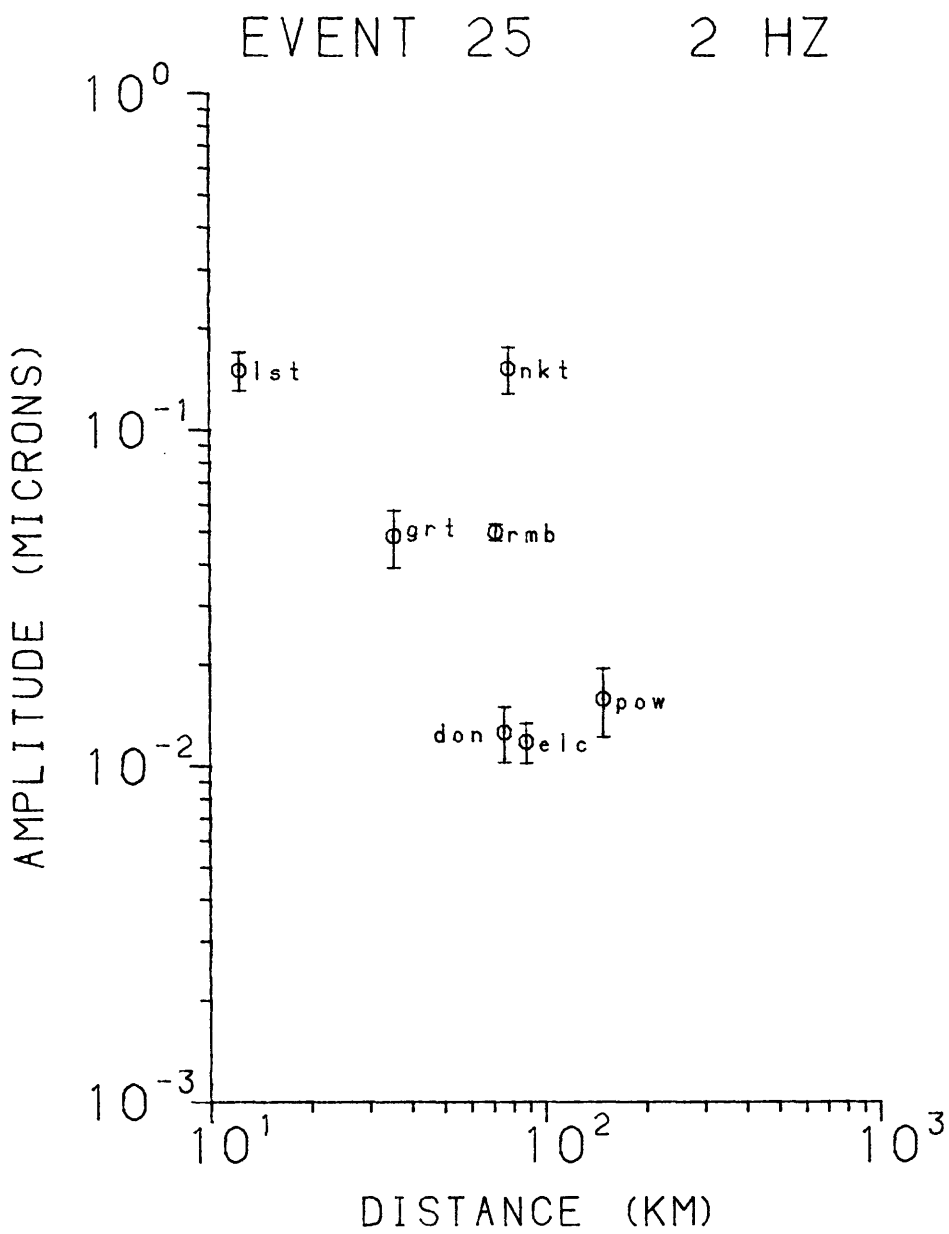

Figure 21. 2-Hz amplitudes of Lg-Z waves for Event No. 25.

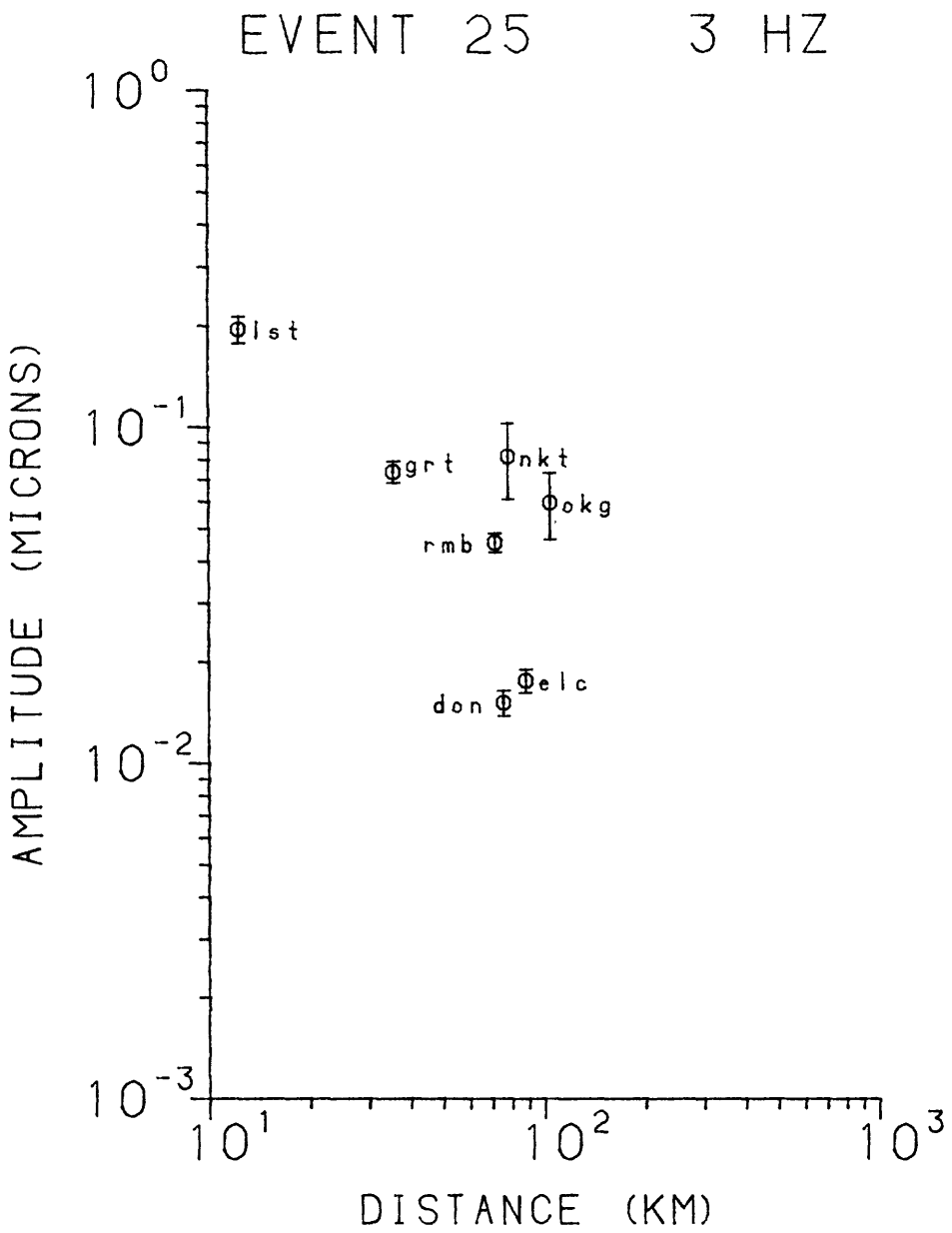

Figure 22. 3-Hz amplitudes of Lg-Z waves for Event No. 25.

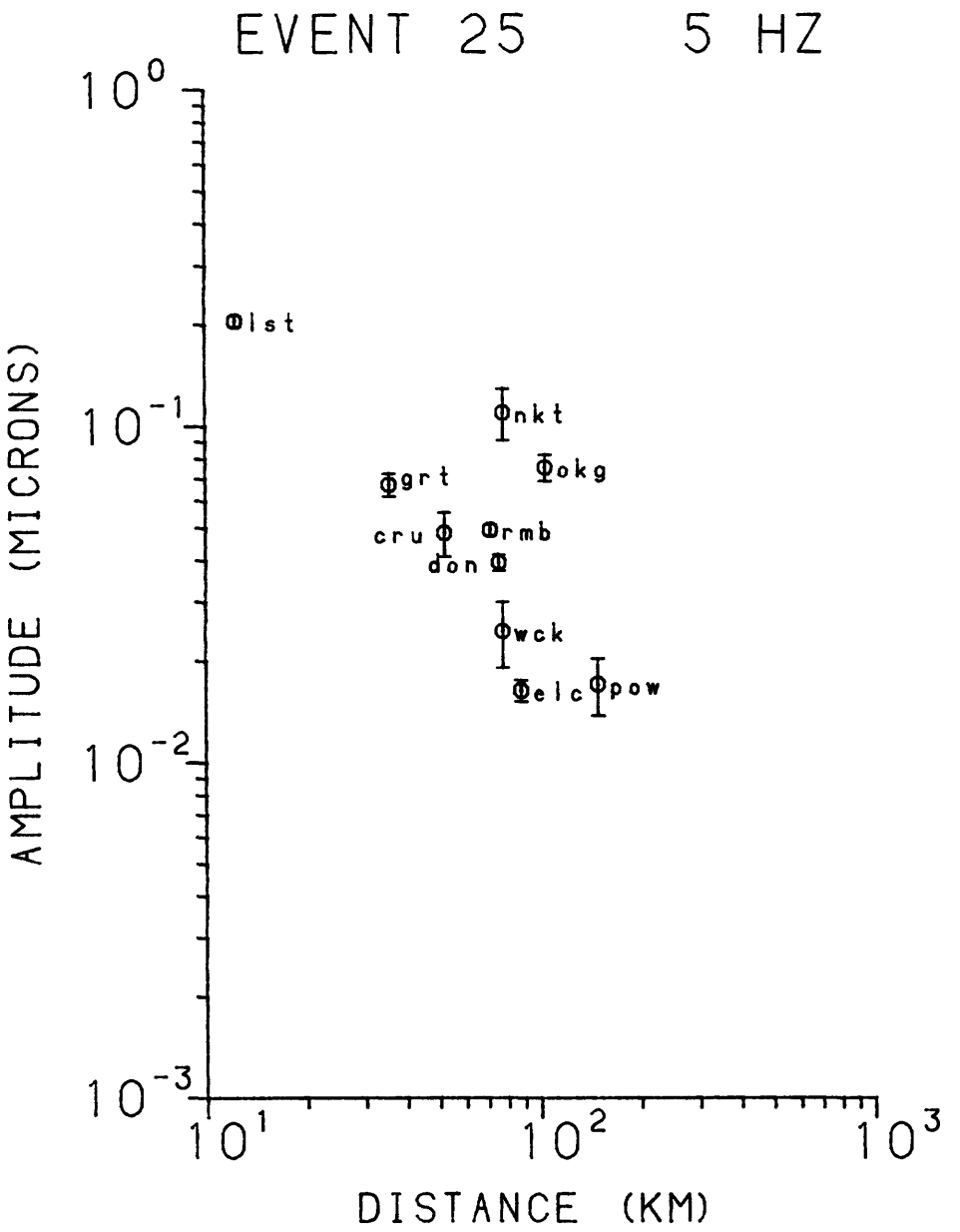

Figure 23. 5-Hz amplitudes of Lg-Z waves for Event No. 25.

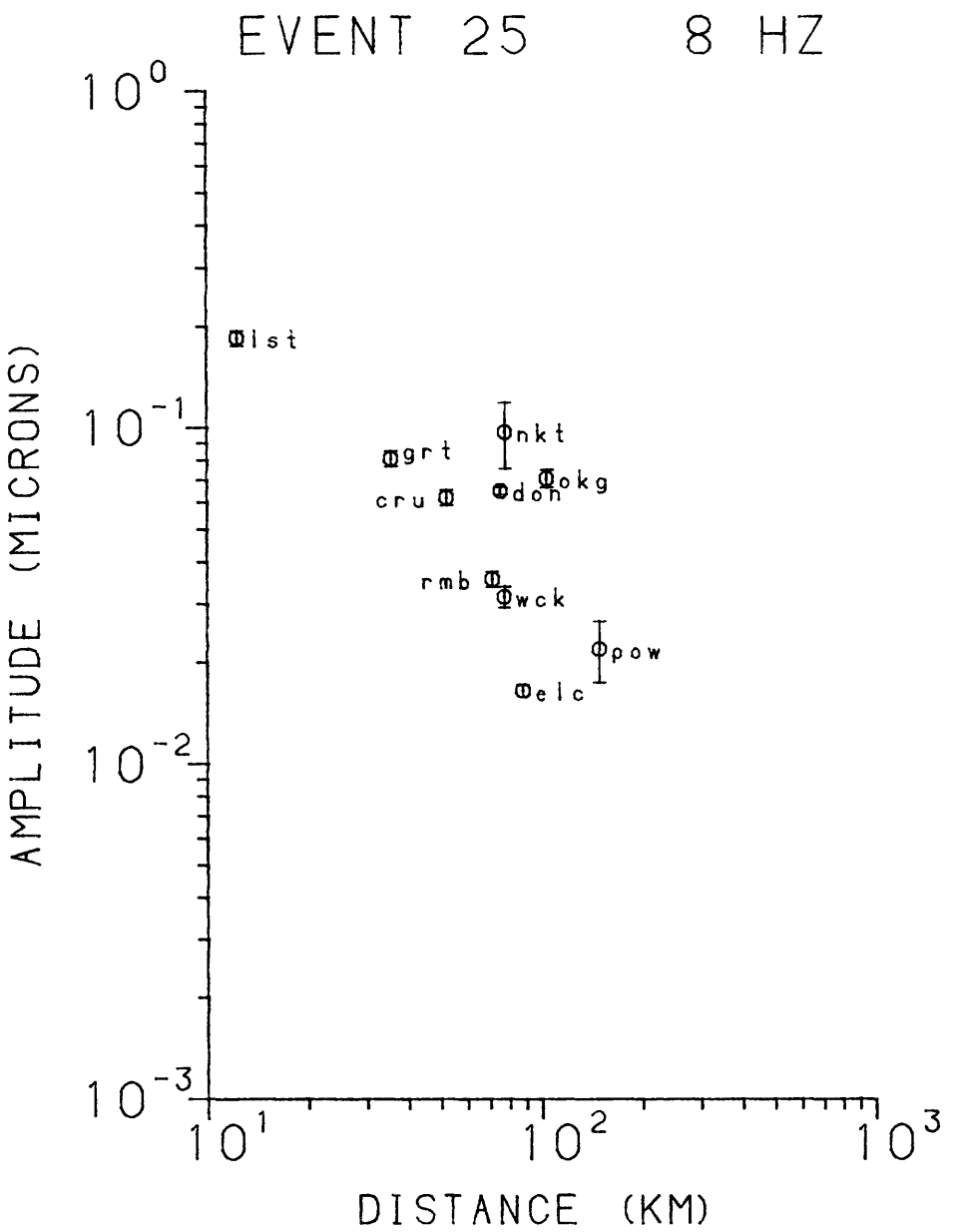

Figure 24. 8-Hz amplitudes of Lg-Z waves for Event No. 25.

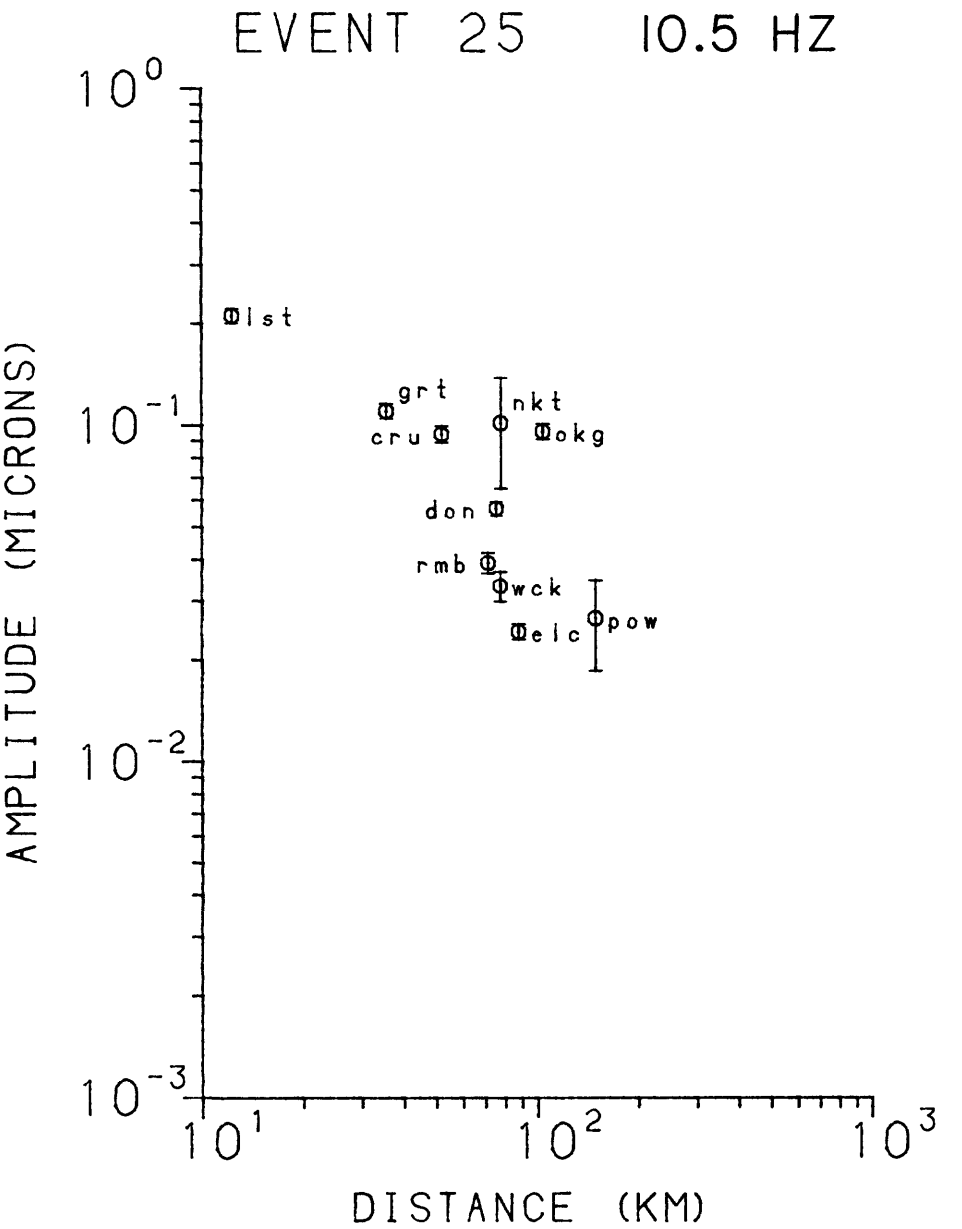

Figure 25. 10.5-Hz amplitudes of Lg-Z waves for Event No. 25.

TABLE 6

AMPLITUDE AND DISTANCE DATA FOR EVENT 31

6a) 1 -Hz Narrow Bandpass Data

Peak Magnification: 195

STA	DIST. (km)	RECORD AMPLITUDE (mm)	RECORD NOISE (mm)	GALVANOMETER GAIN	STATION GAIN	GROUND DISPLACEMENT (μ)	NOISE (μ)	AZIMUTH
TYS	514.4	3.2	.7	8.9	32	.0288	.0081	347
DWM	311.1	4.4	1.0	8.9	8	.1585	.0360	356
LST	282.6	9.6	1.7	8.9	16	.1729	.0306	351
DON	357.2	9.9	1.6	8.9	64	.0446	.0072	350
OKG	187.9	14.9	1.6	8.9	32	.1342	.0144	343
PGA	260.8	11.2	.9	8.9	16	.2017	.0162	331
ECD	236.7	11.8	1.2	8.9	16	.2125	.0216	344
NKT	206.2	19.9	1.4	8.9	16	.3583	.0252	352
POW	297.2	8.7	1.0	8.9	64	.0392	.0045	324

TABLE 6

(continued)

6b) 1.5-Hz Narrow Bandpass Data

Peak Magnification: 290

STA	DIST. (km)	RECORD AMPLITUDE (mm)	RECORD NOISE (mm)	GALVANOMETER GAIN	STATION GAIN	GROUND DISPLACEMENT (μ)	NOISE (μ)	AZIMUTH
TYS	514.4	4.7	1.1	8.9	32	.0284	.0067	347
DWM	311.1	7.2	1.8	8.9	8	.1744	.0436	356
LST	282.6	12.8	1.7	8.9	16	.1550	.0206	351
DON	357.2	19.4	1.2	8.9	64	.0587	.0036	350
OKG	187.9	26.3	1.0	8.9	32	.1592	.0060	343
PGA	260.8	23.8	1.4	8.9	16	.2882	.0170	331
ECD	236.7	20.1	1.3	8.9	16	.2434	.0157	344
NKT	206.2	40.3	1.5	8.9	16	.4879	.0182	352
POW	297.2	17.9	.9	8.9	64	.0542	.0027	324

TABLE 6

(continued)

6c) 2 -Hz Narrow Bandpass Data

Peak Magnification: 480

STA	DIST. (km)	RECORD AMPLITUDE (mm)	RECORD NOISE (mm)	GALVANOMETER GAIN	STATION GAIN	GROUND DISPLACEMENT (μ)	NOISE (μ)	AZIMUTH
TYS	514.4	7.5	1.2	8.9	32	.0274	.0044	347
DWM	311.1	10.9	2.8	8.9	8	.1595	.0410	356
LST	282.6	21.8	2.1	8.9	16	.1595	.0154	351
DON	359.2	27.1	1.1	8.9	64	.0496	.0020	350
OKG	187.9	42.5	1.2	8.9	32	.1554	.0044	343
PGA	260.8	10.0	.8	2	16	.3255	.0260	331
ECD	236.7	12.2	1.0	3.8	16	.2090	.0171	344
NKT	206.2	32.2	.8	3.8	16	.5517	.0137	352
POW	297.2	32.1	1.0	8.9	64	.0587	.0018	324

TABLE 6

(continued)

6d) 3 -Hz Narrow Bandpass Data

Peak Magnification: 810

STA	DIST. (km)	RECORD AMPLITUDE (mm)	RECORD NOISE (mm)	GALVANOMETER GAIN	STATION GAIN	GROUND DISPLACEMENT (μ)	NOISE (μ)	AZIMUTH
TYS	514.4	9.3	1.7	8.9	32	.0202	.0037	347
DWM	311.1	17.8	4.6	8.9	8	.1543	.0399	356
LST	282.6	21.0	1.4	3.8	16	.2132	.0142	351
DON	357.2	12.3	1.0	2	64	.0593	.0048	350
OKG	187.9	26.7	.9	2	32	.2575	.0087	343
PGA	260.8	29.7	1.2	2	16	.5729	.0232	331
ECD	236.7	24.8	1.3	3.8	16	.2518	.0132	344
NKT	206.2	43.8	1.2	3.8	16	.4447	.0122	352
POW	297.2	29.7	.8	3.8	64	.0754	.0020	324

TABLE 6

(continued)

6e) 5 -Hz Narrow Bandpass Data

Peak Magnification: 840

STA	DIST. (km)	RECORD AMPLITUDE (mm)	RECORD NOISE (mm)	GALVANOMETER GAIN	STATION GAIN	GROUND DISPLACEMENT (μ)	NOISE (μ)	AZIMUTH
TYS	514.4	10.8	1.8	8.9	32	.0266	.0038	347
DWM	311.1	26.3	3.1	8.9	8	.2199	.0259	356
LST	282.6	25.7	1.6	3.8	16	.2516	.0157	351
DON	357.2	37.9	1.2	3.8	64	.0928	.0029	350
OKG	187.9	34.3	1.2	2	32	.3190	.0112	343
PGA	260.8	30.0	1.7	2	16	.5580	.0316	331
ECD	236.7	18.6	1.0	2	16	.3460	.0186	344
NKT	206.2	23.7	1.2	3.8	16	.2320	.0118	352
POW	297.2	43.6	1.2	3.8	64	.1067	.0029	324

TABLE 6

(continued)

6f) 8 -Hz Narrow Bandpass Data

Peak Magnification: 1400

STA	DIST. (km)	RECORD AMPLITUDE (mm)	RECORD NOISE (mm)	GALVANOMETER GAIN	STATION GAIN	GROUND DISPLACEMENT (μ)	NOISE (μ)	AZIMUTH
TYS	514.4	7.6	2.2	8.9	32	.0095	.0028	347
DWM	311.1	28.3	2.0	8.9	8	.1420	.0100	356
LST	282.6	26.3	1.7	3.8	16	.1545	.0100	351
DON	357.2	51.5	1.4	2	64	.1437	.0039	350
OKG	187.9	31.8	1.2	2	32	.1775	.0067	343
PGA	260.8	21.1	1.1	2	16	.2355	.0123	331
ECD	236.7	30.0	1.4	3.8	16	.1762	.0082	344
NKT	206.2	31.8	2.0	8.9	16	.0798	.0050	352
POW	297.2	36.8	1.0	2	64	.1027	.0028	324

TABLE 6

(continued)

6g) 12.5-Hz Narrow Bandpass Data

Peak Magnification: 1300

STA	DIST. (km)	RECORD AMPLITUDE (mm)	RECORD NOISE (mm)	GALVANOMETER GAIN	STATION GAIN	GROUND DISPLACEMENT (μ)	NOISE (μ)	AZIMUTH
DWM	311.1	17.7	2.2	8.9	8	.0956	.0119	356
LST	282.2	15.5	1.4	3.8	16	.0980	.0089	351
DON	357.2	33.8	1.2	2	64	.1016	.0036	350
OKG	187.9	47.5	1.2	3.8	32	.1502	.0038	343
PGA	260.8	45.8	2.0	8.9	16	.1237	.0054	331
ECD	236.7	46.4	1.8	8.9	16	.1253	.0049	344
NKT	206.2	11.6	1.7	8.9	16	.0313	.0046	352
POW	297.2	30.9	1.4	2	64	.0928	.0042	324

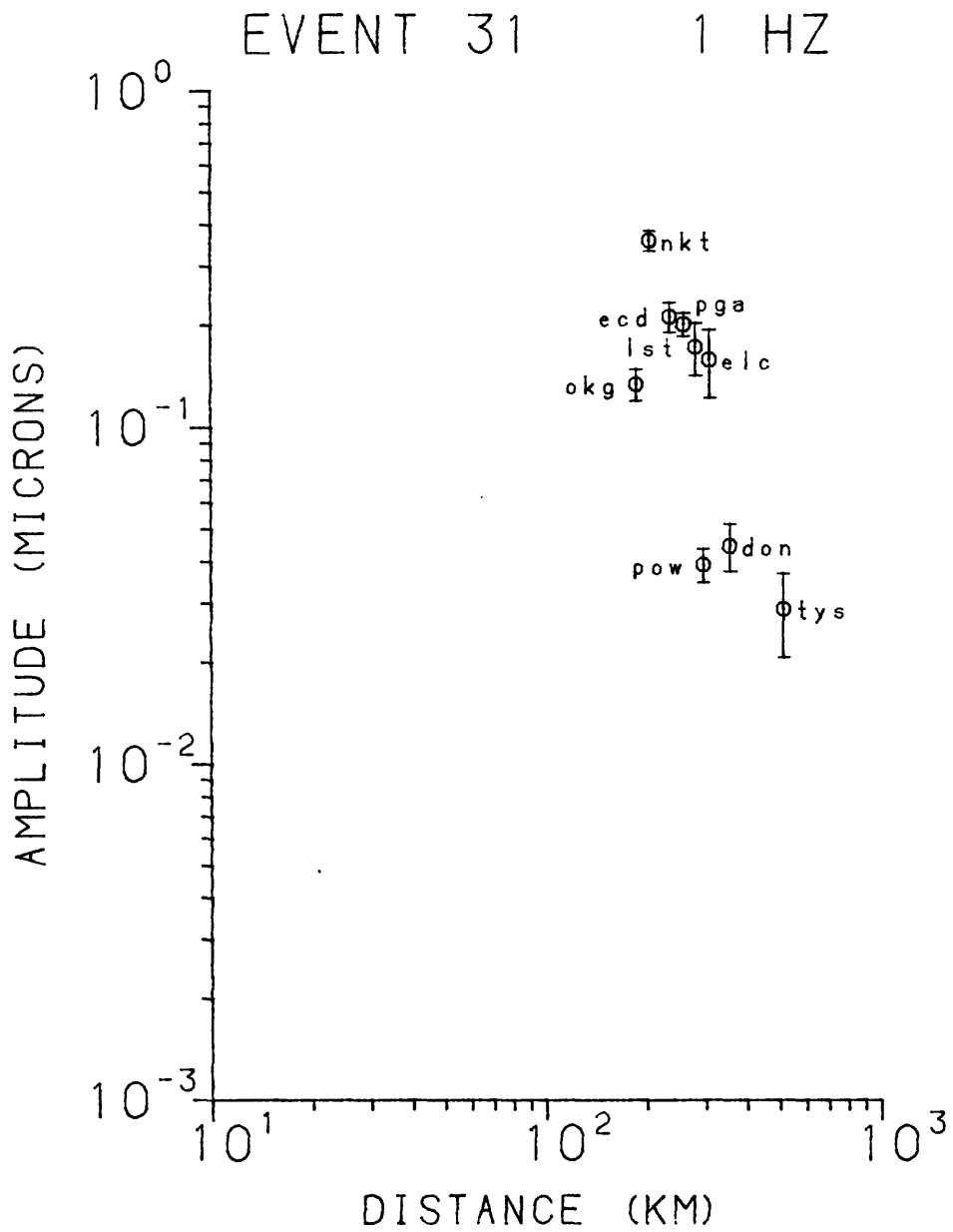

Figure 26. 1-Hz amplitudes of Lg-Z waves for Event No. 31.

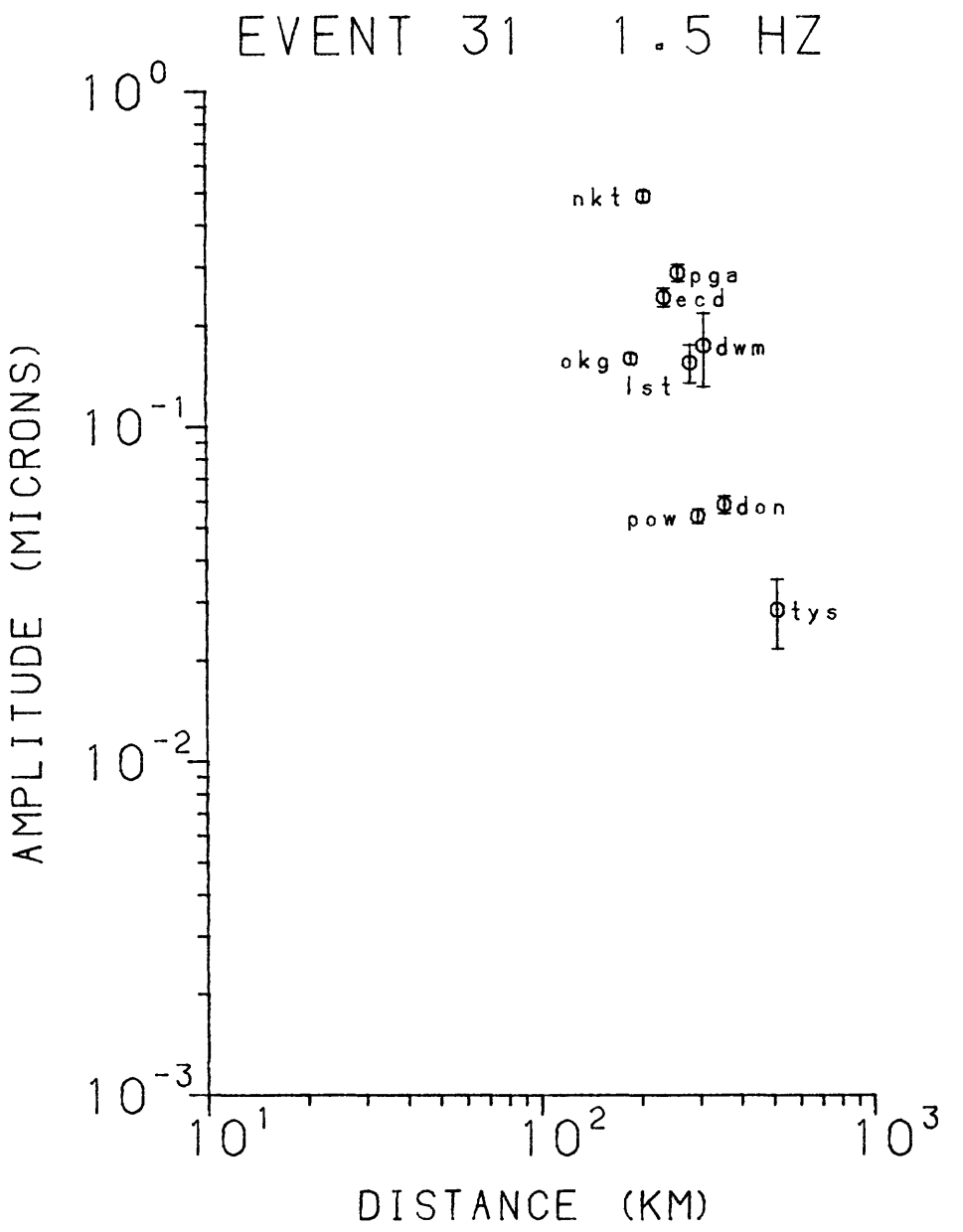

Figure 27. 1.5-Hz amplitudes of Lg-Z waves for Event No. 31.

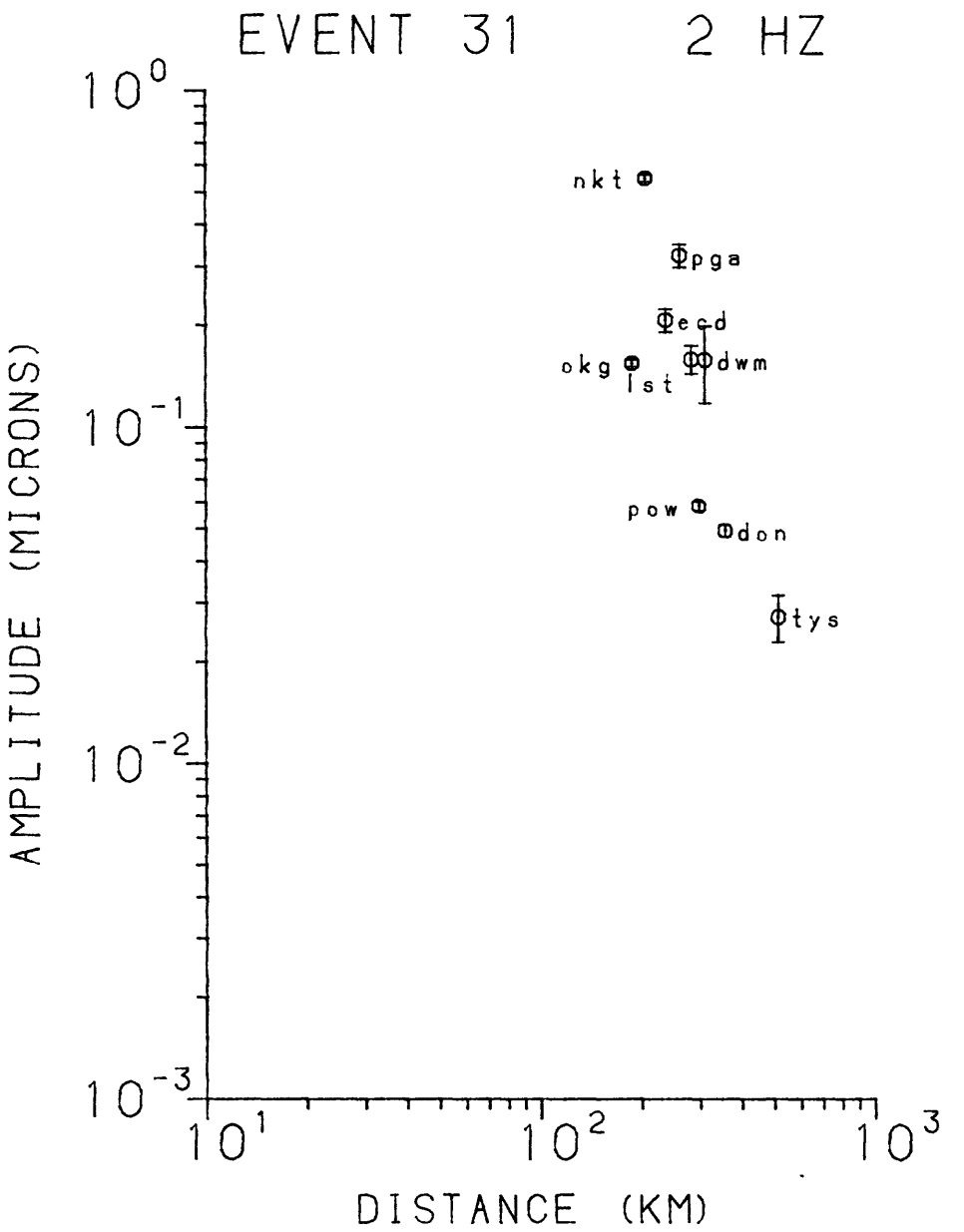

Figure 28. 2-Hz amplitudes of Lg-Z waves for Event No. 31.

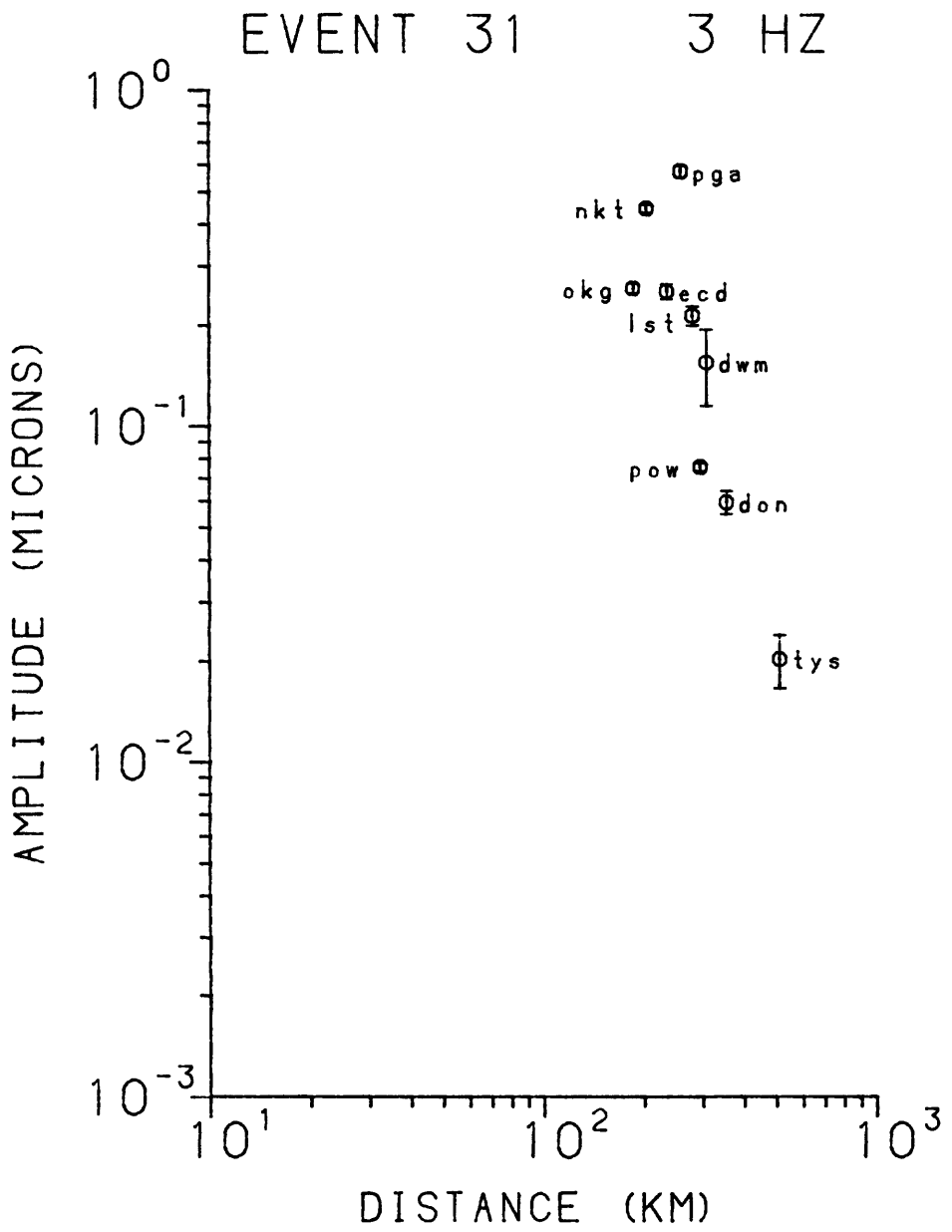

Figure 29. 3-Hz amplitudes of Lg-Z waves for Event No. 31.

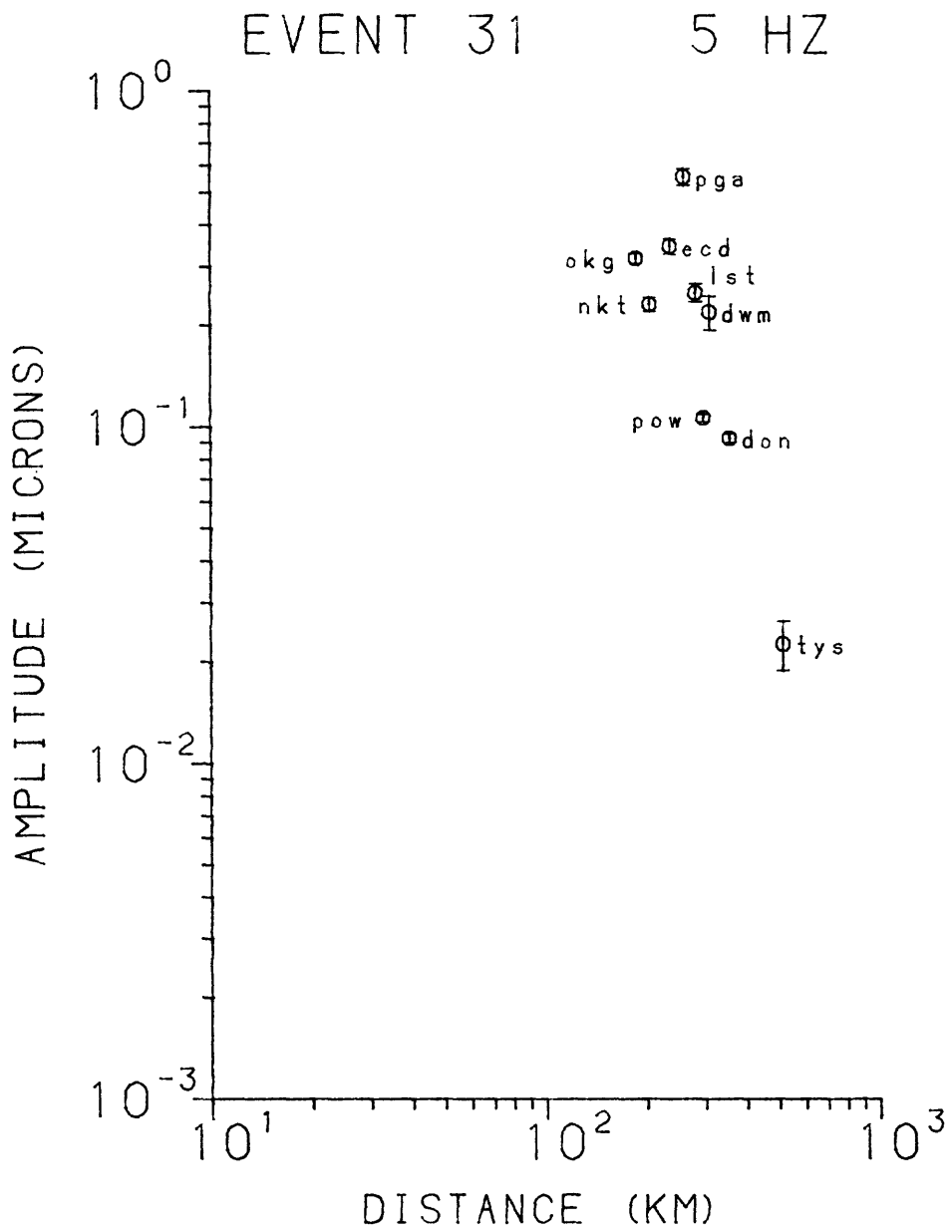

Figure 30. 5-Hz amplitudes of Lg-Z waves for Event No. 31.

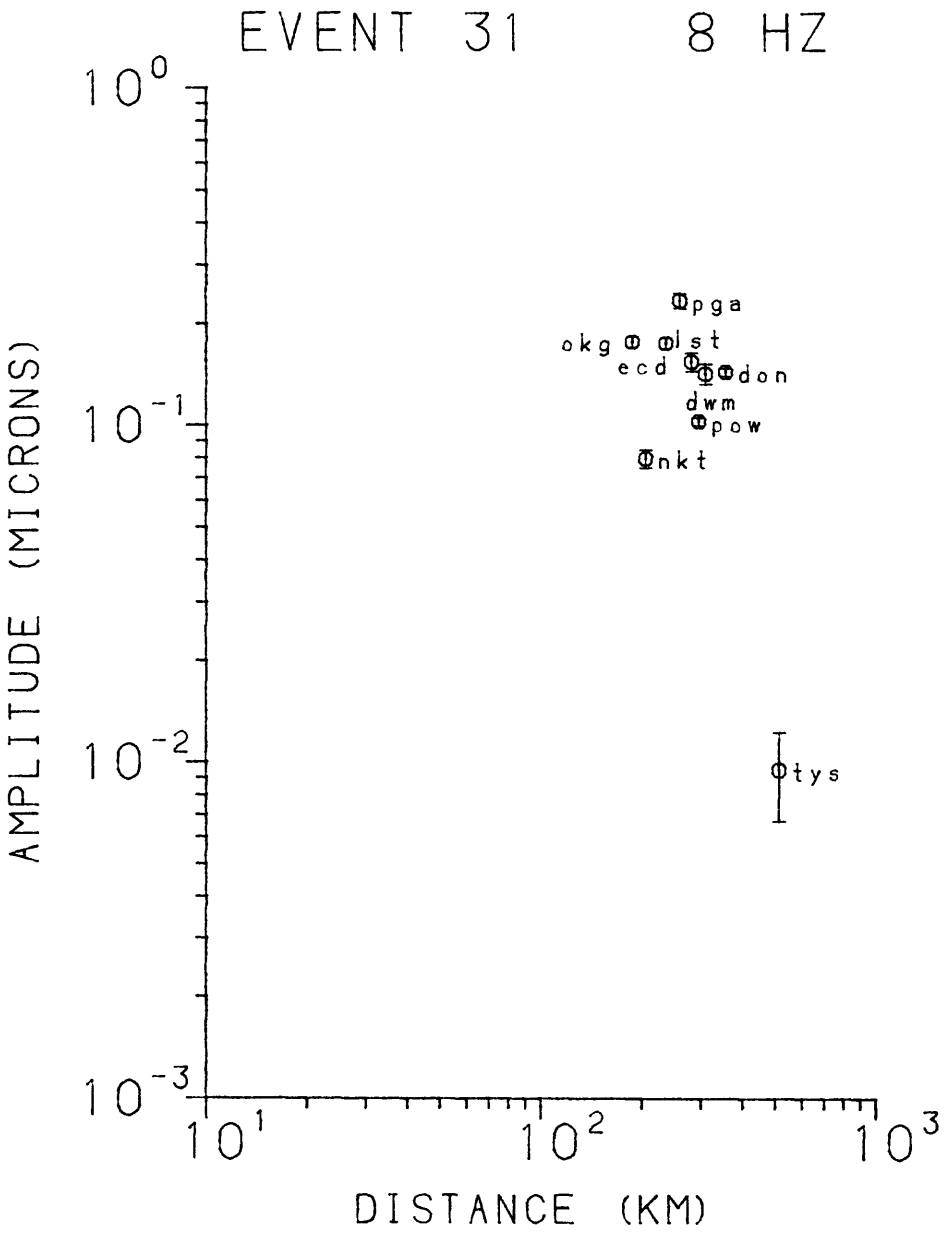

Figure 31. 8-Hz amplitudes of Lg-Z waves for Event No. 31.

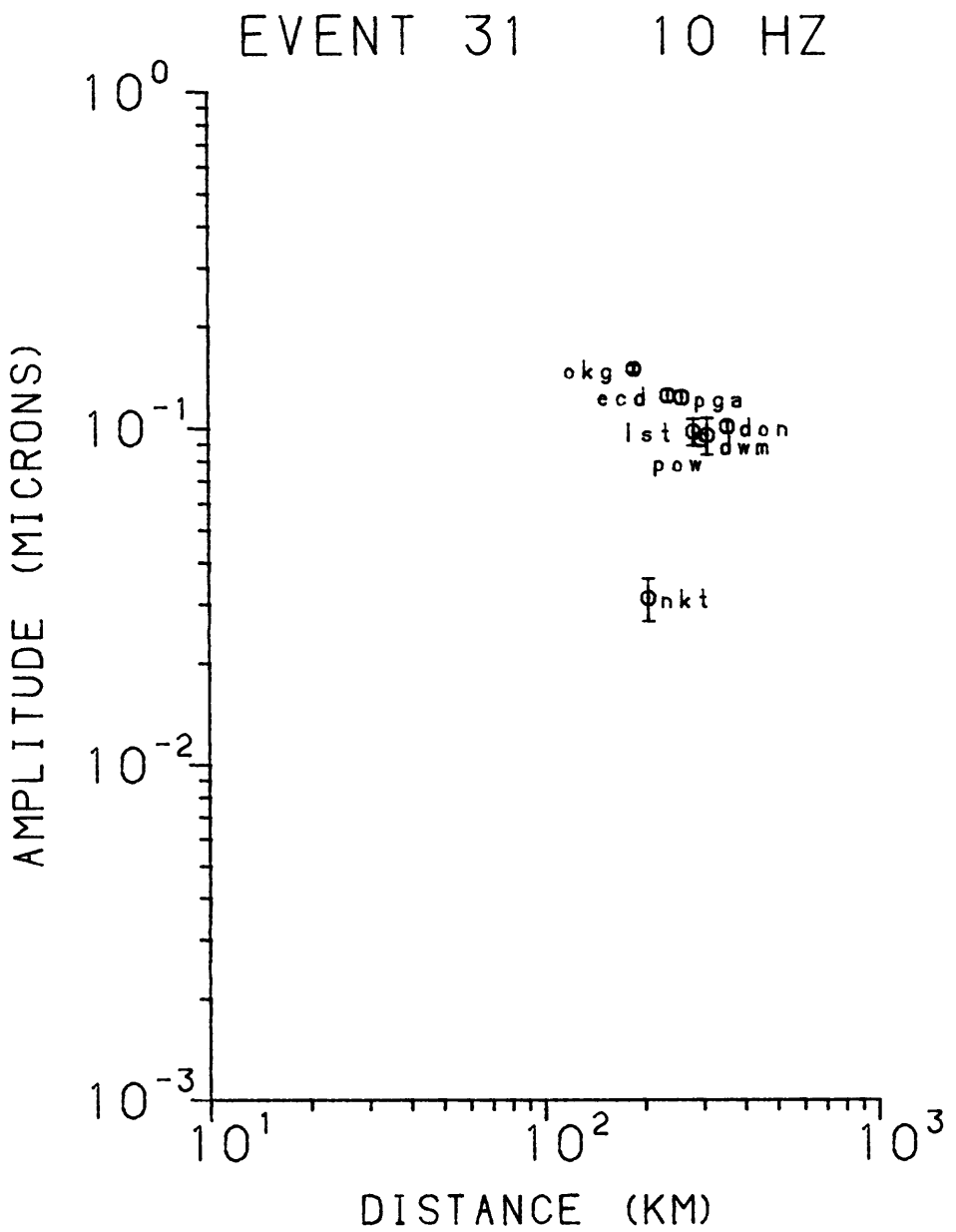

Figure 32. 10.5-Hz amplitudes of Lg-Z waves for Event No. 31.

ANALYSIS

In the time domain, the Lg phase amplitude data are assumed to satisfy the relation (Ewing et al., 1957)

$$A = A_o \Delta^{-1/3} (R_o \sin \Delta^o)^{-1/2} \exp(-\gamma\Delta) \quad (1)$$

where A is the observed amplitude at epicentral distance Δ, A_o is a constant for a given frequency and is related to the source spectrum, and γ is the coefficient of anelastic attenuation. The term $(R_o \sin \Delta^o)^{-1/2}$ represents the amplitude decrease due to a geometrical spreading, where Δ^o is the epicentral distance in degrees and R_o is the radius of the earth, and the term $\Delta^{-1/3}$ represents the decrease in amplitude due to dispersion, where Lg is assumed to be an Airy phase (Nuttli, 1973). The term $\exp(-\gamma\Delta)$ accounts for frequency-dependent absorption. The parameter γ is frequency dependent, and is related to the specific quality factor, Q, by

$$\gamma = \pi f/QU \quad (2)$$

where U is the group velocity of the wave, which for the Lg phase is 3.5 km/sec, and f is the frequency of the wave. The parameter Q is usually considered to be frequency independent, although there is some evidence that at periods of 0.1 to 10 sec it may vary with frequency.

Consider the constant term A_o in equation (1). We know that for a given frequency,

$$A \propto \Delta^{-1/3} (R_o \sin \Delta^o)^{-1/2} \exp(-\gamma\Delta) \quad (3)$$

Therefore, given an amplitude A at an arbitrary distance Δ, and an

amplitude A_o at a distance of 1 km, then from (3)

$$\frac{A}{A_o} = \frac{\Delta^{-1/3} \, (R_o \sin \Delta^o)^{-1/2} \exp(-\gamma\Delta)}{(1)^{-1/3} \, (R_o \sin (1/111.1))^{-1/2} \exp(-\gamma \cdot 1.)}$$

or

$$A = A_o \, \Delta^{-1/3} \, (R_o \sin \Delta^o)^{-1/2} \exp(-\gamma\Delta) \exp(\gamma)$$

with the multiplicand of A_o now unitless. If we also assume that the value of γ is small ($<< 1$) then $\exp(\gamma) \sim 1$ and we have

$$A = A_o \, \Delta^{-1/3} \, (R_o \sin \Delta^o)^{-1/2} \exp(-\gamma\Delta) \qquad (4)$$

which is of the same form as (1), except that A_o is now the amplitude of the Lg wave at a distance of one kilometer from the source. It is important to note that this is only a value extrapolated from a far-field equation, and that Lg, being a superposition of higher-mode surface waves, does not actually exist at an epicentral distance of 1 km. This value A_o will be referred to as the source amplitude.

To study the attenuation of Lg amplitudes with distance, we can use equation (4) to form a family of curves, log-log plots of A vs Δ, where each curve represents a different value of γ (Figure 33). If we then plot Lg amplitude vs epicentral distance data for an event on the same log-log scale, we can determine the value of γ by hand-fitting the curves to the data (e.g., fitting the curves in Figure 33 to the data in Figures 5-32). This is a widely used method of determining the coefficient of anelastic attenuation (Nuttli, 1973; Street, 1976; Nuttli and Dwyer, 1978; Bollinger, 1979), and has been previously used with a portion of the data used in this study (Dwyer and Nuttli, 1978). The method does, however, present certain problems: we use only certain

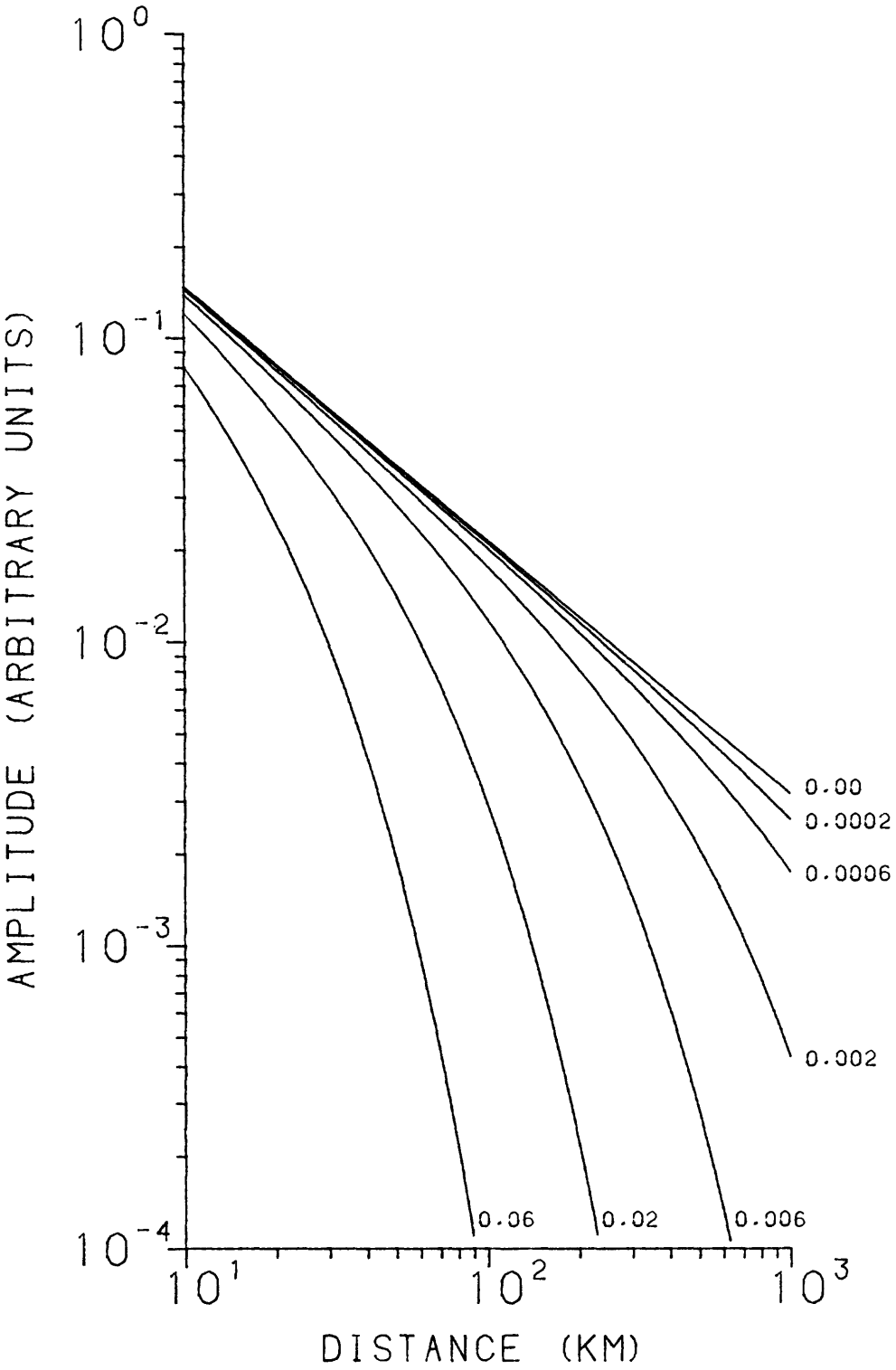

Figure 33. Theoretical curves of attenuation with distance of Lg amplitude, using different values of γ.

discrete values for γ in our curve fitting, and we have only a rough feel for the goodness of fit of the chosen curve. We would overcome these problems if we were able to determine the value of γ numerically from the amplitude data.

In an attempt to find another method of determining γ, we look again at equation (4). If we multiply both sides of the equation by $\Delta^{1/3} (R_o \sin \Delta^o)^{1/2}$, and then take the natural logarithm of each side, we obtain

$$\ln (A \Delta^{1/3} (R_o \sin \Delta^o)^{1/2}) = \ln A_o - \gamma\Delta \tag{5}$$

Making the substitutions

$$y = \ln (A \Delta^{1/3} (R_o \sin \Delta^o)^{1/2})$$

and

$$B = \ln A_o$$

we have

$$y = B - \gamma\Delta \tag{6}$$

We note in passing that if for all measurements $\Delta^o < 15^o$, then we may approximate

$$\Delta^{-1/3} (R_o \sin \Delta^o)^{-1/2} = \Delta^{-5/6}$$

and therefore

$$y = \ln (A \Delta^{5/6})$$

In equation (6), at a given frequency and for a given event, B and γ are constants, and we have a linear equation. If we have a number N of stations recording an event, we then have, for a given station i,

$$y_i = B - \gamma\Delta_i \tag{7}$$

We can now perform a least-squares fit to the data. We form the sum of the squares of the differences between the observed and calculated y values for our N stations

$$\chi^2 = \sum_{i=1}^{N} (y_i - (B - \gamma\Delta_i))^2 \tag{8}$$

We then take the derivative with respect to B and set it equal to zero, in order to minimize χ^2 with respect to B

$$\frac{\partial\chi^2}{\partial B} = -2 \sum_{i=1}^{N} (y_i - (B - \gamma\Delta_i)) = 0$$

or

$$\sum_{i=1}^{N} y_i = NB - \gamma \sum_{i=1}^{N} \Delta_i \tag{9}$$

We do the same with respect to γ:

$$\frac{\partial\chi^2}{\partial\gamma} = 2 \sum_{i=1}^{N} \Delta_i (y_i - (B - \gamma\Delta_i)) = 0$$

or

$$\sum_{i=1}^{N} \Delta_i y_i = B \sum_{i=1}^{N} \Delta_i - \gamma \sum_{i=1}^{N} \Delta_i^2 \tag{10}$$

Since we know the values of Δ_i and can calculate the y_i's from amplitude data, we have two equations in two unknowns and can solve for γ and B.

Although this is a straight forward method, it needs data that are fairly well constrained. Unfortunately, the number of data points and the scatter involved for a single event, as seen is Figures 5-32, severely limit the worth of our resulting γ values, which are likely to vary greatly from one event to the next, and have large standard deviations. What we should like to do is combat this problem by combining many events in order to increase our number of data points. This may be done by scaling the source constant A_o for each event to match a reference A_o by assuming a relation between seismic moment, corner frequency, and magnitude, and then adjusting the record amplitudes accordingly (Bollinger, 1979). There is, however, a numerical method which allows us to combine separate events, and which needs no assumptions about A_o (Chouet et al., 1978).

Let us look again at equation (7). If we assume that γ is a constant for a region at a given frequency, then for the data from station i and event j,

$$y_{ji} = B_j - \gamma\Delta_{ji} \tag{11}$$

We can obtain for one event the sum of the squares of the differences between observed and calculated y values for our N stations used for this event (N(j))

$$\chi^2 = \sum_{i=1}^{N(j)} (y_{ji} - (B_j - \gamma\Delta_{ji}))^2$$

but we can also sum M events

$$\chi^2 = \sum_{j=1}^{M} \sum_{i=1}^{N(j)} (y_{ji} - (B_j - \gamma\Delta_{ji}))^2 \tag{12}$$

We can also recognize that some of the data might be more reliable than others, and can seek a method of weighting each of the data points using some weighting function w_{ji}. This gives us

$$\chi^2 = \sum_{j=1}^{M} \sum_{i=1}^{N(j)} w_{ji} \, (y_{ji} - (B_j - \gamma \Delta_{ji}))^2 \tag{13}$$

We now seek to minimize χ^2 with respect to each of the B_j's

$$\frac{\partial \chi^2}{\partial B_K} = -2 \sum_{i=1}^{N(K)} w_{Ki} (y_{Ki} - (B_K - \gamma \Delta_{Ki}))^2 = 0$$

or

$$\sum_{i=1}^{N} w_{Ki} \, y_{Ki} = B_K \sum_{i=1}^{N(K)} w_{Ki} - \gamma \sum_{i=1}^{N(K)} \Delta_{Ki} \tag{14}$$

and also with respect to γ

$$\frac{\partial \chi^2}{\partial \gamma} = -2 \sum_{j=1}^{M} \sum_{i=1}^{N(j)} w_{ji} \, \Delta_{ji} \, (y_{ji} - (B_j - \gamma \Delta_{ji})) = 0$$

or

$$\sum_{j=1}^{M} \sum_{i=1}^{N(j)} w_{ji} \, \Delta_{ji} \, y_{ji} = B_j \sum_{j=1}^{M} \sum_{i=1}^{N(j)} w_{ji} \, \Delta_{ji} - \gamma \sum_{j=1}^{M} \sum_{i=1}^{N(j)} w_{ji} \, \Delta_{ji}^2 \tag{15}$$

We now have M + 1 equations in M + 1 unknowns. If we let

$$X = \begin{bmatrix} \sum_{i=1}^{N(1)} W_{1i} & 0 & 0 & \cdots & \sum_{i=1}^{N(1)} W_{1i} \, \Delta_{1i} \\ 0 & \sum_{i=1}^{N} W_{2i} & 0 & \cdots & \sum_{i=1}^{N} W_{2i} \, \Delta_{2i} \\ 0 & 0 & \sum_{i=1}^{N(3)} W_{3i} & \cdots & \sum_{i=1}^{N(3)} W_{3i} \, \Delta_{3i} \\ \vdots & \vdots & \vdots & & \\ \sum_{i=1}^{N(1)} W_{1i} \Delta_{1i} & \sum_{i=1}^{N(2)} W_{2i} \, \Delta_{2i} & \sum_{i=1}^{N(3)} W_{3i} \, \Delta_{3i} & \cdots & \sum_{j=i}^{M} \sum_{i=i}^{N(j)} W_{ji} \, \Delta^2_{ji} \end{bmatrix}$$

$$C = \begin{bmatrix} B_1 \\ B_2 \\ B_3 \\ \vdots \\ Bm \\ -\gamma \end{bmatrix} \quad \text{and} \quad Y = \begin{bmatrix} \sum_{i=1}^{N(1)} W_{1i}\, y_{1i} \\ \sum_{i=1}^{N(2)} W_{2i}\, y_{2i} \\ \sum_{i=1}^{N(3)} W_{3i}\, y_{3i} \\ \vdots \\ \sum_{j=1}^{M} \sum_{i=1}^{N(j)} W_{ji}\, y_{ji}\, \Delta_{ji} \end{bmatrix} \tag{16}$$

then from Equations (14) and (15) we have

$$XC + Y \tag{17}$$

If we take the inverse of X and multiply, we have

$$X^{-1}XC = X^{-1}Y \tag{18}$$

or

$$C = X^{-1}Y \tag{19}$$

Looking back at our definition of C, we find that we have solved for a single regional γ and for the natural logarithms of the source amplitudes of each of the events using just the amplitude and epicentral distance data.

To determine confidence limits on the B and γ values, we use, following Herrmann and Mitchell (1975)

$$\text{est. err. } B_K = t(m,p)\ \sqrt{V(B_K)}$$

and (20)

$$\text{est. err. } \gamma = t(m,p)\ \sqrt{V(\gamma_K)}$$

where t(m,p) is the p percentage confidence point of the student's t-distribution with m degrees of freedom (we will use 95% confidence

limits), and

$$V(B_K) = S^2 X^{-1} (K,K)$$

and

$$V(\gamma) = S^2 X^{-1} (M+1, M+1)$$

where X^{-1} (K,K) is the K^{th} diagonal element of the covariance matrix in equation (19). For our weighted data set, the sample variance, S^2, is given by (Bevington, 1969)

$$S^2 = \frac{\frac{1}{(L-M-1)} \sum_{j=1}^{M} \sum_{i=1}^{N(j)} \{w_{ij} [y_{ij} - (B_j - \gamma \Delta_{ij})]^2\}}{\frac{1}{L} \sum_{j=1}^{M} \sum_{i=1}^{N(j)} w_{ij}} \qquad (21)$$

where L is the total number of data points, i.e.

$$L = \sum_{j=1}^{M} N(j)$$

and (L-M-1) is the number of degrees of freedom. Note that if all data are given equal weight, $w_{ij} = 1$, then the denominator in equation (20) becomes equal to unity, and equation (20) reduces to the usual definition of sample variance.

This, then, is the method used in the present study to determine a value for the coefficient of anelastic attenuation over a range of frequencies. It seems ideally suited to our time domain study of narrow bandpass filtered data.

RESULTS: UNFILTERED DATA

Before analyzing our filtered data, we sought to test the least-squares method, using events which had a wide epicentral distance range and fairly large magnitudes. To do this, we used two sets of 1-sec period Lg amplitude data: one given by Bollinger (1979) for the southeastern United States, and one using events studied by Nuttli for the central United States. (In both cases, the actual data given is the amplitude divided by period (A/T), so the A_o obtained by our method in this case has units of μ/sec.)

Utilizing the data from 14 events given by Bollinger, we determined a value of γ at 1 Hz of 0.0011 km^{-1} ± 0.0002 km^{-1} for the southeastern United States, which corresponds to a Q of 816 (within the limits $690 < Q < 997$). This agrees very well with other estimates given for the eastern United States γ values (Street, 1976).

In plotting out the data, we use equation (11)

$$y_{ji} = B_j - \gamma\Delta_{ji}$$

Recalling that

$$B_j = \ln A_{oj}$$

and

$$y_{ji} = \ln (A_j \ \Delta_{ji}^{5/6})$$

we have

$$\ln (A_j \ \Delta_{ji}^{5/6}/A_{oj}) = -\gamma\Delta_{ji},$$

or, for plotting on a semi-log scale,

$$\log (A_j \ \Delta_{ji}^{5/6}/A_{oj}) = -\gamma\Delta_{ji} \log(e) \qquad (22)$$

Thus, if we divide the data for each event by the source amplitude for that event, we arrive at a value referred to as the reduced amplitude (Y), which allows us to plot the data from all events together, as seen in Figure 34. The solid line shown is a plot of

$$Y = (-.0011 \text{ km}^{-1}) \ \Delta \log (e)$$

We can see that this line is a good fit to the data, showing a well measured value for γ. There seems to be no evidence of a change in attenuation rates at a distance of approximately 1000 km, as suggested by Bollinger.

As a further test of the method, we used the source amplitudes obtained for each event to obtain an m_b magnitude for each event. We used our calculated values of A_o and γ, and equation (4), to determine the value of A/T at a distance of one degree (assuming T = 1 sec). This value was then used to calculate the magnitude, using (Nuttli, 1973)

$$m_b = 3.75 + 0.90 \ (\log \Delta^o) + \log A/T \qquad 0.5^o \leq \Delta \leq 4.0^o \qquad (23)$$

The errors in A_o were used to determine the error in m_b.

We also determined an average m_b magnitude for each event. For this we took the A/T and Δ values at each station, and solved for m_b using equation (23) and

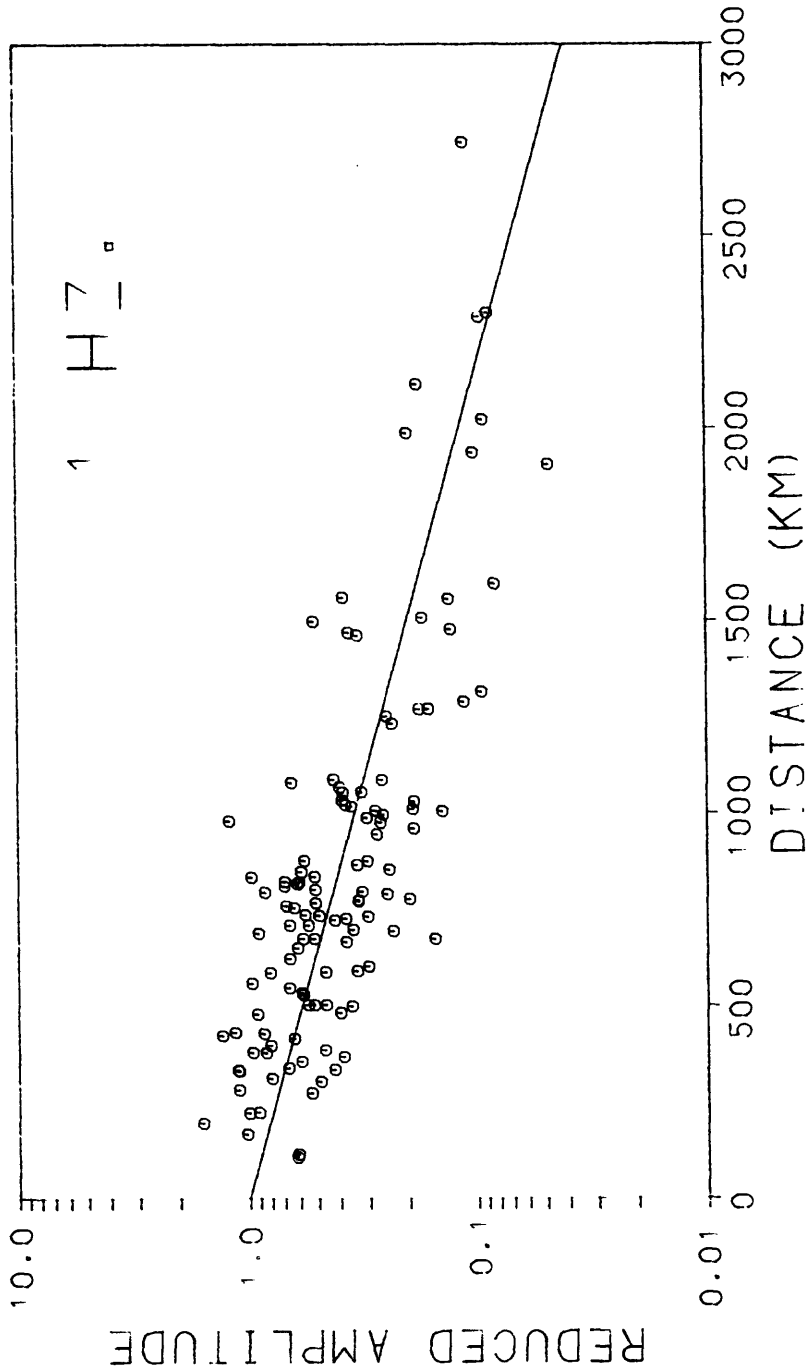

Figure 34. 1-Hz Lg attenuation data of Bollinger (1979) for the southeastern United States.

$$m_b = 3.30 + 1.66\ (\log \Delta^o) + \log A/T \qquad 4^o \leq \Delta \leq 30^o \qquad (24)$$

We then averaged over all the stations for each event, obtaining an average m_b and a standard deviation.

Finally we plotted the source-amplitude magnitude versus the average magnitude for each event. The result is given in Figure 35. The straight line shown is for the case of the source-amplitude magnitude equalling the average magnitude. We can see that we do have a very good straight line fit with the source-amplitude magnitude measuring consistentaly approximately one-tenth of a magnitide unit higher than the average magnitude. This is due to the fact that the magnitude formulas given in equations (23) and (24) were formulated using a Q of 1500. However, for Bollinger's data we obtained a Q of 816. This means that when we calculated the average magnitudes, we were not correcting the magnitudes properly for the effects of attenuation with distance (the second term on the right hand side of both equations (22) and (23)). Hence the average magnitudes were undercorrected by about one-tenth of a magnitude unit.

The second set of 1-sec period amplitude data analyzed consisted of six events that occurred in the central United States. These events are listed in Table 7. Amplitude data were taken from stations of the World Wide Standard Seismic Network (WWSSN) and the Seismological Service of Canada. Only stations east of the Rocky Mountains were used. From these data, we determined a value for γ at 1 Hz of $0.0007\ km^{-1} \pm .0002\ km^{-1}$ for the central United States, which corresponds to a Q of 1282 (within the limits $997 < Q < 1795$), which is a higher value than that obtained for the southeastern United States, as is expected,

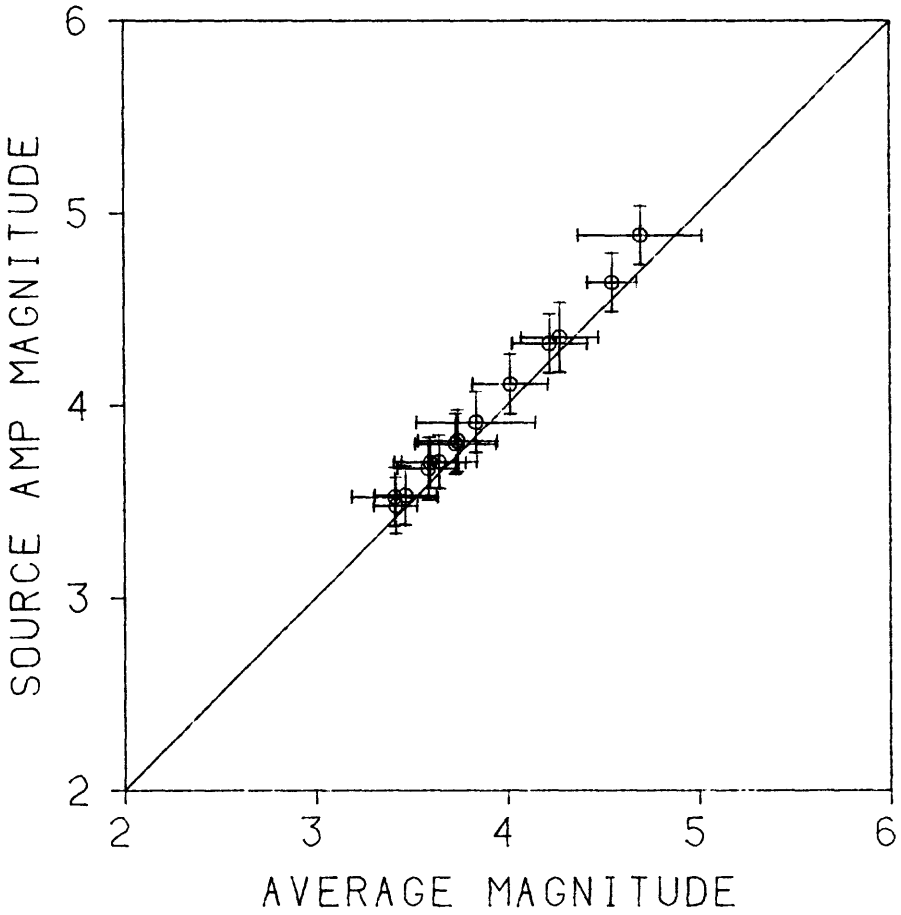

Figure 35. Source amplitude magnitude versus average magnitude for 1-Hz data for southeastern United States.

TABLE 7

Date	Origin Time U.T.	Latitude °N	Longitude °N	m_b
14 AUG 65	13:13:54	37.1	89.2	3.8
21 OCT 65	02:02:38	37.5	91.0	4.9
04 JUN 67	16:14:14	33.6	90.9	4.5
21 JUL 67	09:14:49	37.5	90.4	4.3
01 JAN 69	23:35:36	34.8	92.6	4.5
17 NOV 70	01:13:55	35.9	90.1	4.4

and which also agrees very nicely with Nuttli's value of 1500 for 1 Hz Q in the central United States (Nuttli, 1973). The data are plotted in Figure 36, with the solid line corresponding to the equation

$$Y = (-.0007 \text{ km}^{-1}) \Delta \log (e)$$

where, as before, Y is the reduced amplitude. Once again you can see that we have a good fit to the data, showing a well measured value for γ. In Figure 37, we have the plot of source-amplitude magnitude versus the average magnitude. Note that since our measured Q of 1282 is close to the Q of 1500, which Nuttli used for his magnitude formulas, we can see that in this case the source-amplitude magnitude is equal to the average magnitude, i.e. the effects of attenuation with distance are properly accounted for.

Along with the two sets of 1-Hz amplitude data, we also analyzed a set of unfiltered 10-Hz data from the New Madrid area. This data, obtained from stations of the Saint Louis University microearthquake seismic array, had already been analyzed using the calibration curve fitting method (Nuttli, 1978). From this analysis, Nuttli determined a γ of 0.006 km^{-1} for the New Madrid seismic zone. This corresponds to a Q of 1500, which is equal to the Q found for 1 Hz Lg waves. Our least-squares analysis of these same data yields a γ of 0.0029 ± 0.0010 km^{-1}, corresponding to a Q of 3095 (within the limits $2301 < Q < 4724$). The data are plotted in Figure 38, where the solid line corresponds to the equation

$$Y = (-0.0029 \text{ km}^{-1}) \Delta \log (e)$$

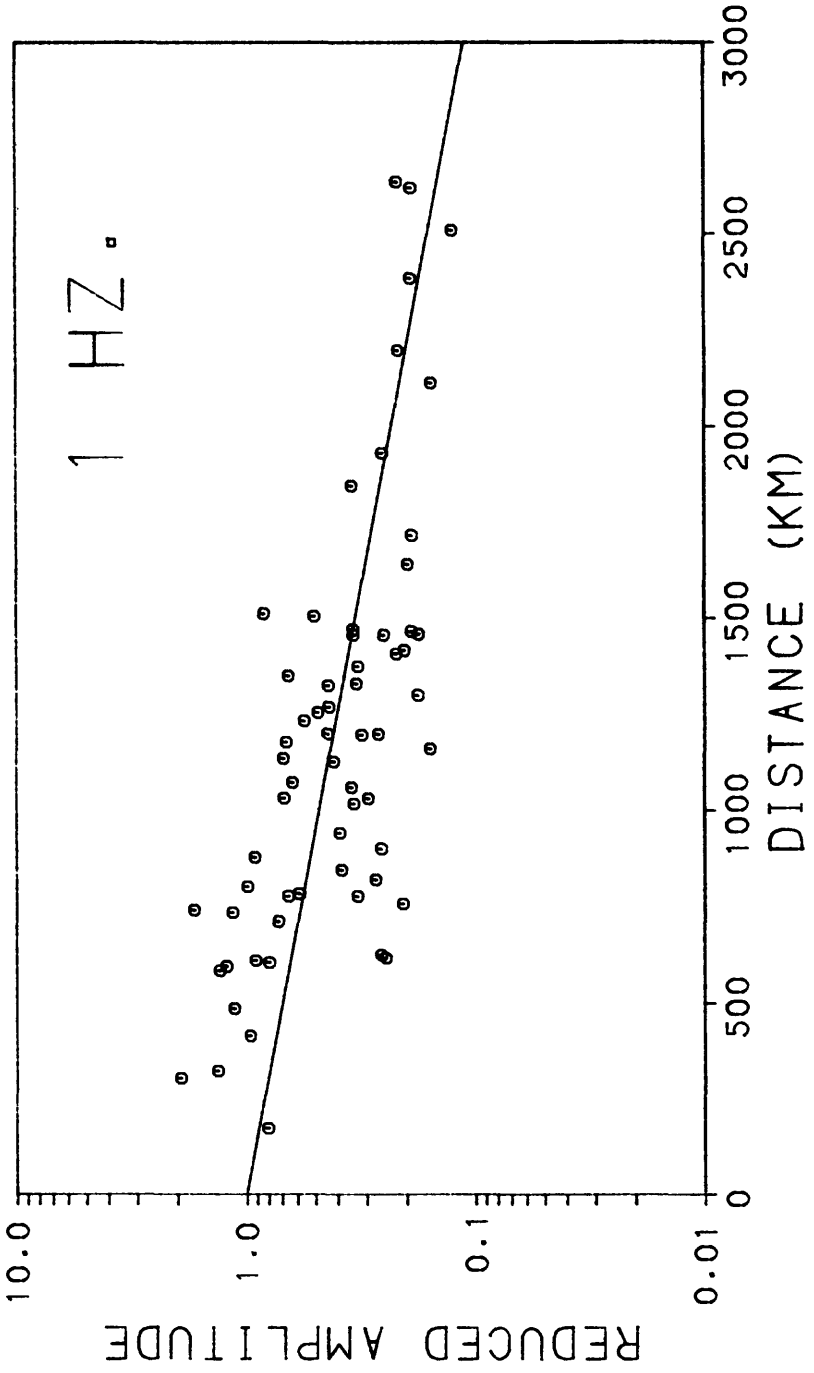

Figure 36. 1-Hz Lg attenuation data for the central United States.

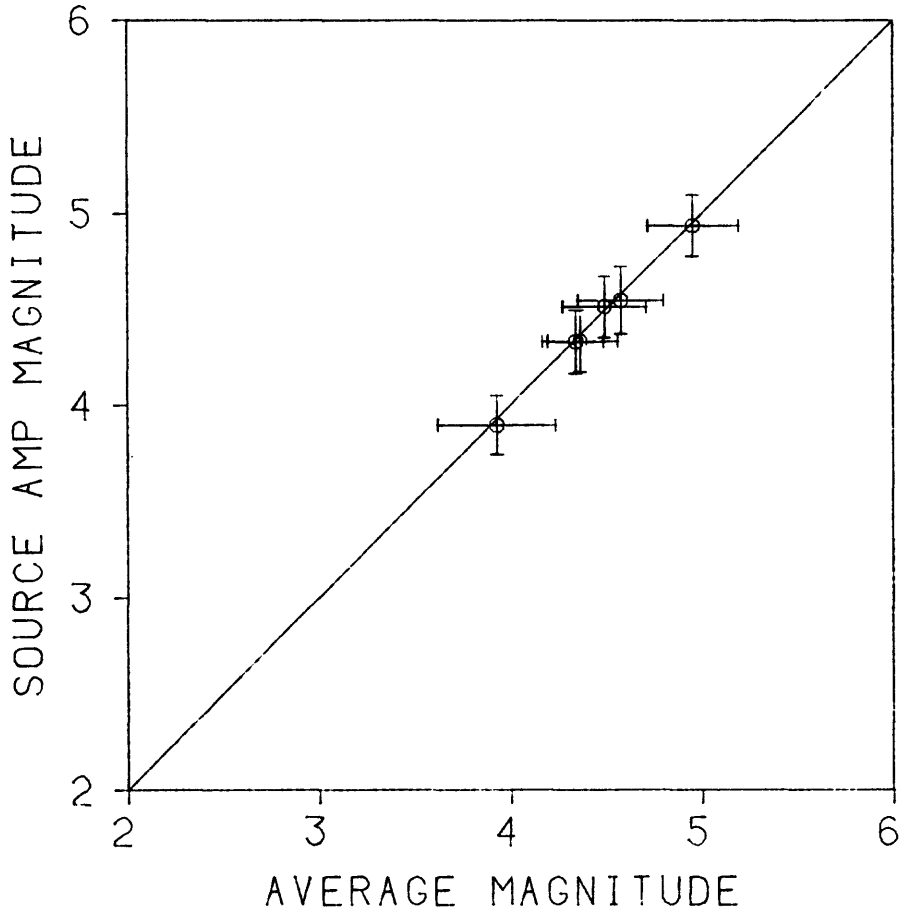

Figure 37. Source amplitude magnitude versus average magnitude for 1-Hz data for central United States.

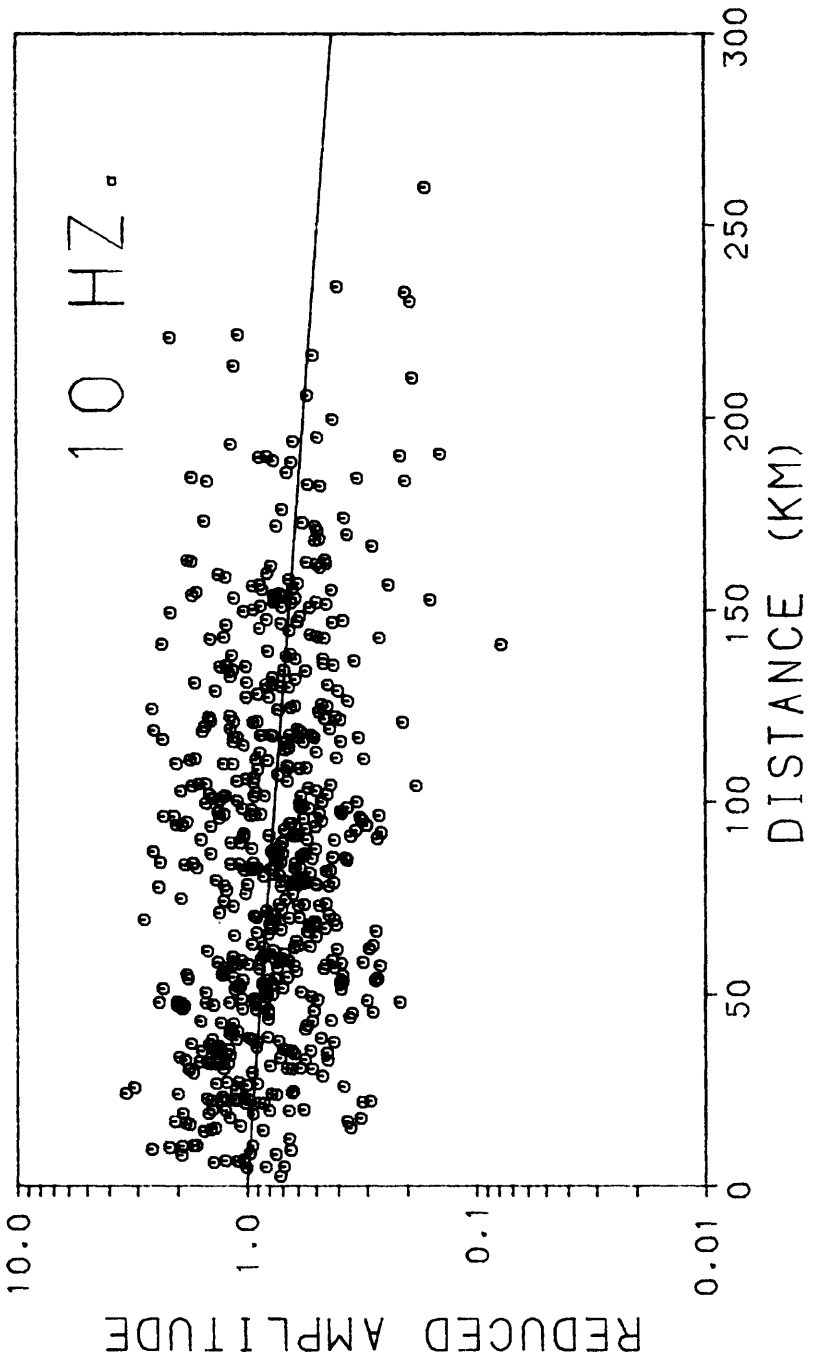

Figure 38. 10-Hz Lg attenuation data of Nuttli (1978) for the New Madrid seismic region.

It can be seen that although there is some scatter, the line is a good fit to the data, indicating that the value of Q for Lg waves at 10 Hz is greater than at 1 Hz by about a factor of two. The question of Q dependence on frequency has recently been examined by Mitchell (1980). Using Lg waves at 1 sec and fundamental- and higher-mode Rayleigh waves, and assuming that Q varies with depth and frequency as

$$Q_\beta\ (\omega,z) = C(z)\omega^\zeta,$$

he indicates that a constant value of ζ between 0.3 and 0.5 can satisfy the available data over the entire period range between 1 and 40 sec (Mitchell, 1980). If we assume a similar form for Q of Lg waves, namely

$$Q(\omega) = C\ \omega^\zeta$$

and use our computed values of Q for Nuttli's data at 1 and 10 Hz, we obtain a value of 0.4 for ζ, which is **consistent** with Mitchell's work thus far.

In Figure 39, we see a plot of source-amplitude magnitude versus average magnitude for the 10-Hz data. The magnitude formulas used to calculate these values were those used for the St. Louis micro-earthquake seismic array (Stauder et al., 1979):

$$\begin{aligned}
m_{b10hz} &= 0.95 \log \Delta\ (\text{km}) + \log A\ (\text{m}\mu) - 1.05 \quad && 10\ \text{km} \leq \Delta \leq 40\ \text{km} \\
m_{b10hz} &= 1.25 \log \Delta\ (\text{km}) + \log A\ (\text{m}\mu) - 1.50 \quad && 40\ \text{km} \leq \Delta \leq 100\ \text{km} \\
m_{b10hz} &= 1.55 \log \Delta\ (\text{km}) + \log A\ (\text{m}\mu) - 2.10 \quad && 100\ \text{km} \leq \Delta \leq 200\ \text{km} \\
m_{b10hz} &= 2.50 \log\ \ (\text{km}) + \log A\ (\text{m}\mu) - 4.30 \quad && 200\ \text{km} \leq \Delta \leq 300\ \text{km}
\end{aligned} \tag{25}$$

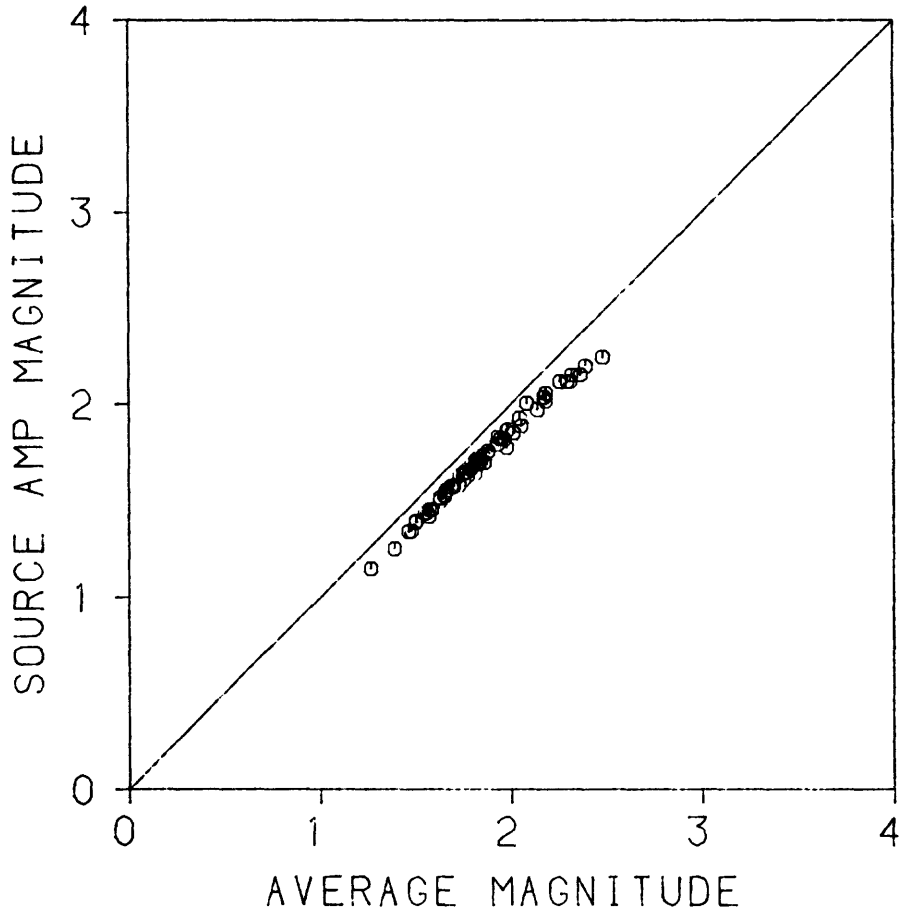

Figure 39. Source amplitude magnitude versus average magnitude for 10-Hz data for New Madrid seismic region.

(The source-amplitude magnitudes were determined by using values of γ and A_o, and equation (4), to determine the value of A at a distance of 10 km, and then using the first of the four formulas listed above.) Once again, we can see that the plot is fairly linear, and that this time the average magnitudes are approximately one-tenth magnitude unit greater than the source-amplitude magnitudes. This is due to the fact that equations (25) assume a Q of 1500, but for this data we found a Q of 3095. This means that the average magnitudes were overcorrected for the effects of attenuation with distance. If this were the case, then for larger magnitude earthquakes, where the closer stations saturate and more distant ones are used for amplitude measurement, we would expect to see a larger discrepancy in magnitudes than for smaller magnitude events. This effect is visible in Figure 39. To show that this overcorrection with distance was indeed the source of the discrepancy in magnitudes, a set of magnitude formulas similar to equations (25) were drawn up, using a γ of 0.0029 km^{-1}. When the average magnitude for an event was calculated using these formulas, it was found to equal the source-amplitude magnitude.

The results of the least-squares analysis of the 1-Hz and 10-Hz unfiltered data showed the merits of our numerical method, giving reasonable values for Q and for source amplitudes at both 1 and 10 Hz. We can now use it on filtered data to cover a range of frequencies between 1 and 10 Hz.

RESULTS: FILTERED DATA

As we have seen, in order to determine the coefficient of anelastic attenuation from Lg amplitude and epicentral distance data, we simply required that all amplitude data be measured at the same frequency. Thus, if we applied our numerical method to data gathered using a particular narrow-bandpass filter setting, we could determine a value for γ at the peak frequency of that filter setting. As mentioned in the data section, we had seven such sets of data from the New Madrid seismic region, spanning a frequency range of 1 to 10.5 Hz. In applying our numerical method, each set of data was analyzed three times, each analysis using a different weighting function (w_{ij} in Equations(13) through (21)). The first time, all data were given equal weight ($w_{ij} = 1$). The second time, the data were weighted according to the square of the signal-to-noise ratio (S_n) of the data (Bevington, 1969). The third time, a ramp function was used to weight the data:

$$w_{ij} = \begin{cases} 0, & S_n \leq 2 \\ \dfrac{S_n - 2}{2}, & 2 \leq S_n \leq 4 \\ 1, & S_n \leq 4 \end{cases}$$

The resulting values of γ and their associated 95% confidence limits for the filtered data can be seen in Table 8, along with the corresponding values for Q. Also listed are the correlation coefficients for the fit of y-observed to y-calculated. In order to provide a visual check on our data, we made plots, for each of the frequencies, of the reduced amplitudes versus epicentral distance, as was done with the unfiltered data in the preceding section. The results are seen in Figures 41-47. Figure 40

TABLE 8

VALUES OF γ AND Q CALCULATED FROM THE NARROW BANDPASS FILTERED DATA, USING DIFFERENT WEIGHTING FUNCTIONS, W

Table 8a
W = 1

FREQ	γ	$Q_- < Q < Q_+$	CORRELATION COEFFICIENT	# OF EVENTS	# OF DATA POINTS
1	.0028 ± .0029	157 < 320 < ---	.963	8	54
1.5	.0038 ± .0026	210 < 354 < 1122	.938	11	73
2	.0032 ± .0023	326 < 560 < 1990	.972	20	142
3	.0043 ± .0019	434 < 625 < 1122	.955	35	238
5	.0029 ± .0015	1020 <1544 < 2992	.970	35	264
8	.0021 ± .0014	2052 <3412 <11968	.984	34	261
10.5	.0017 ± .0015	2945 <5532 <47124	.990	34	260

TABLE 8

VALUES OF γ AND Q CALCULATED FROM THE NARROW BANDPASS FILTERED DATA, USING DIFFERENT WEIGHTING FUNCTIONS, W

Table 8b
$W = (\text{Signal/Noise})^2$

FREQ	γ	$Q_- < Q < Q_+$	CORRELATION COEFFICIENT	# OF EVENTS	# OF DATA POINTS
1	.0029 ± .0003	280 < 310 < 345	.973	8	54
1.5	.0029 ± .0003	421 < 464 < 518	.975	11	73
2	.0047 ± .0002	366 < 382 < 399	.943	20	142
3	.0066 ± .0002	396 < 408 < 421	.888	35	238
5	.0046 ± .0001	955 < 976 < 997	.906	35	264
8	.0024 ± .0001	2872 <2991 <3116	.977	34	261
10.5	.0017 ± .0001	5225 <5532 <5878	.985	34	260

TABLE 8

VALUES OF γ AND Q CALCULATED FROM THE NARROW BANDPASS FILTERED DATA, USING DIFFERENT WEIGHTING FUNCTIONS, W

Table 8c
W = Ramp Function

FREQ	γ	$Q_- < Q < Q_+$	CORRELATION COEFFICIENT	# OF EVENTS	# OF DATA POINTS
1	$.0028 \pm .0026$	$166 < 320 < 4488$	.963	8	54
1.5	$.0037 \pm .0023$	$224 < 363 < 962$	.942	11	73
2	$.0032 \pm .0019$	$375 < 560 < 1378$	.972	20	142
3	$.0047 \pm .0016$	$427 < 572 < 869$	.942	35	238
5	$.0033 \pm .0012$	$997 < 1358 < 2137$	.960	35	264
8	$.0021 \pm .0012$	$2176 < 3412 < 7979$	.984	34	261
10.5	$.0020 \pm .0012$	$2945 < 4703 < 11781$	.984	34	260

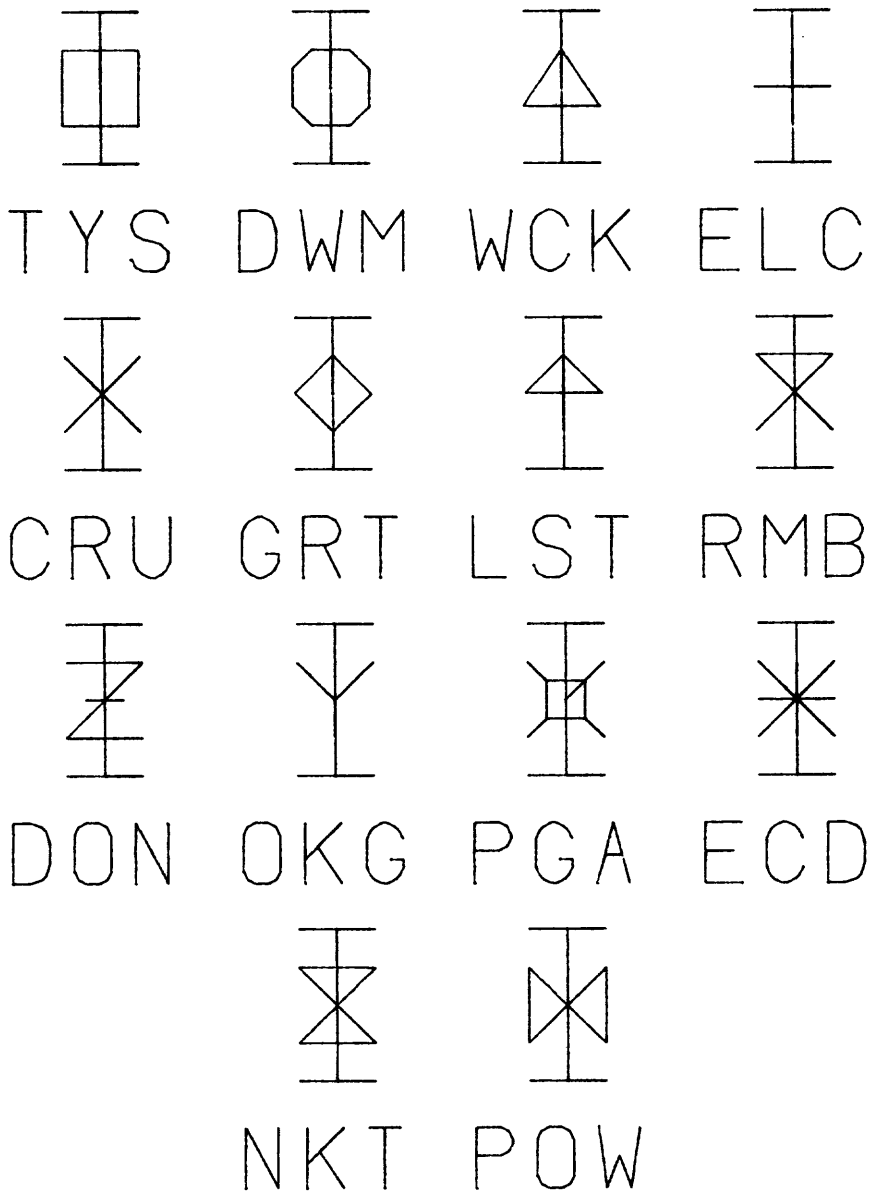

Figure 40. Station symbols used in Figures 41-54.

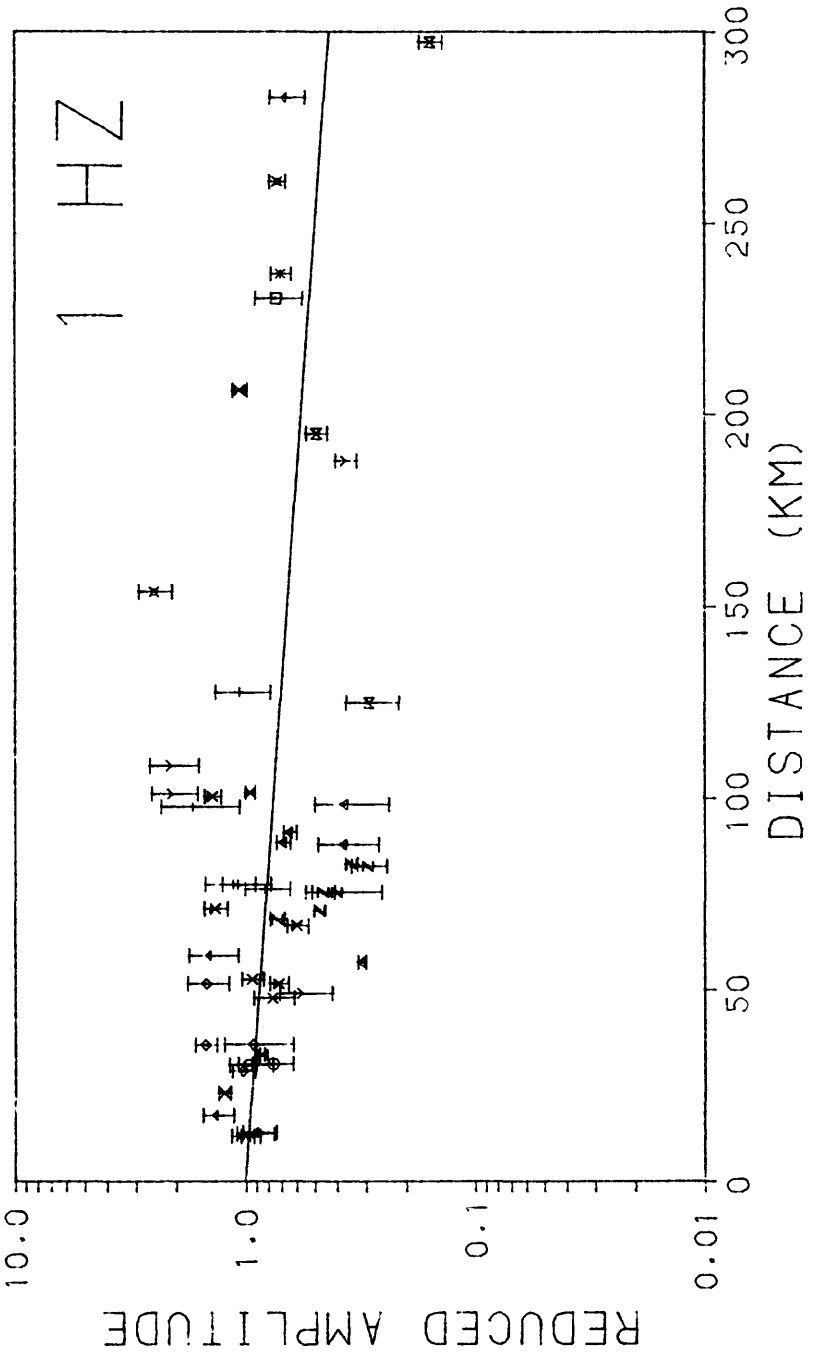

Figure 41. 1-Hz Lg attenuation using ramp weighting function. Error bars represent the level of background noise at each station.

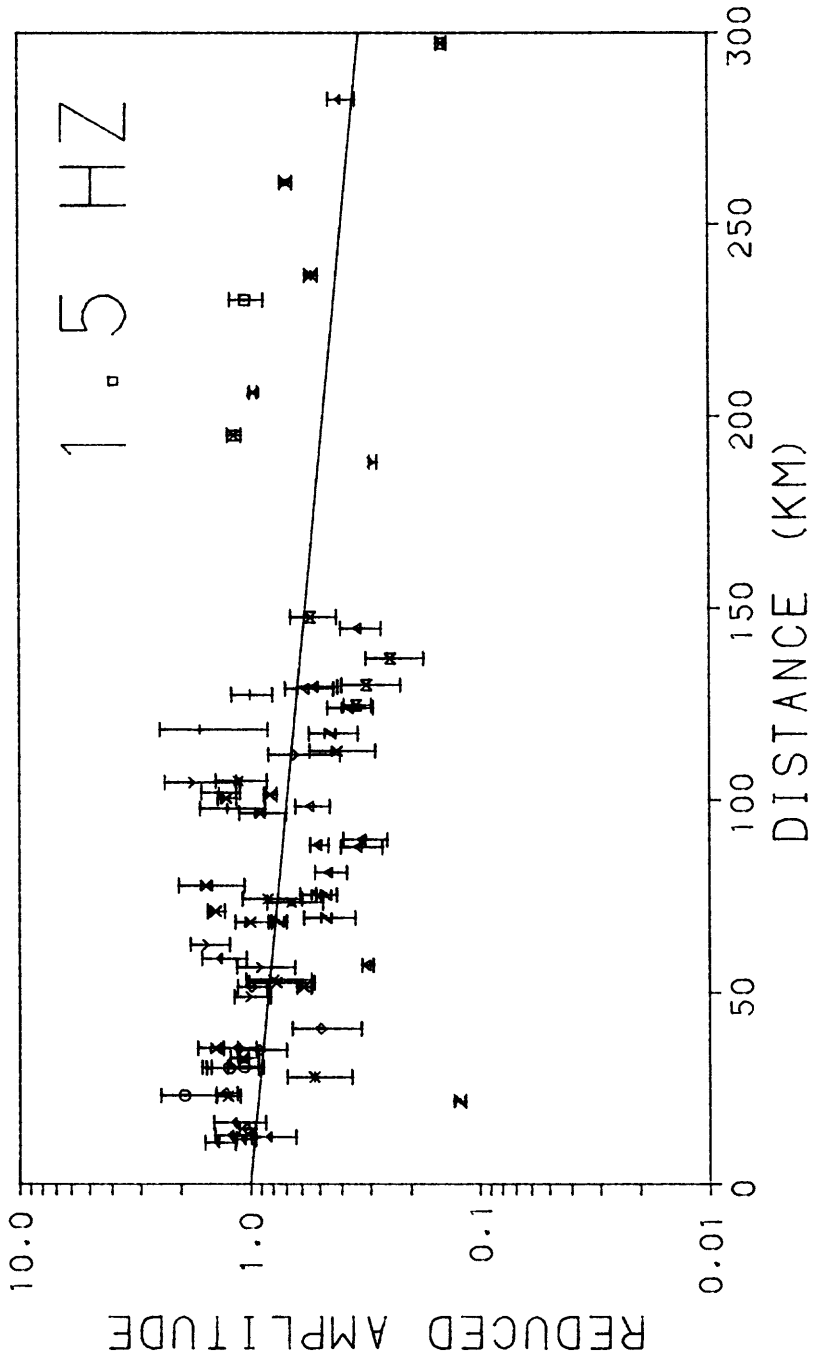

Figure 42. 1.5-Hz Lg attenuation using a ramp weighting function.

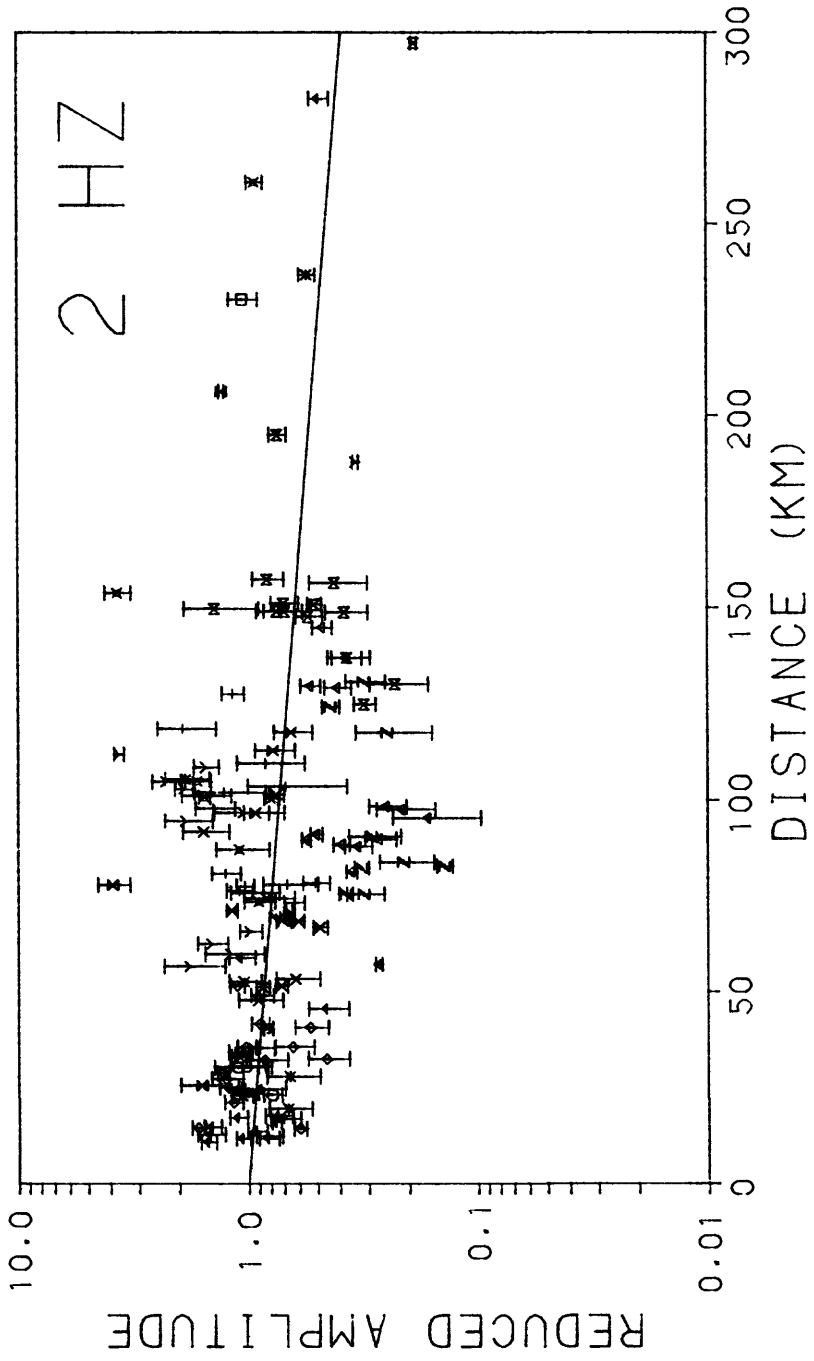

Figure 43. 2-Hz Lg attenuation using a ramp weighting function.

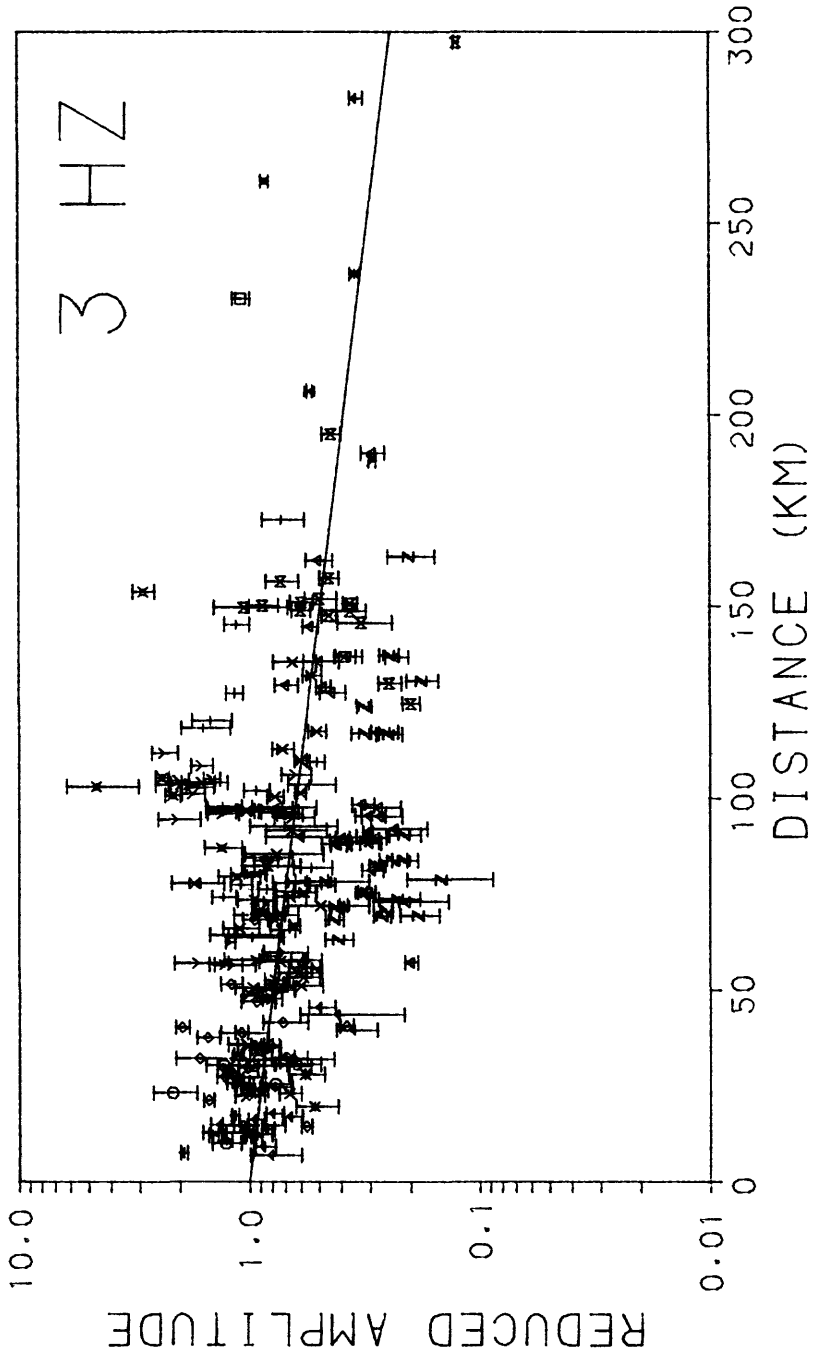

Figure 44. 3-Hz Lg attenuation using a ramp weighting function.

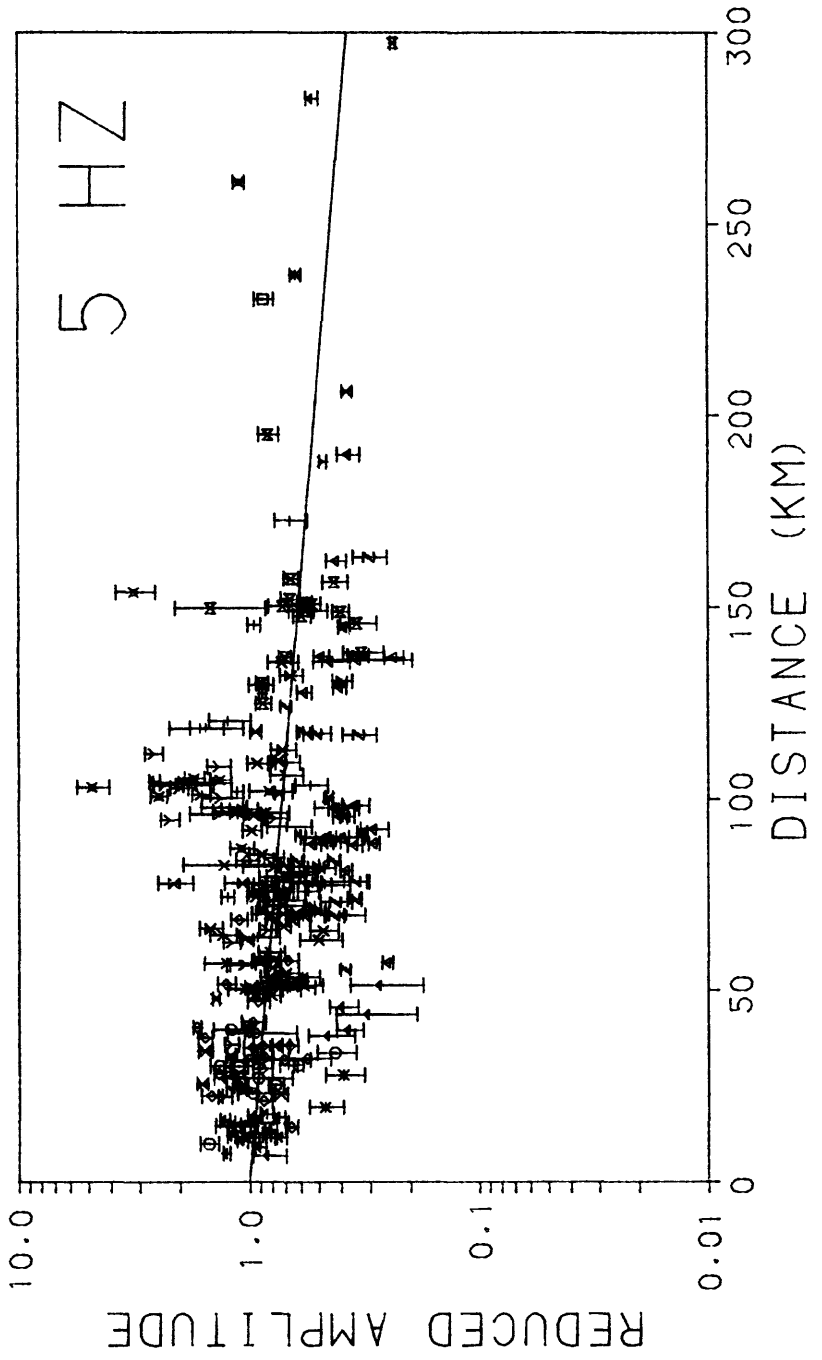

Figure 45. 5-Hz Lg attenuation using a ramp weighting function.

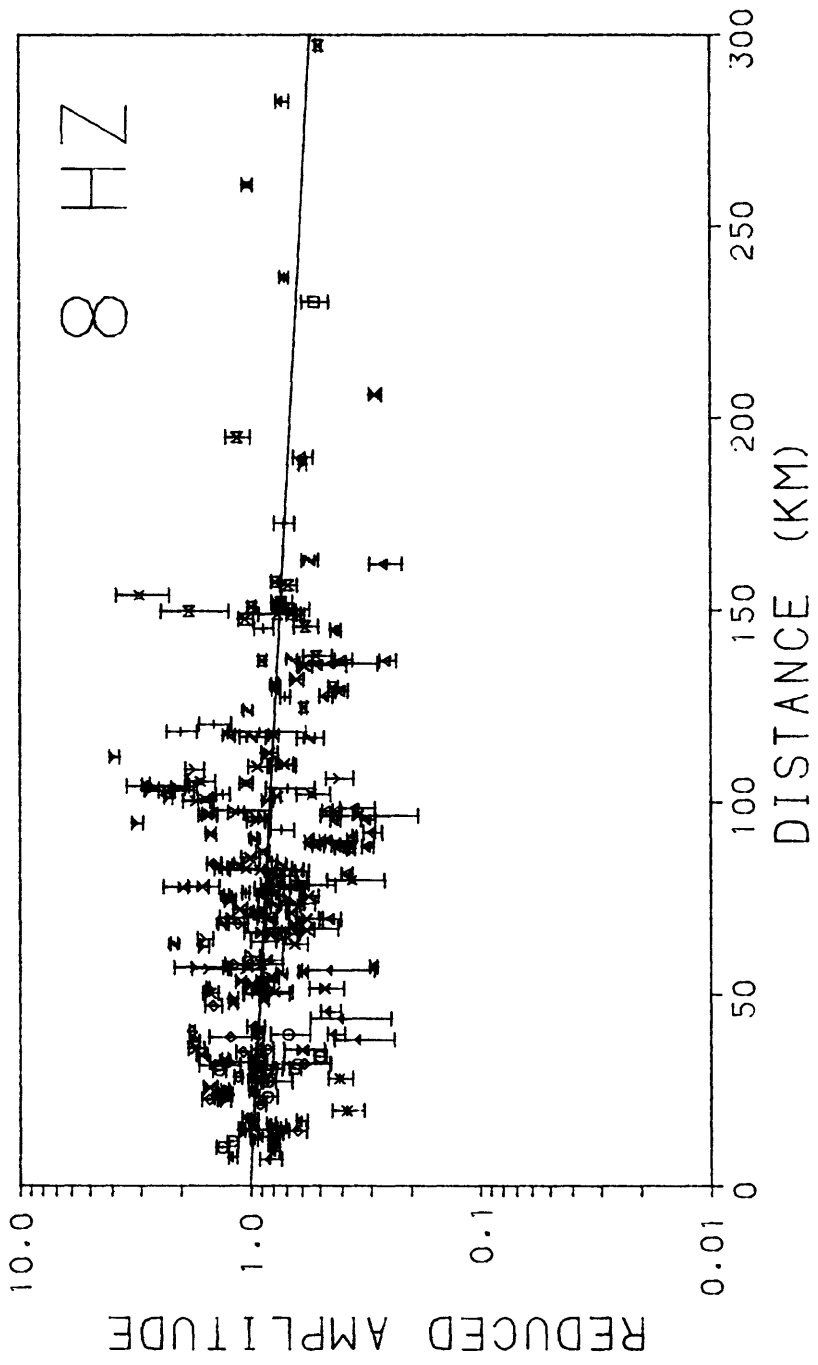

Figure 46. 8-Hz attenuation using a ramp weighting function.

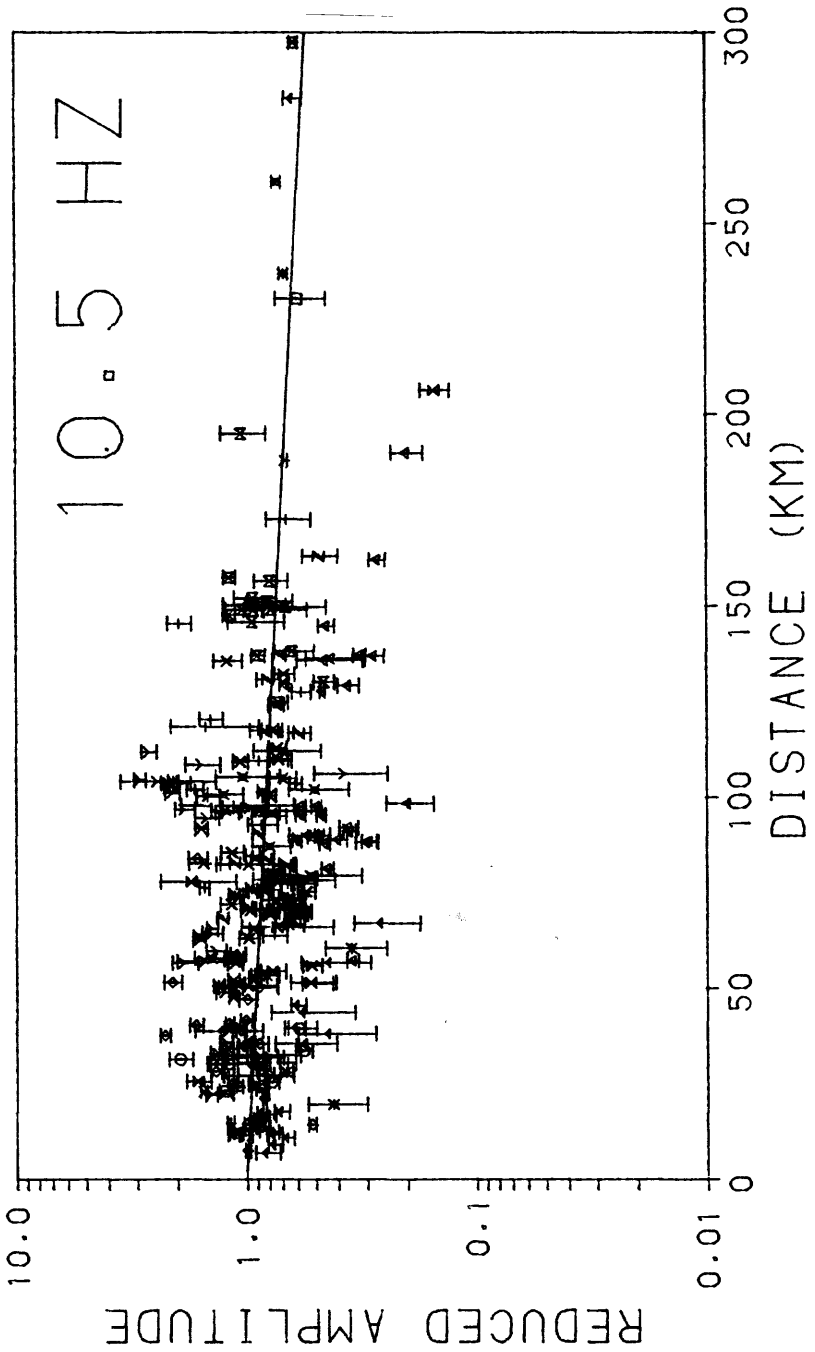

Figure 47. 10.5-Hz attenuation using a ramp weighting function.

gives the symbols used for each of the fourteen network stations. The results plotted are those obtained with the ramp weighting function, which seemed the most reasonable to use. (Poor signal-to-noise ratio seemed a likely source of error, so it did not appear reasonable to give equal weight to all the data. On the other hand, a weighting function proportional to the square of the signal-to-noise ratio risked giving too much weight to data from normally quiet sites and from close-in stations, increasing possible azimuthal or station bias errors.)

Perhaps the most obvious observation to make from Table 8, regardless of the weighting function used, is the dependence of the quality factor, Q , on the frequency. The values of Q previously obtained by Nuttli (1973,1978) seemed to indicate a constant Q of 1500 between 1 and 10 Hz for the New Madrid seismic region. As we have shown, our unfiltered data seemed to indicate an increase in Q between 1 and 10 Hz, with a value for Q at 1 Hz of 1292, and at 10 Hz of 3090. The filtered results also show an increase in Q with frequency, but the Q values at the lower frequencies are much less than would have been expected from the results using unfiltered data. This effect, however, can be understood as we consider sources of possible error in our Q values. First of all, it must be pointed out that there is a sparsity of data for the lower frequencies, especially for 1 and 1.5 Hz, as compared with the higher frequencies. Second, as we can see from Figures 41-47, we have a predominance of data, for all frequencies, in the epicentral range of 10-150 km. A wider range of distances would be an obvious asset to the determination of γ, particularly at the larger distances where the effect of absorption dominates over that of geometric spreading. Third, it has been noticed that stations located in the Mississippi

embayment seem to have a background noise level with a predominant frequency range of 1-3 Hz, while this effect has not been noticed for highland stations. As can be seen in Figure 2, for most of the events used, the stations closest to the epicenters are located in the embayment. This means that for the lower frequencies, the closest stations will have their measured amplitudes enhanced by the background noise level, while the more distant highland stations will be unaffected. The result of this will be an apparently larger attenuation of the Lg amplitude with distance than would normally be observed, hence a lower Q value than expected. If this is indeed a reason for the low Q values, it means that a spectral study of the background noise level in different parts of the region under study could be important in determining the proper rate of attenuation of Lg waves in that region.

Other possible errors in our measured values of γ are those introduced by possible azimuthal or station bias effects. To see if such effects are present here, we plotted the normalized amplitude versus azimuth, where the normalized amplitude is corrected for source function and attenuation. From Equation (4):

$$A = A_o \Delta^{-1/3} (R_o \sin \Delta^\circ)^{-1/2} \exp(-\gamma\Delta)$$

so

$$[(A \Delta^{1/3} (R_o \sin \Delta^\circ)^{1/2}) / A_o] \exp(+\gamma\Delta) = 1$$

This normalized amplitude should be equal to unity, and systematic azimuthal or station effects should be obvious as gross trends in the data. In figures 48-54, the normalized amplitude versus azimuth is plotted for each of the filter frequencies, using the station symbols

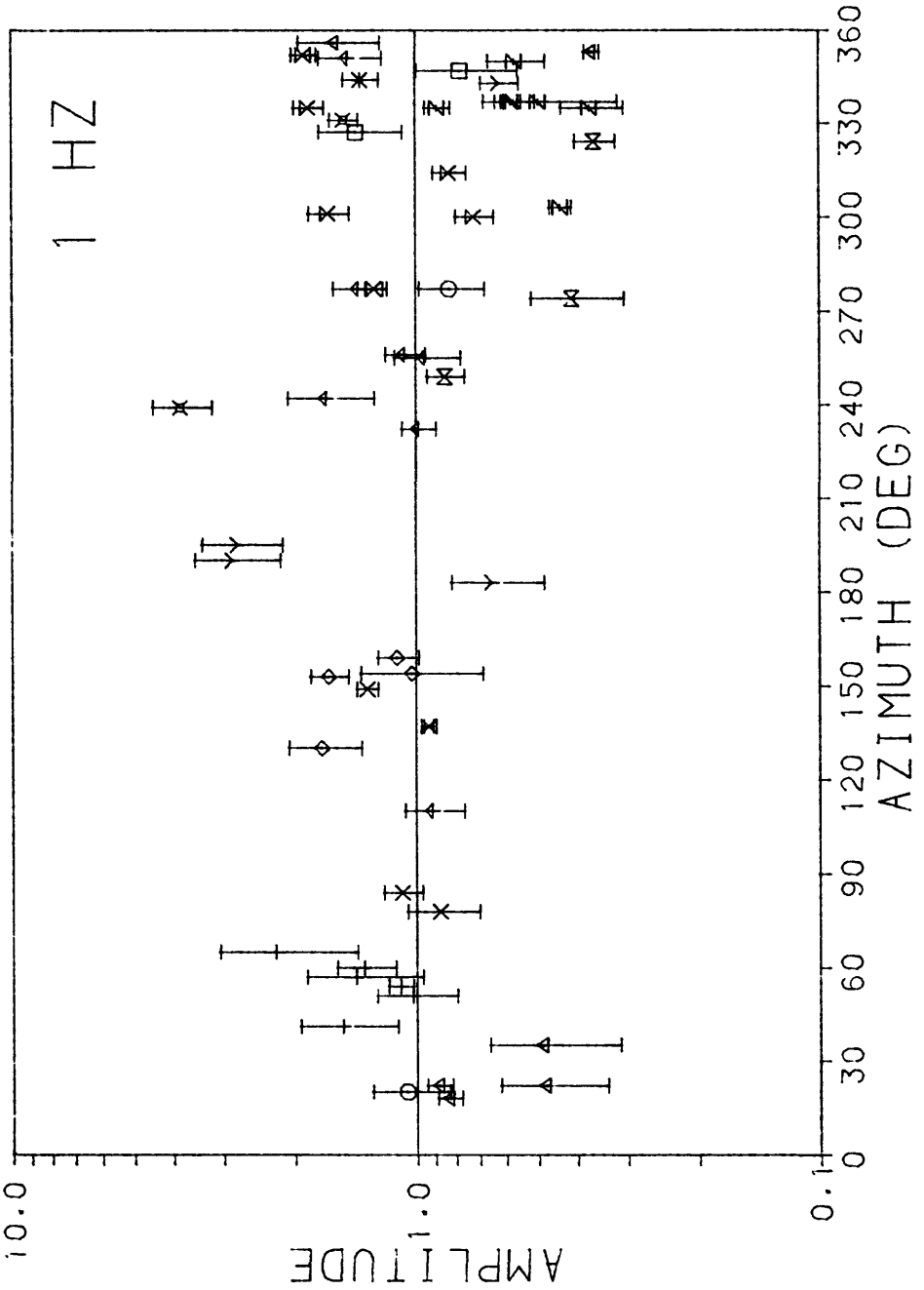

Figure 48. Normalized 1-Hz amplitudes as a function of azimuth from epicenter to staion. Error bars represent the level of background noise at each station.

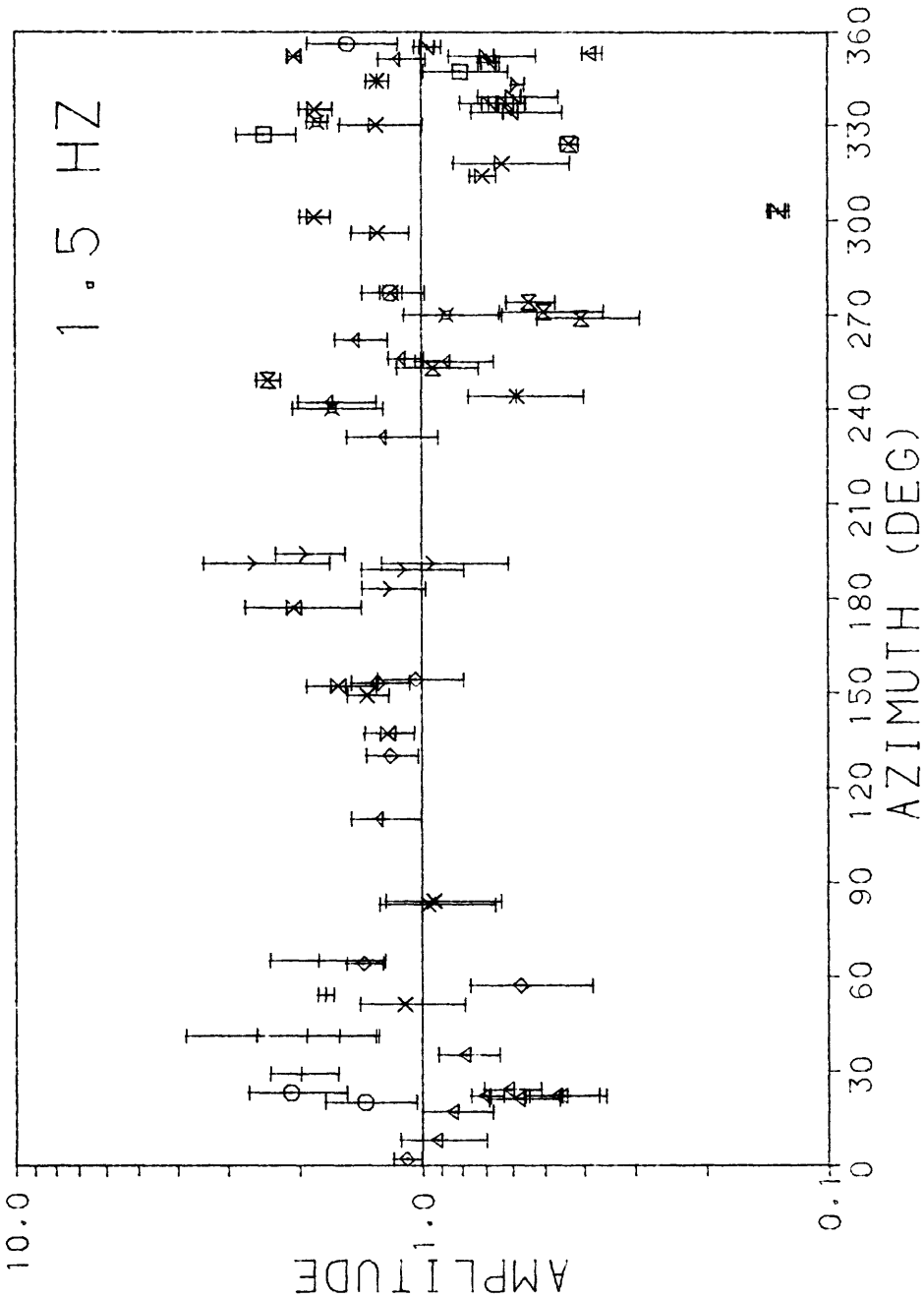

Figure 49. Normalized 1.5-Hz amplitudes as a function of azimuth from epicenter to station.

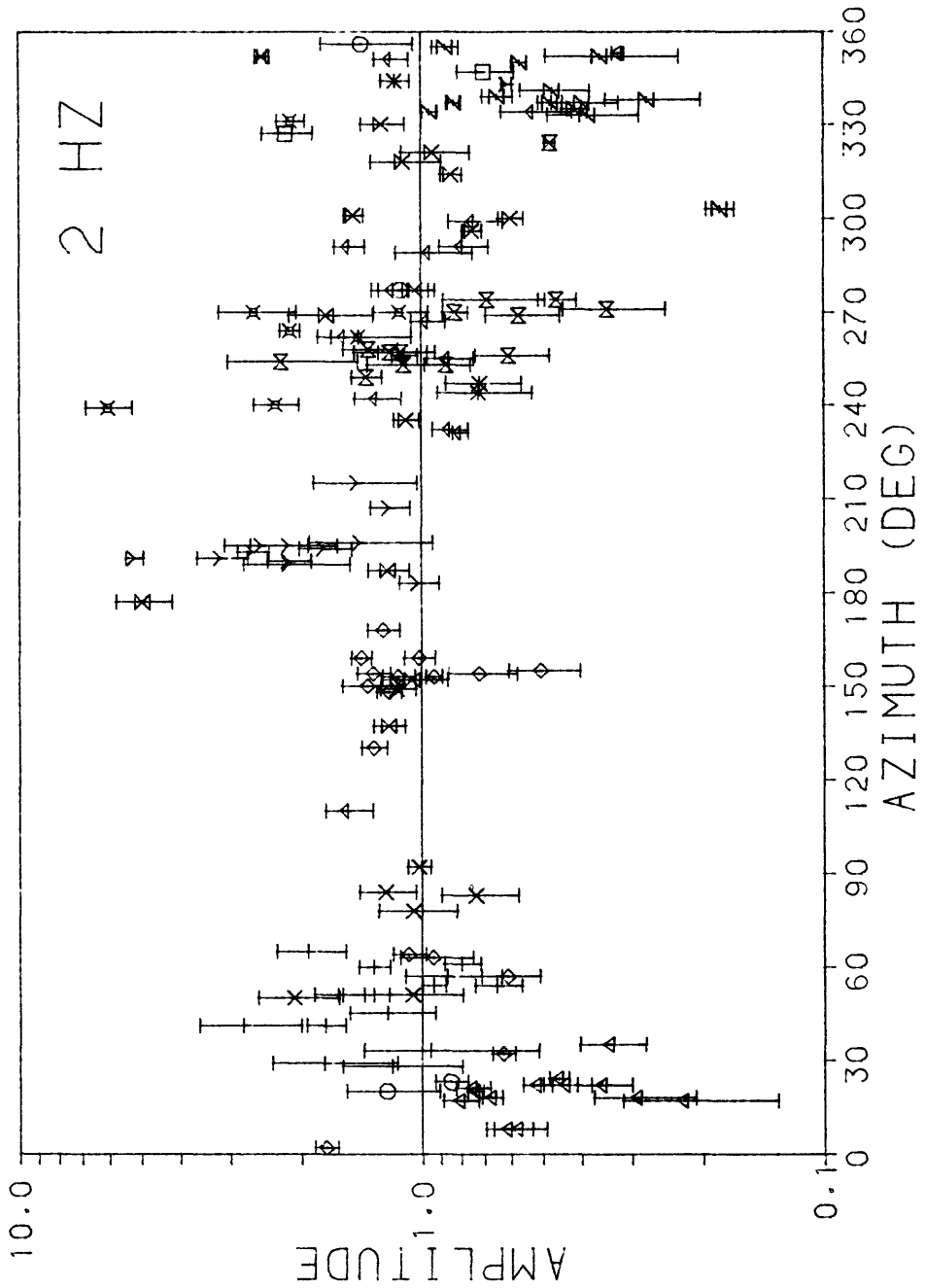

Figure 50. Normalized 2-Hz amplitudes as a function of azimuth from epicenter to station.

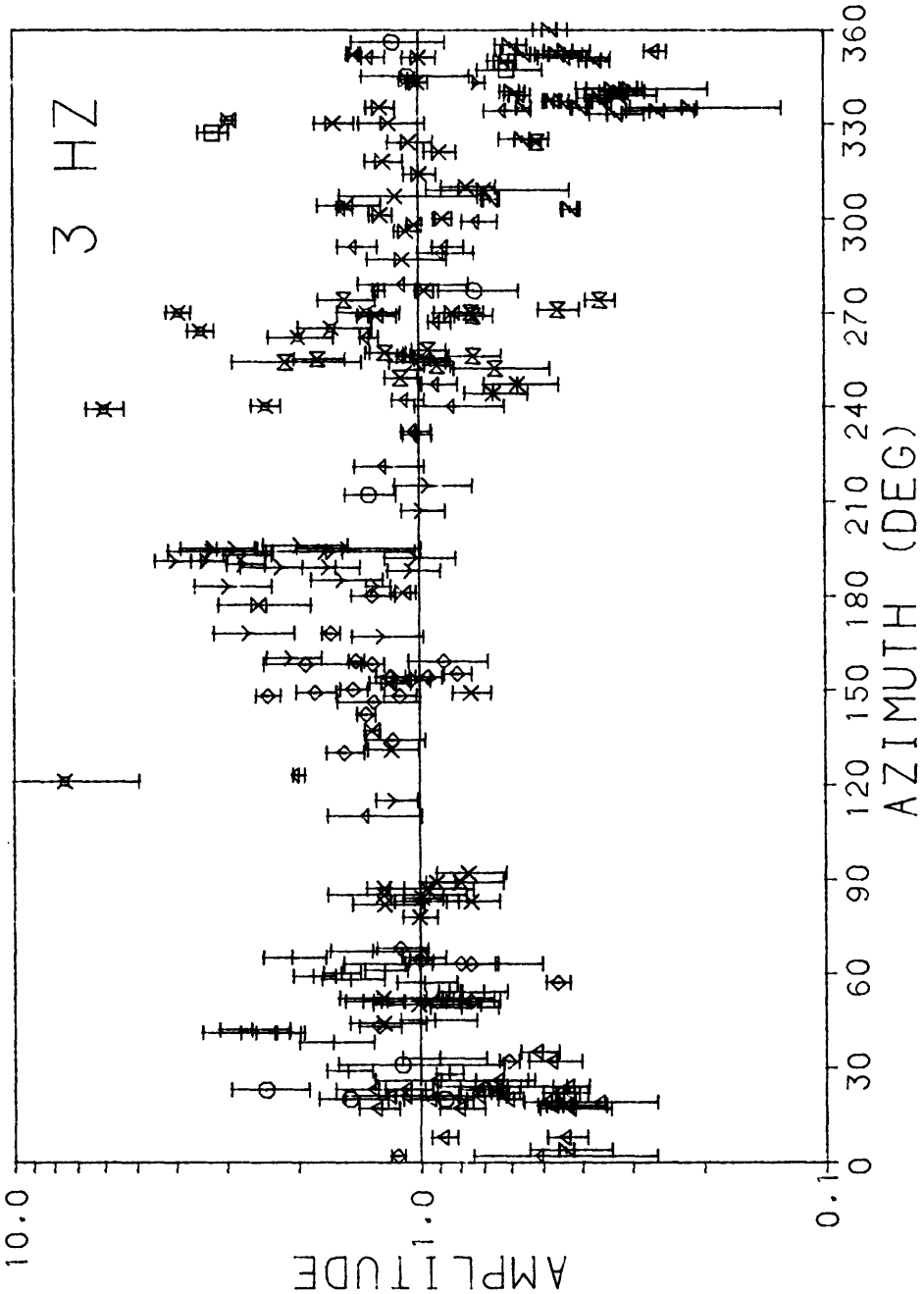

Figure 51. Normalized 3-Hz amplitudes as a function of azimuth from epicenter to station.

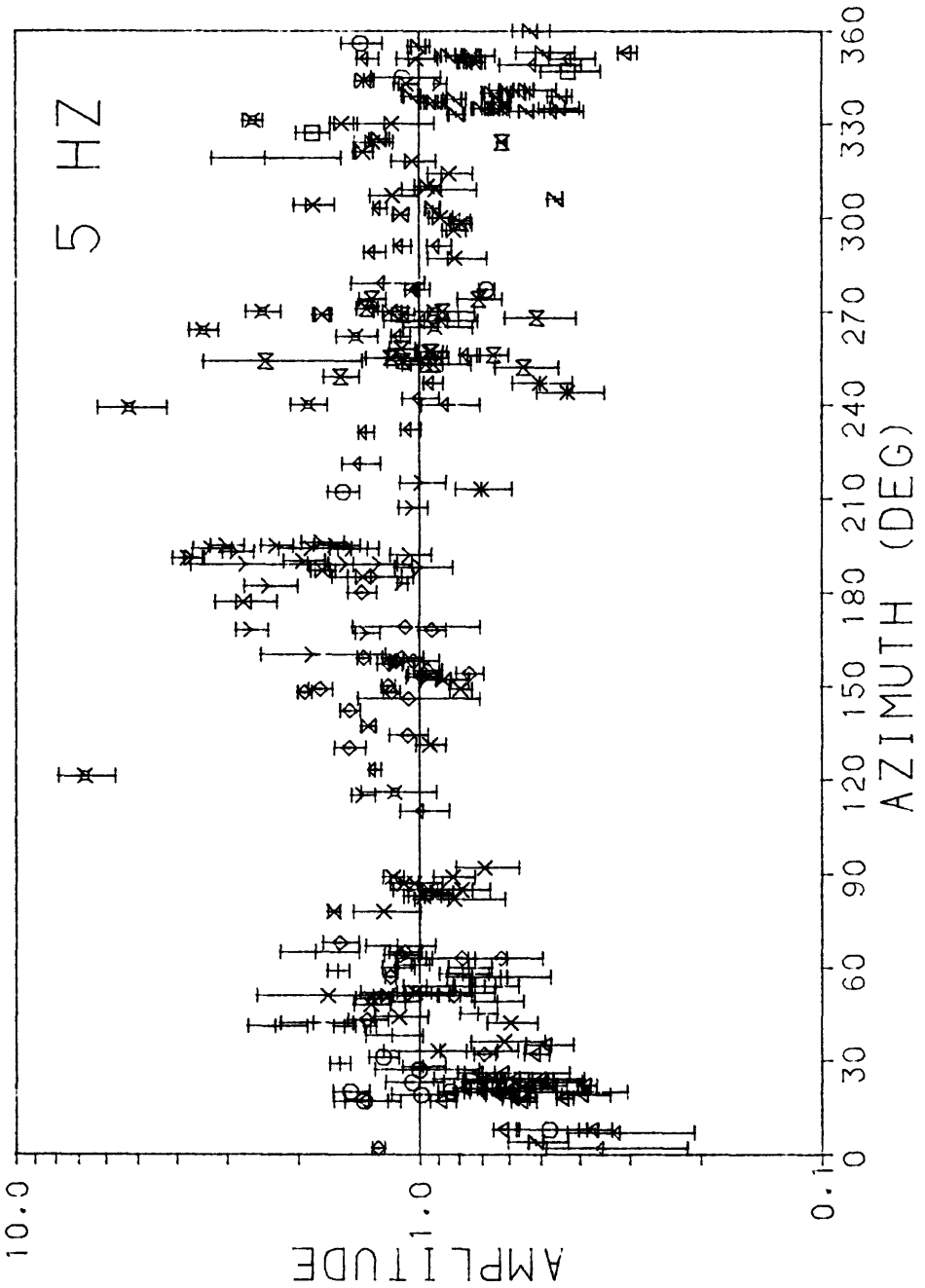

Figure 52. Normalized 5-Hz amplitudes as a function of azimuth from epicenter to station.

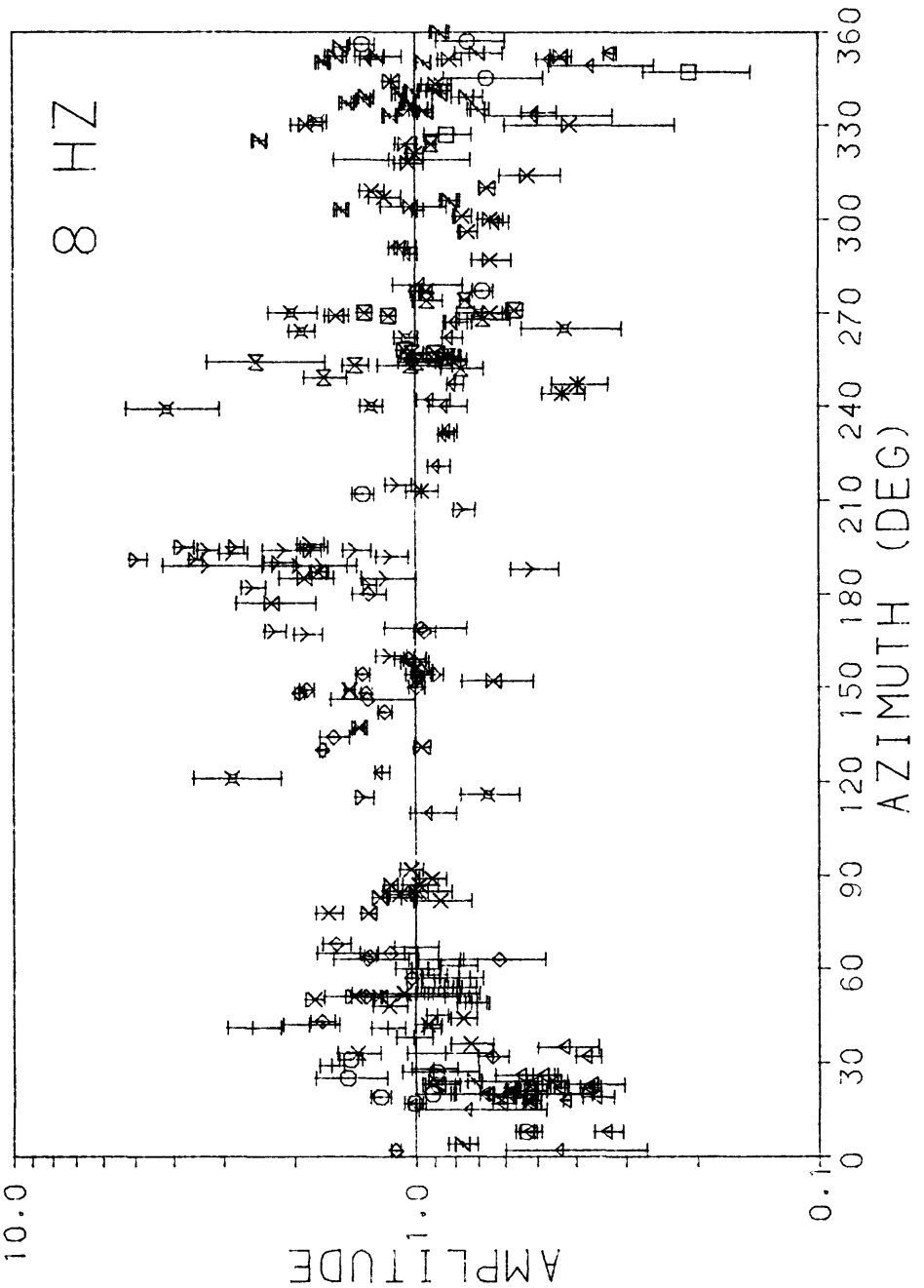

Figure 53. Normalized 8-Hz amplitudes as a function of azimuth from epicenter to station.

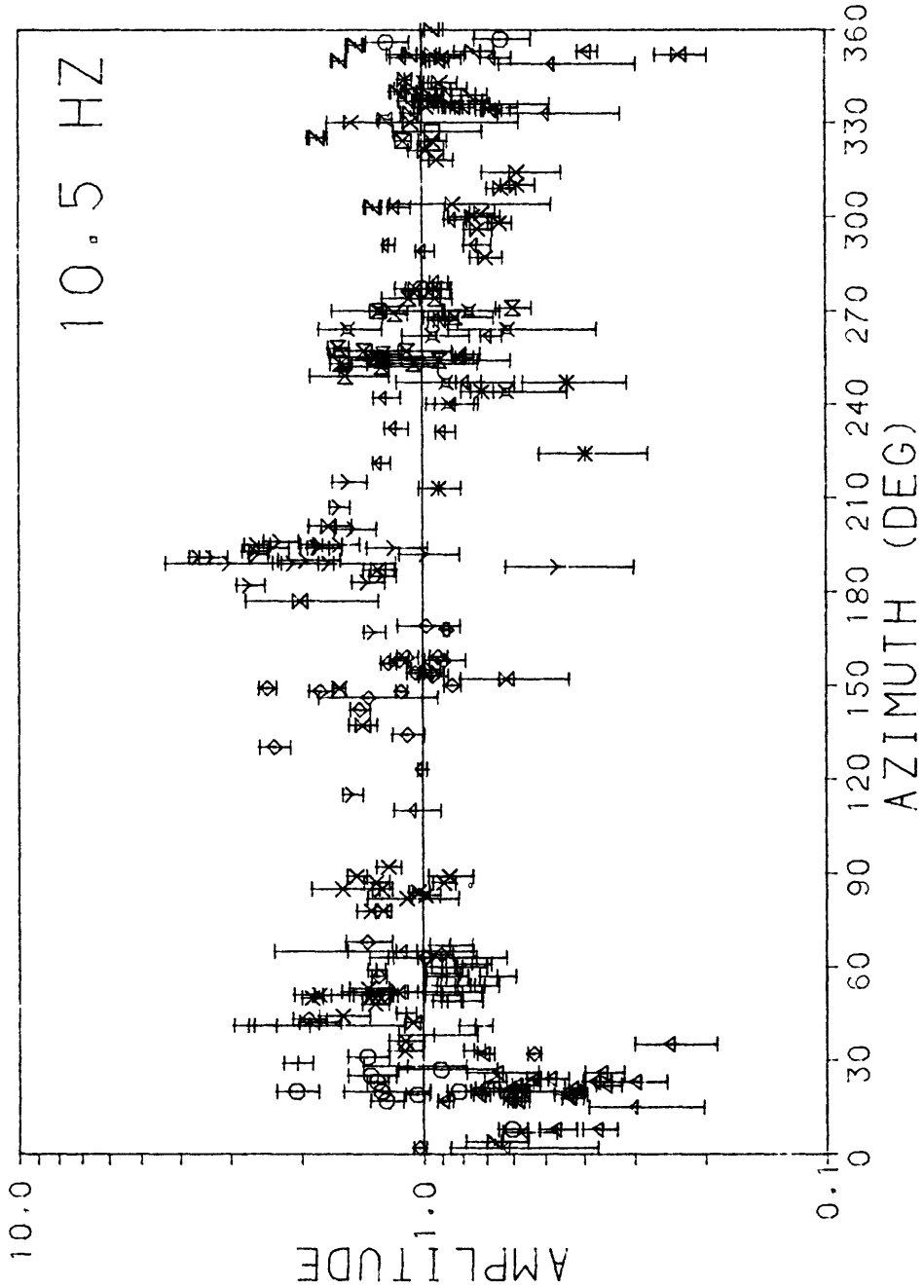

Figure 54. Normalized 10.5-Hz amplitudes as a function of azimuth from epicenter to station.

from Figure 40. Looking at these data, we can see a definite trend toward high values at approximately 170°-200°, consisting largely of data from OKG, and an obvious trend toward low values in the range of 350°-40°. These consist mainly of data from two stations, DON and WCK. The normalized amplitudes at DON seem to be frequency dependent, while those of WCK are low at all frequencies. These observations could be interpreted in two ways. The first and most obvious is that the bias is inherent in the stations themselves, as perhaps in the case of DON. However, if we look at our map of the network (Figure 1), we can see that WCK, which has consistently low normalized amplitudes, lies on a line along the embayment upriver from the chosen events, while OKG, which has rather consistently high normalized amplitudes, lies on a line along the embayment downriver from the chosen events. Perhaps this also has a bearing on the problem.

Along with the values of γ obtained by the numerical fit, we also obtained source amplitudes for each of the events at each of the frequencies. These values are given in Table 9. If, for each event, we were to plot source amplitude versus frequency, the result would be a time-domain source "spectrum". This would give the ground displacement at 1 km for Lg waves of a specific frequency (or,more accurately, the displacement measured using a Kronhite filter centered at that specific frequency.) Empirically, from a study of the Kronhite filters, if we divide the source amplitude at each frequency by the square root of the bandwidth (half-width) of the filter, we obtain the spectral level of the frequency-domain spectrum at that frequency. Hence, if we plot these corrected amplitudes versus frequency, we arrive at the frequency-domain source spectrum. This

TABLE 9

SOURCE AMPLITUDES (MICRONS) FOR THE
EVENTS USED FOR EACH BANDPASS FILTER FREQUENCY

EVENT	1	1.5	2	3	5	8	10.5
1	**1.46**	**1.53**	1.27	1.31	1.26	1.30	1.28
2	---	---	---	1.39	1.62	1.30	1.87
3	---	---	---	.49	.47	.35	1.91
4	---	---	---	2.50	2.92	---	3.02
5	---	---	---	.76	.82	.62	---
6	---	1.66	1.15	2.60	2.39	1.87	1.96
7	3.29	---	2.56	3.03	2.83	2.31	2.08
8	---	---	---	1.19	.66	.20	1.58
9	---	---	---	2.09	1.92	1.51	1.49
10	---	---	---	1.25	.84	.83	1.98
11	---	---	---	.62	.44	.41	1.12
12	2.73	2.10	1.68	2.31	2.43	2.30	2.68
13	3.90	---	2.54	3.87	3.59	2.96	3.67
14	---	.82	1.40	1.54	1.38	1.32	1.88
15	---	---	---	.24	.27	.34	.85
16	---	.78	.70	1.22	1.51	1.10	1.48
17	---	---	**.85**	2.08	1.62	1.17	1.29
18	5.03	3.19	2.81	4.76	3.68	2.06	2.30
19	2.74	2.37	1.47	2.30	2.48	1.66	2.29
20	---	---	1.98	2.33	2.35	2.18	2.01
21	---	---	1.52	1.73	1.83	1.66	1.77
22	---	---	3.31	3.00	2.38	2.05	2.47
23	---	---	---	1.56	2.18	1.46	1.66
24	---	---	3.75	5.21	4.29	3.20	3.85
25	1.20	1.33	1.46	**1.79**	1.96	1.88	2.23
26	---	---	---	1.25	1.46	1.37	1.53
27	---	---	---	1.09	1.04	1.02	1.23
28	---	---	---	1.90	2.62	2.47	2.14
29	---	---	---	1.38	1.36	1.18	1.53
30	---	---	.31	.78	.99	1.77	1.72
31	28.75	43.29	**36.17**	69.60	52.59	23.80	17.49
32	---	---	1.37	1.46	1.97	2.14	1.91
33	---	1.58	1.48	1.88	2.16	1.86	1.88
34	---	---	---	1.12	.94	.91	.94
35	---	1.41	1.72	2.29	2.20	1.84	2.21

procedure was followed for all events which had a frequency range of 10 Hz. The spectra of thirteen such events are plotted in Figures 55-67.

The bandwidths of the various filter settings are as follows:

freq (Hz)	bandwidth (Hz)
1	.95
1.5	1.5
2	1.9
3	2.7
5	3.8
8	5.1
10.5	5.8

Looking at the time-domain "spectra", we notice that they are fairly level in the frequency range 1 to 10 Hz. They do not resemble the typical frequency-domain source spectra, which have an ω^{-2} fall off for higher frequencies, in spite of the fact that for the magnitudes of the events used in this study, the corner frequencies of the source spectra should have a value between 1 and 10 Hz. (For m_b = 2.5, the corner frequency is 3.1 Hz; for m_b = 1.5, the corner frequency is 6.8 Hz.) (Street et al., 1975). This discrepency was thought to be due to the fact that the bandwidth of the filter increased as the center frequency of the filter increased; thus although the source spectrum at high frequencies might have had an ω^{-2} fall off, the observing window for energy was wider at higher frequencies, which would have compensated for the drop in spectral amplitudes. However, it is still quite difficult to pick a corner frequency from most of the frequency-domain spectra, which have been corrected for bandwidth. The major exception to this is Event 31 (Figure 65), where a drop in amplitude with frequency of approximately ω^{-2} is readily observable on the frequency-domain

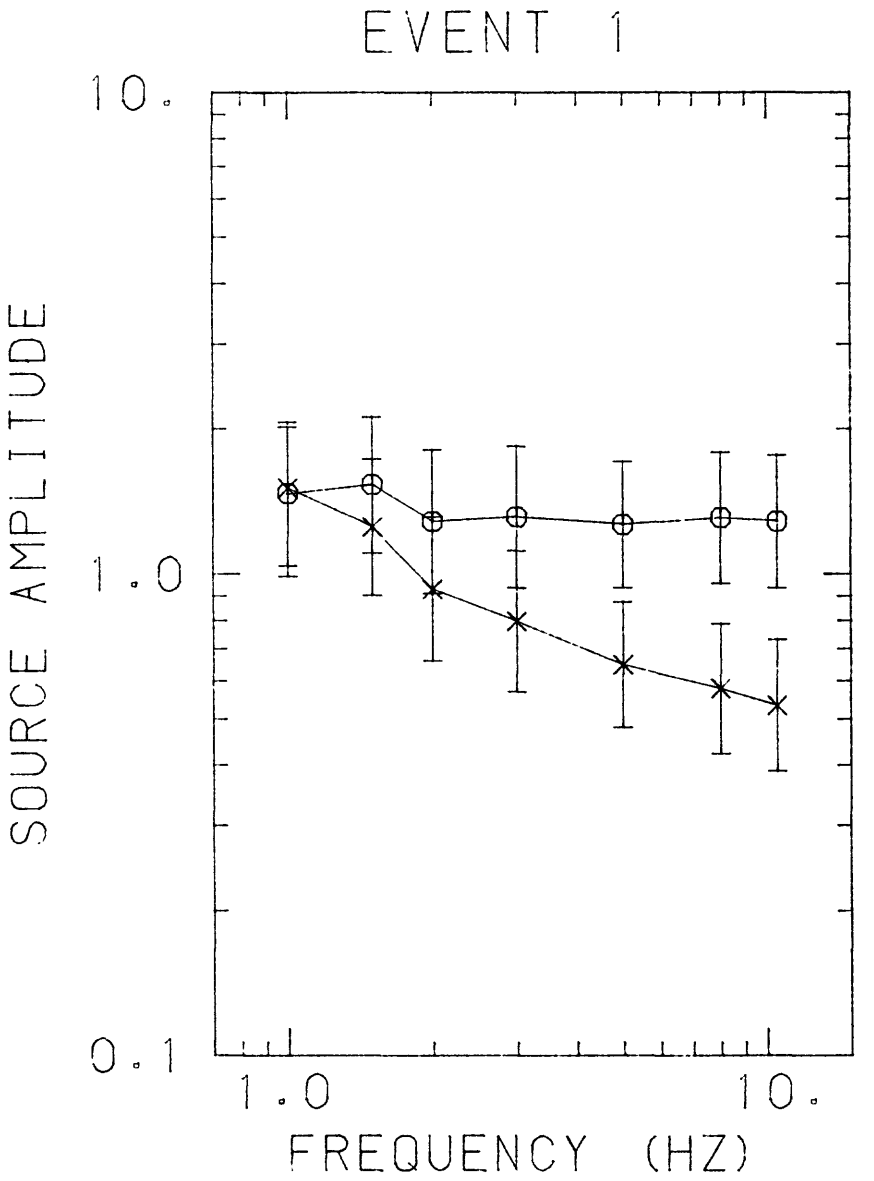

Figure 55. Source spectra for Event 1. The circles represent the time domain "spectrum" with the source amplitude in units of microns; the crosses represent the frequency spectrum in units of micron-seconds.

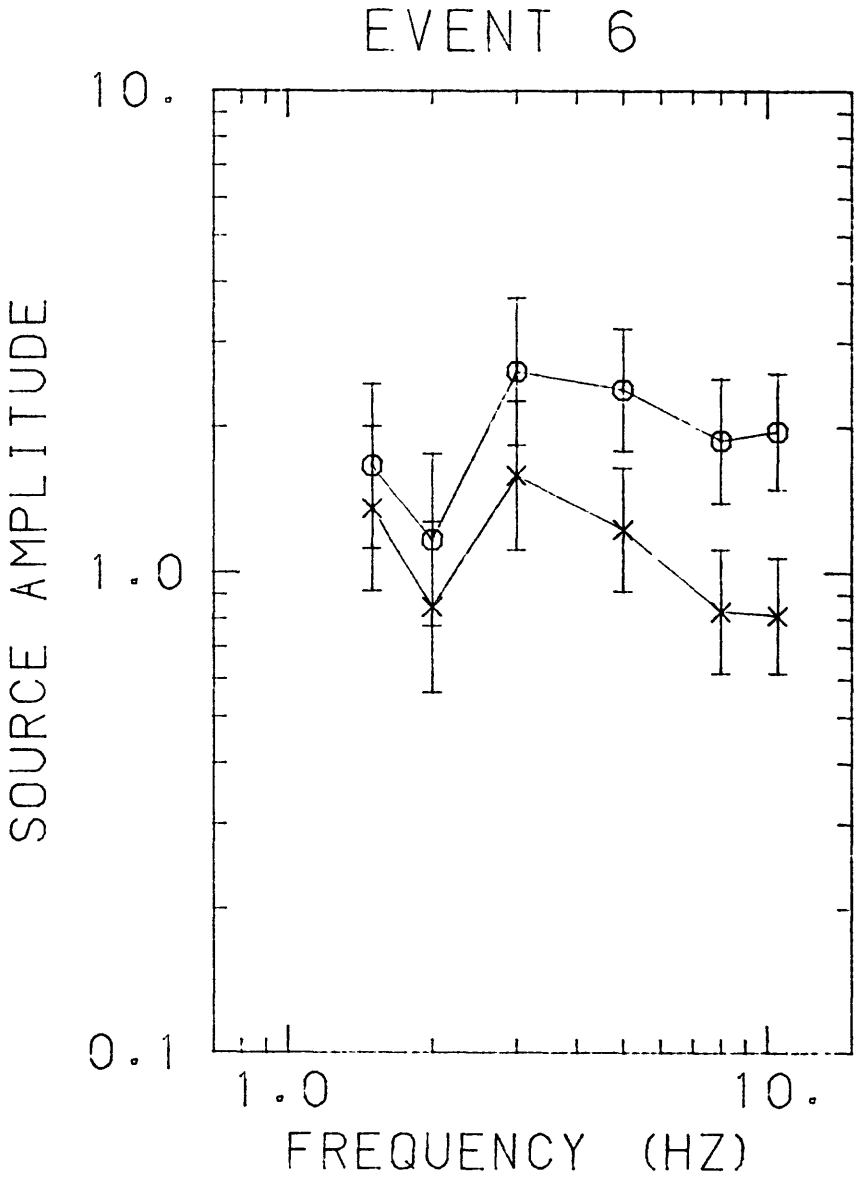

Figure 56. Source spectra for Event 6.

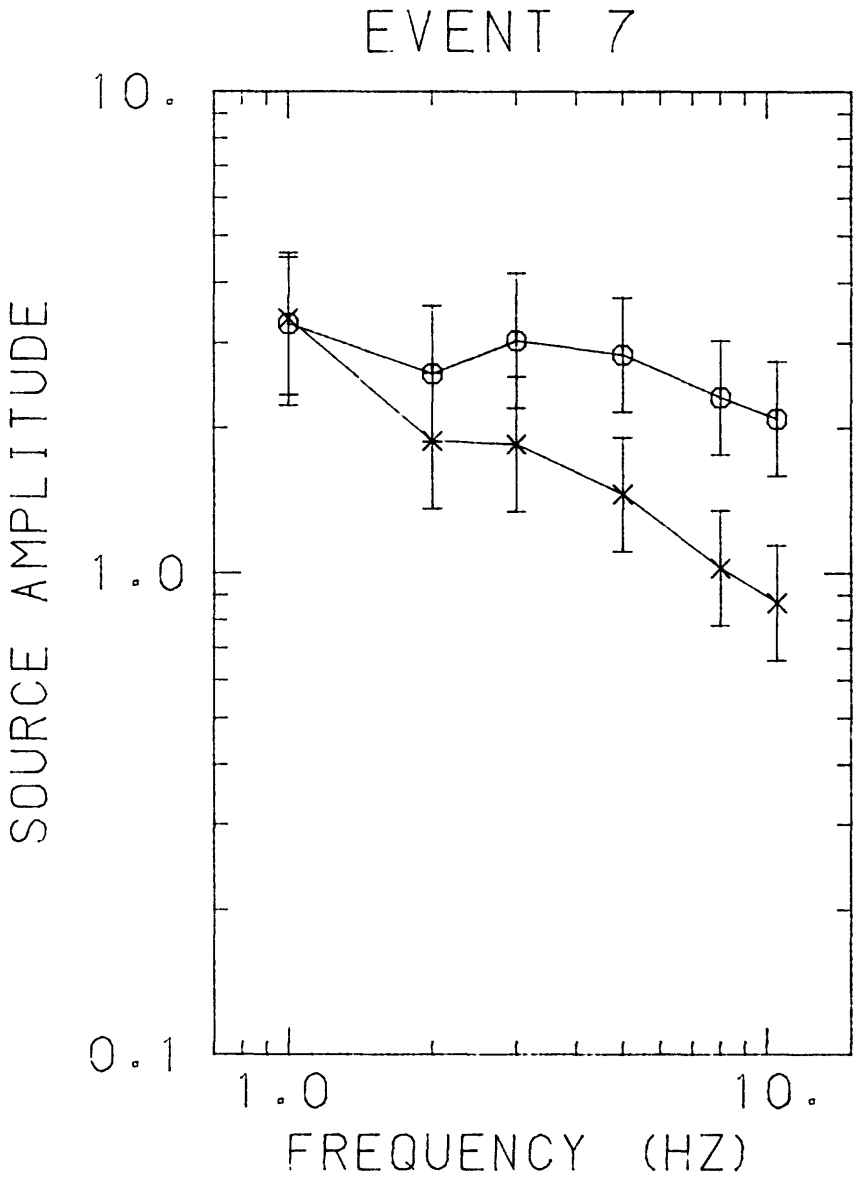

Figure 57. Source spectra for Event 7.

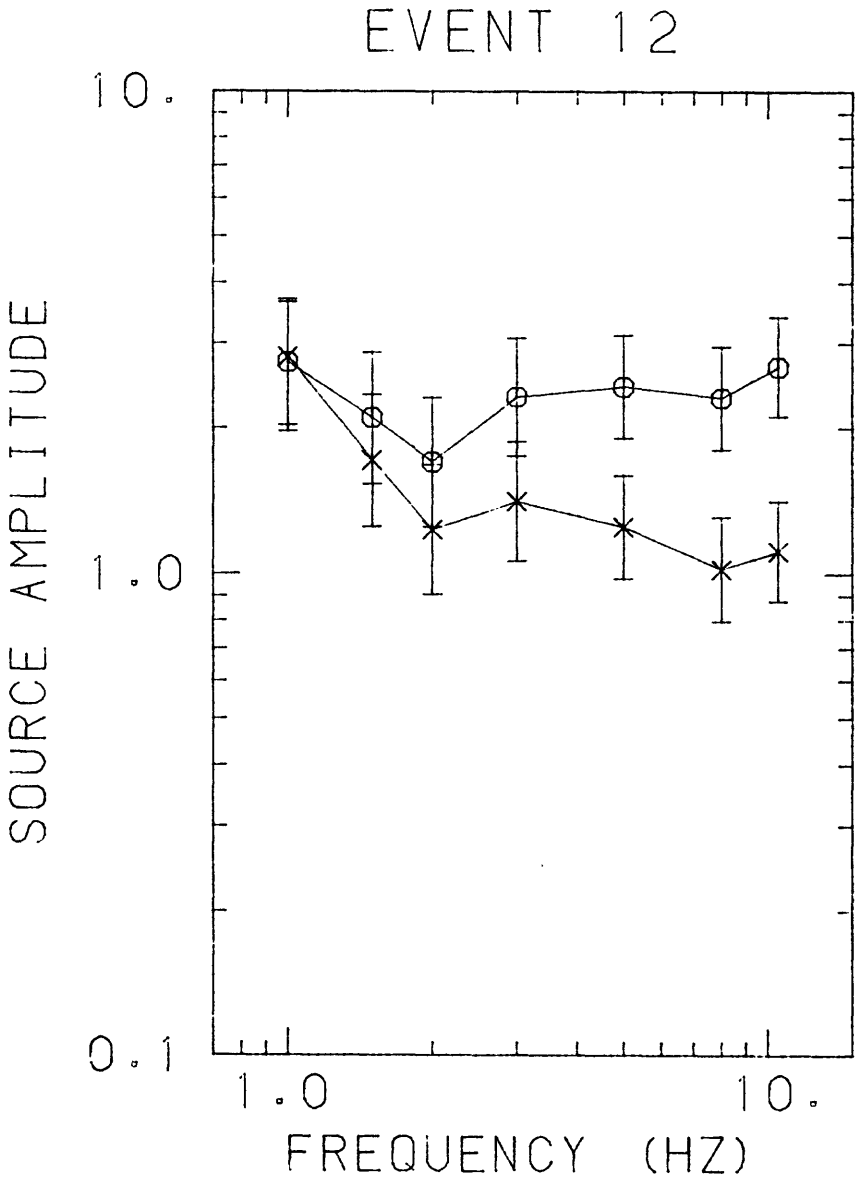

Figure 58. Source spectra for Event 12.

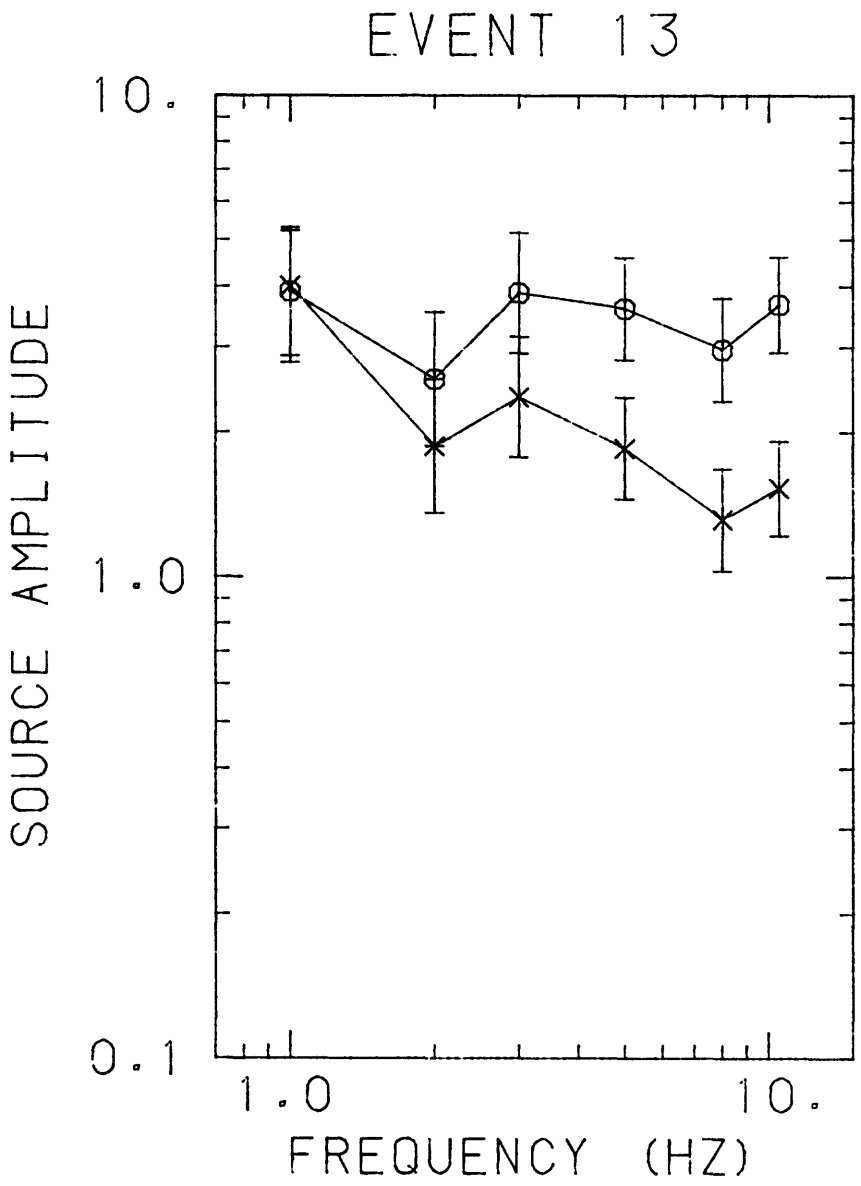

Figure 59. Source spectra for Event 13.

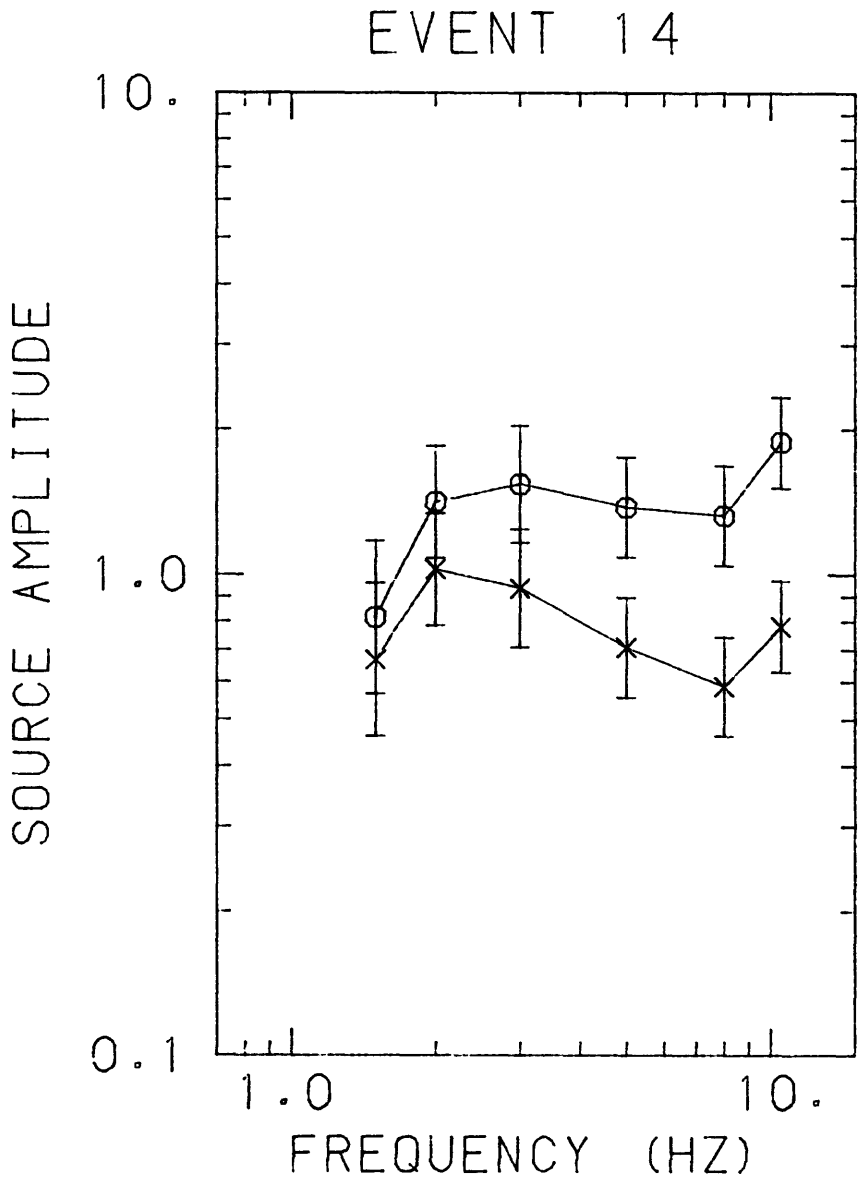

Figure 60. Source spectra for Event 14.

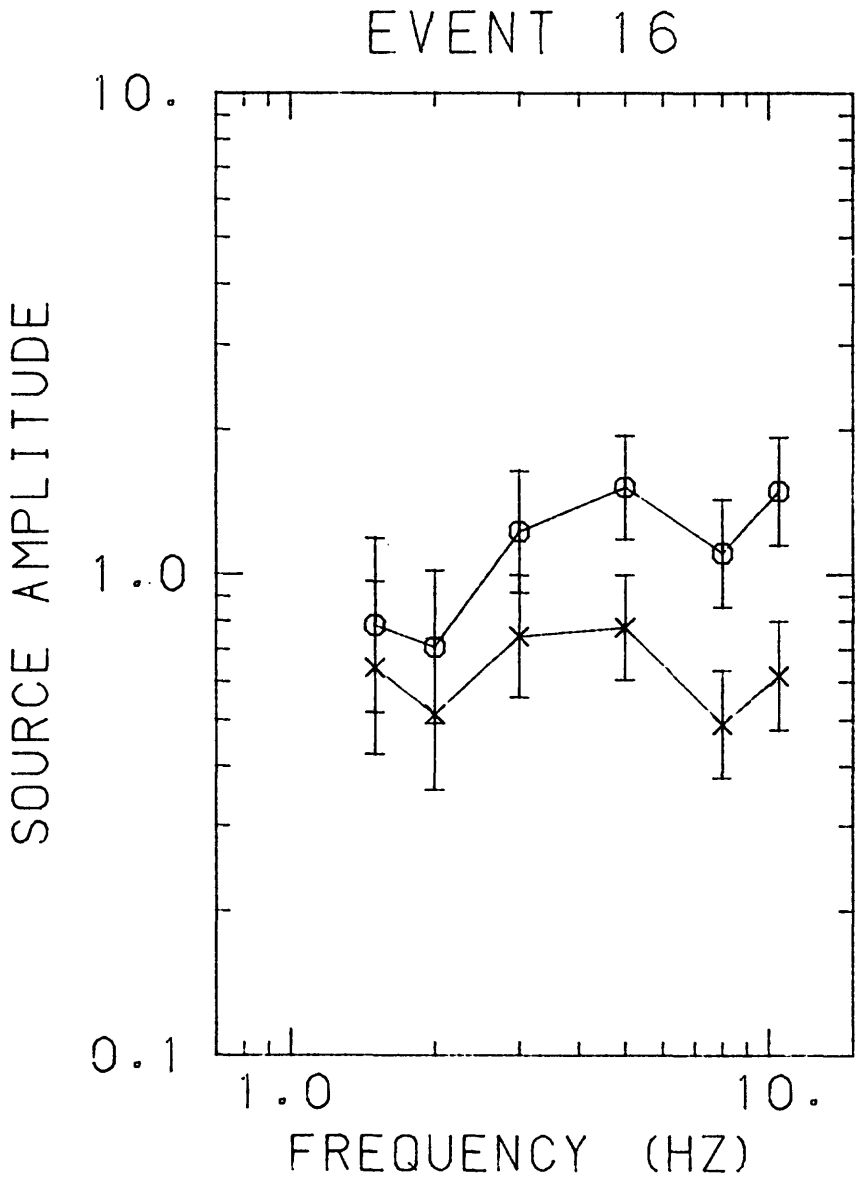

Figure 61. Source spectra for Event 16.

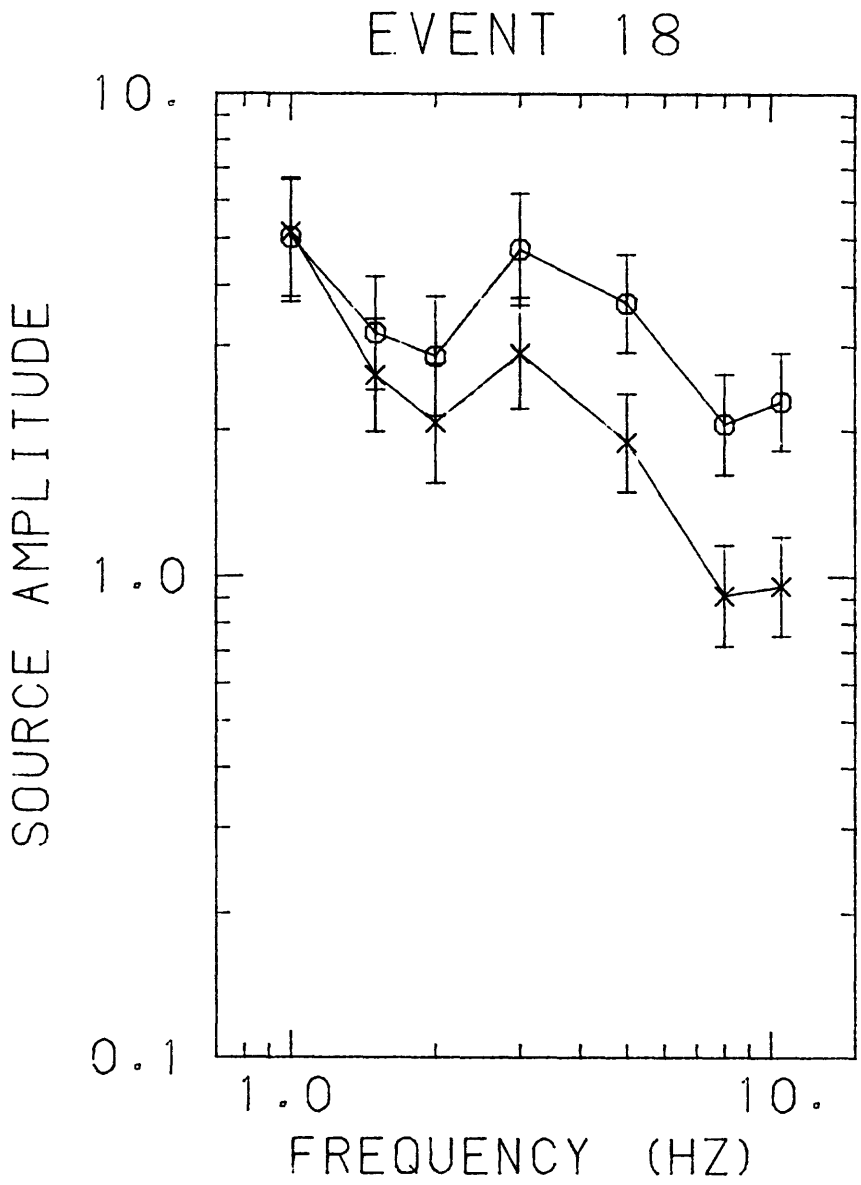

Figure 62. Source spectra for Event 18.

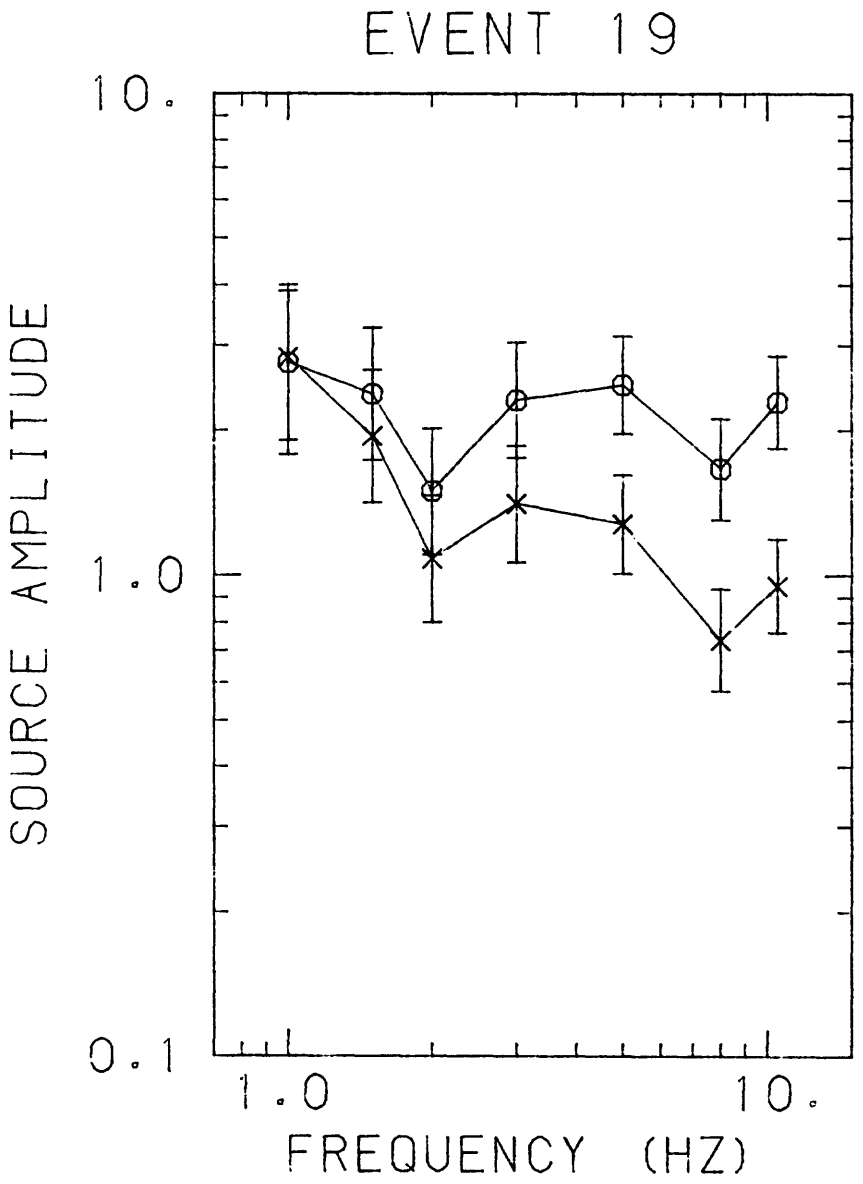

Figure 63. Source spectra for Event 19.

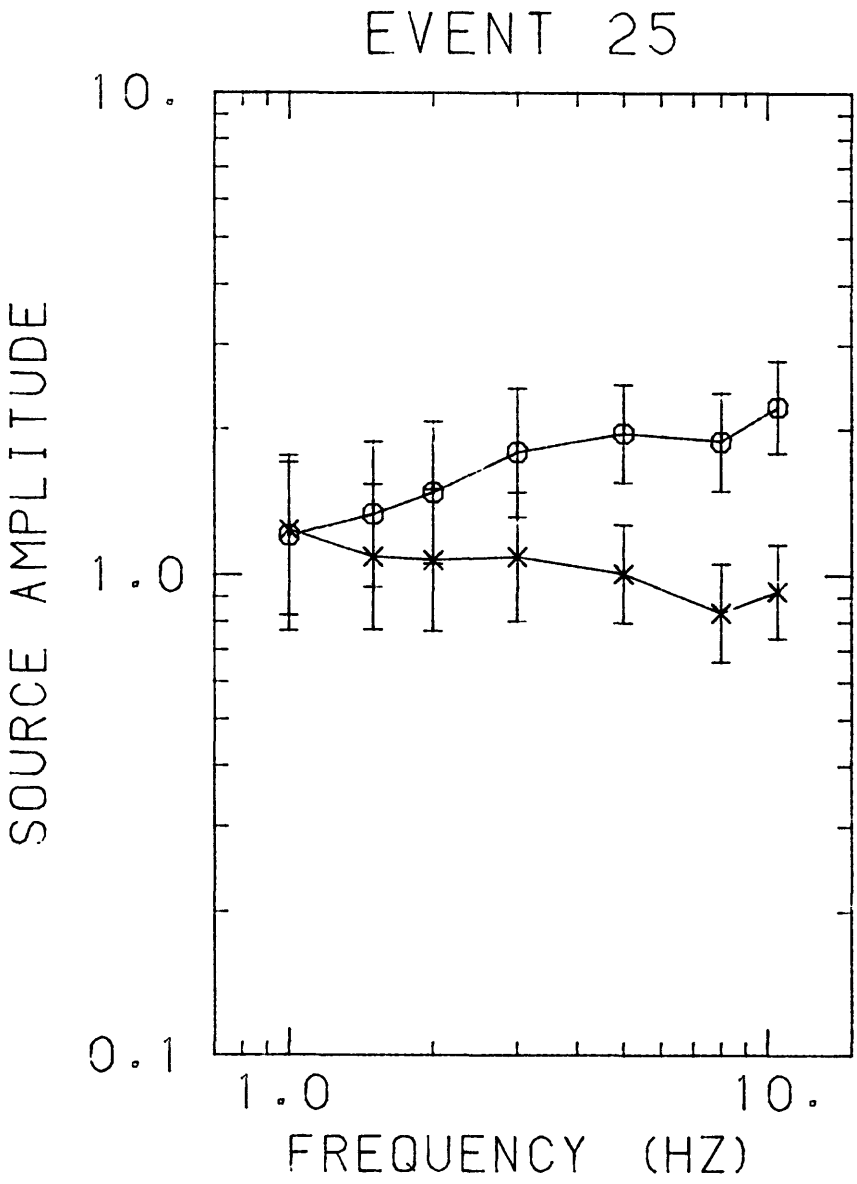

Figure 64. Source spectra for Event 25.

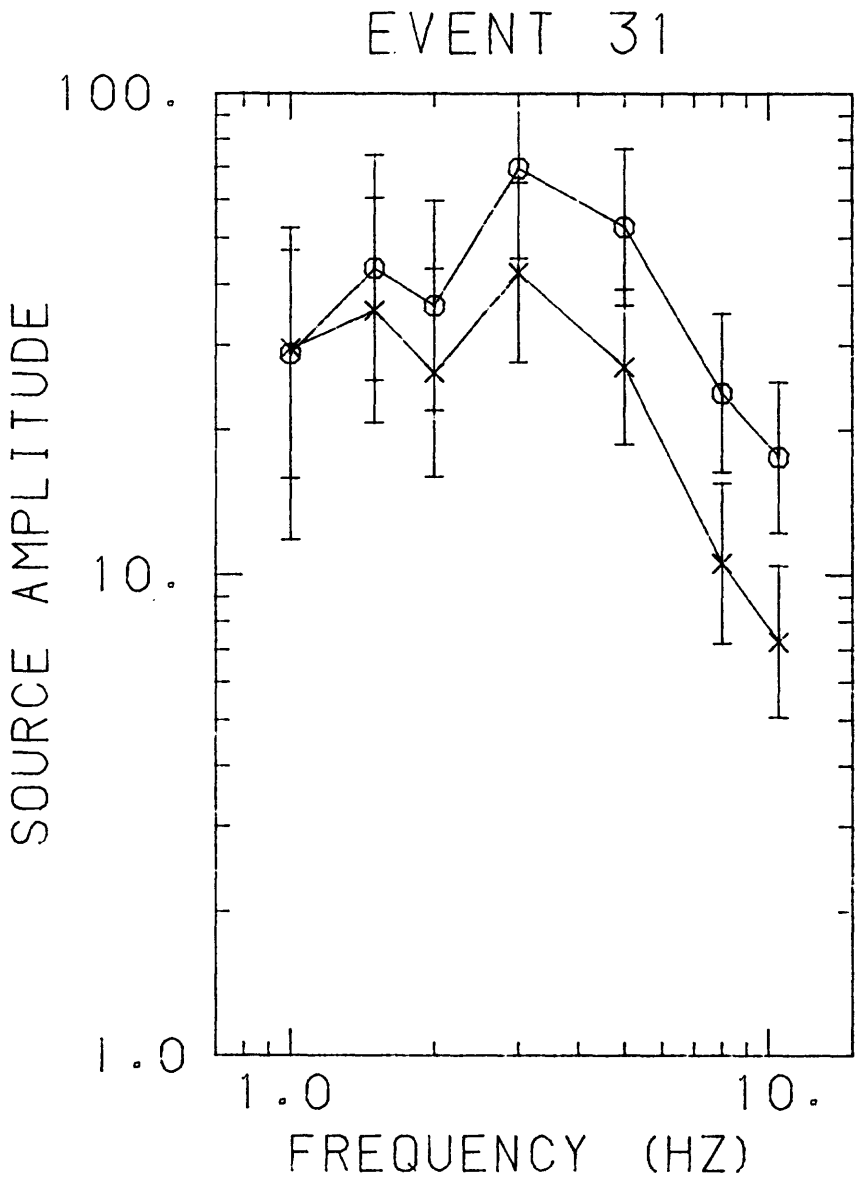

Figure 65. Source spectra for Event 31.

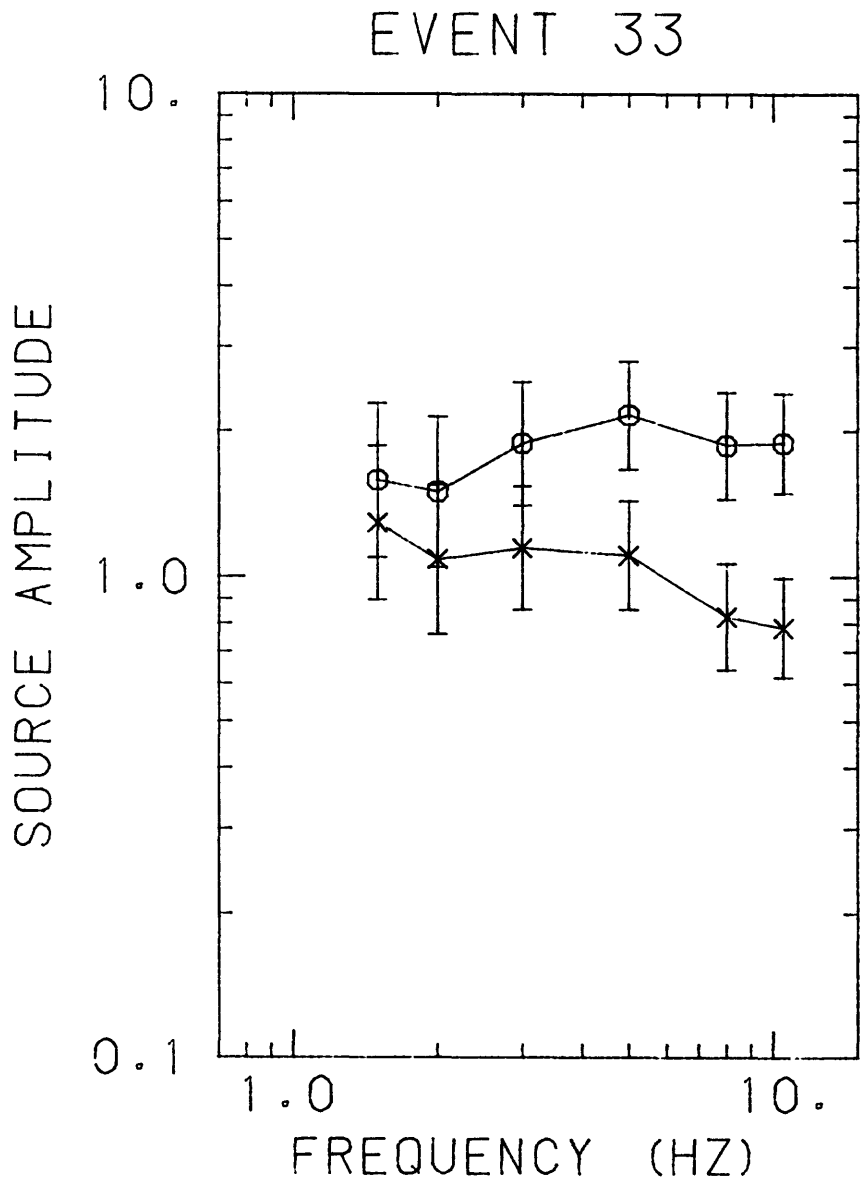

Figure 66. Source spectra for Event 33.

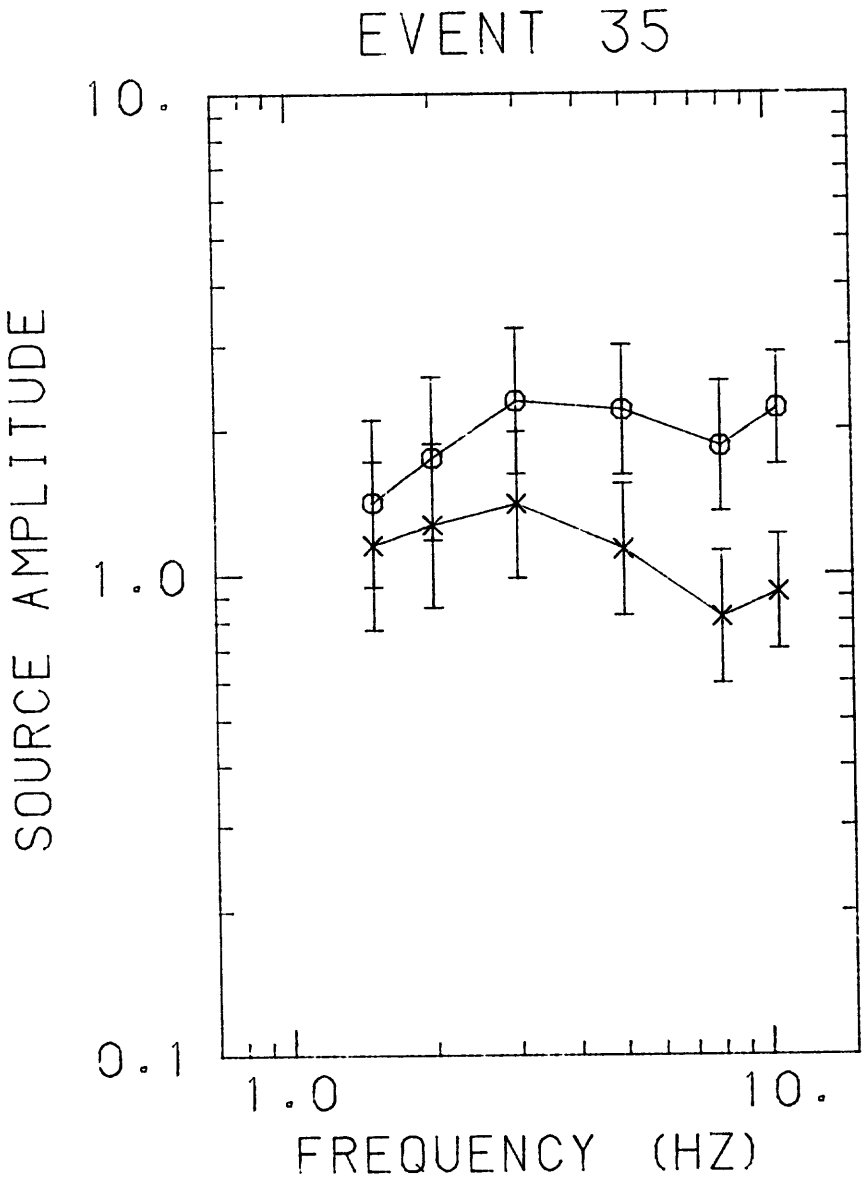

Figure 67. Source spectra for Event 35.

spectrum. We find a corner frequency of approximately 3 Hz, and can estimate a seismic moment of approximately 4.3×10^{20} dyne-cm, which agrees with moment values for events of similar magnitude (Street et al., 1975). This moment should correspond to a corner frequency of approximately 2 Hz. This event has a magnitude $m_b = 3.5$, whereas all the other events are in the magnitude range $1.5 \leq m_b \leq 2.2$. The lack of observable corner frequencies for the smaller events is probably due to a lack of resolution in the range of frequencies beyond the corner frequencies. The corner frequencies should be in the range 3.1 to 6.8 Hz, but we only sample three frequencies (5,8 and 10.5 Hz) beyond this range.

DISCUSSION AND CONCLUSIONS

The principal contribution of the research presented in this report is the developement of a methodology to determine γ and Q values for high frequency seismic phases by statistical methods, which allow one to place confidence limits on the values of γ and Q so determined.

The statistical method used was shown to give excellent results for 1-Hz Lg attenuation data of Bollinger (1979) for the southeastern United States, as well as for 1-Hz Lg data for the central United States. Our findings agree with those of Street (1976) in indicating that the rate of attenuation with distance of 1-Hz Lg waves in the central U.S. (Q=1300) is slightly less than that observed in the southeastern U.S. (Q = 820). Both regions, however, show a much lower attenuation rate than California (Q = 200). This agrees with studies by Sutton et al. (1967), who found that Q for 0.5-2 Hz waves in California was approximately 200, and in New Madrid approximately 1000. In other parts of the United States they found $200 < Q < 1000$, with values generally less than 500 west of the Rocky Mountains and greater than 500 east of the Rocky Mountains. Recently Herrmann (1980) used coda shape and coda dispersion of events recorded by WWSSN instruments to determine Q values for several regions of the United States, and found a Q of 135 for California using data from Berkeley (BKS), a Q of 325 for the Basin and Range Province using data from Dugway, Utah (DUG), and a Q of 1040 for the southeastern United States using data from Blacksburg, Virginia (BLA).

The importance of high Q values for strong ground motion studies

lies in the fact that it results in relatively large amplitude high-frequency wave motion at large epicentral distances. In other words, in high Q regions one can expect large areas of damaging ground shaking, as is typically observed in the central and eastern United States.

A second important result of this study is the indication of the dependence of the quality factor, Q , on frequency. Although Q is usually considered frequency independent, there is some evidence that at frequencies of 0.1 to 10 Hz it may vary with frequency. Our present results, from both the filtered and unfiltered data, indicate an increase in Q with frequency in the range of 1 to 10 Hz. This finding coincides with the results of Mitchell (1980), which indicated an increase in Q with frequency in the range of 0.1 to 1 Hz.

There are only a very limited set of data for the attenuation of high frequency ground motion as a function of wave frequency. One such study was done by Espinosa (1977), using spectra of strong-motion records of the 1971 San Fernando, California earthquake. Espinosa's data were principally in the range of 0-150 km, where geometric spreadin accounts for most of the attenuation, with absorption having only a minor effect. On log A-log Δ plots Espinosa fitted the data by straight lines, which corresponds to a relation

$$A = A_o \Delta^{-n}$$

Converting Espinosa's frequency-domain measurements to time-domain values, we have n = 1.17 for southern California and 1.11 for New Madrid for 1-Hz waves. For 3-Hz waves the southern California value is 1.60 and the New Madrid value is 1.19. For 10-Hz waves the values are 1.48 and 1.04, respectively. Test values of n show that for

distances out to 150 km attenuation is almost the same in the two regions for 1-hz waves, i.e. it is controlled by geometric spreading which is similar for the two regions. The higher-frequency waves are more affected by absorption in California, and thus have relatively high n values. (For no absorption the value of n would be 0.83.)

Peak accelerations in strong-ground motion usually occur at frequencies of 3 hz and greater. Thus it can be expected that peak accelerations will fall off more rapidly with distance in California than in New Madrid. Peak velocities for large earthquakes, on the other hand, often occur at frequencies near 1 hz. Thus out to distances of 150 km the fall-off of peak velocity with distance will be similar in California and New Madrid. We need more strong-motion data to confirm these conclusions which are based on microearthquake data for New Madrid.

ACKNOWLEDGMENTS

This research was supported by the U.S. Geological Survey, purchase order no. 9950-7312. We wish to thank A.F. Espinosa of the U.S. Geological Survey, Golden, Colorado, for helpful comments.

REFERENCES

Bevington, Philip, Data Reduction and Error Analysis for the Physical Sciences, Chapter Six, McGraw Hill, New York, 1969.

Bollinger, G.A., Attenuation of the Lg phase and the determination of m_b in the southeastern United States, Bull. Seis. Soc. Am., 69, 45-62, 1979.

Chouet, B., K. Aki, and M. Tsujiura, Regional variations of the scaling law of earthquake source spectrum, Bull. Seism. Soc. Am., 68, 49-79, 1978.

Dwyer, J., and O. Nuttli, Attenuation of high-frequency Lg waves in the New Madrid seismic zone, Report submitted to U.S. Geological Survey, Golden, CC, 1978.

Espinosa, A.F., Particle-velocity attenuation relations: San Fernando earthquake of February 9, 1971, Bull. Seism. Soc Am., 67, 1195-1214, 1977.

Ewing, M., W.S. Jardetzky, and F. Press, Elastic Waves in Layered Media, p. 358, McGraw-Hill, New York, 1957.

Herrmann, R.B., Q estimates using the coda of local earthquakes, Bull. Seism. Soc. Am., 70, 447-468, 1980.

Herrmann, R.B. and B.J. Mitchell, Statistical analysis and interpretation of surface wave anelastic attenuation data for the stable interior of North America, Bull. Seism. Soc. Am., 65, 1115-1128, 1975.

Mitchell, B.J., Frequency dependence of shear wave internal friction in the continental crust of eastern North America, J. Geophys. Res., in print.

Nuttli, O.W., Seismic wave attenuation and magnitude relations for eastern North America, J. Geophys. Res., 78, 876-885, 1973.

Nuttli, O.W., A time domain study of the attenuation of 10-Hz waves in the New Madrid seismic zone, Bull. Seism. Soc. Am., 68, 343-355, 1978.

Nuttli, O.W., and J. Dwyer, State-of-the-Art for Assessing Earthquake Hazards in the United States; "Attenuation of High Frequency Seismic Waves in the Central Mississippi Valley," Miscellaneous Paper S-73-1, Report 10, U.S. Army Engineer Waterways Experiment Station, CE, Vicksburg, Miss., 1978.

Stauder, W., R. Herrmann, S.T. Morrissey, J. Best, S.H. Cheng, J. Fischer, M. Kramer, C. Nicholson, R. Perry, S. Singh, M. Woods and J. Zollweg, Southeast Misspuri Regional Seismic Network Quarterly Bulletins, Saint Louis University, Nos. 1-19, 1974-1979.

Street, R., Scaling northeastern United States/southeastern Canadian earthquakes by their Lg waves, Bull. Seism. Soc. Am., 66, 1525-1537, 1976.

Street, R., R.B. Herrmann, and O.W. Nuttli, Spectral Characteristics of the Lg wave generated by central United States data, Geophys. J. R. Astr. Soc., 41, 51-63, 1974.

Sutton, G.H.,W. Mitronovas and P.W. Pomeroy, Short-period seismic energy radiation patterns from underground nuclear explosions and small-magnitude earthquakes, Bull. Seism. Soc. Am., 57, 249-267, 1967.

☆ U. S. GOVERNMENT PRINTING OFFICE 1980 - 778-734/232 Reg. 8